

MOLECULAR MODELLING OF VOLTAGE-GATED ION CHANNELS

**MOLECULAR MODELLING OF
VOLTAGE-GATED POTASSIUM, SODIUM AND CALCIUM CHANNELS
COMPLEXED WITH METAL IONS AND SMALL-MOLECULE LIGANDS**

By

IVA BRUHOVA, B. Sc.

A Thesis

Submitted to the School of Graduate Studies

in Partial Fulfilment of the Requirement

for the Degree of

Doctor of Philosophy

McMaster University

© Copyright by Iva Bruhova, May 2009

DOCTOR OF PHILOSOPHY (2009)
(Biochemistry and Biomedical Sciences)

McMaster University
Hamilton, Ontario

TITLE: Molecular modelling of voltage-gated potassium, sodium and calcium channels complexed with metal ions and small-molecule ligands

AUTHOR: Iva Bruhova, B. Sc. (McMaster University)

SUPERVISOR: Professor Boris S. Zhorov

NUMBER OF PAGES: xi, 139

ABSTRACT

Voltage-gated potassium, sodium, and calcium channels play fundamental roles in cell physiology. They are targets for numerous drugs that are used to treat pain, cardiovascular, autoimmune, and other disorders. Atomic-resolution structures of ion channels and their complexes with ligands are necessary to understand the mechanisms of drug action of ligands. Electrophysiological and crystallographic studies have advanced our understanding of ion channels, but the binding sites, access pathways, and the mechanism of state-dependent action of medically important drugs remain unclear. During my graduate studies, I investigated the structure-function relationships of voltage-gated ion channels and their complexes with drugs by using energy calculations with experimental constraints. My work has helped resolve controversial interpretations of experiments addressing structural similarity between prokaryotic and eukaryotic K^+ channels. Our model of the open *Shaker* K^+ channel was confirmed by the later published X-ray structure of $K_v1.2$. Our $Ca_v2.1$ model reinterprets substituted-cysteine accessibility experiments, validates the proposed alignment between K^+ and Ca^{2+} channels, and suggests a similar folding of voltage-gated K^+ and Ca^{2+} channels. These results allowed me to model eukaryotic K^+ and Na^+ channels in the resting and open/slow-inactivated states, and to predict the binding sites of local anaesthetics, correolide, and chromanol 293B. In these studies, we proposed the involvement of metal ions in the binding of nucleophilic drugs and suggested that the deficiency of permeating ion(s) in the outer pore of the slow-inactivated channels stabilizes the ligands. Simultaneous studies of K^+ , Na^+ , and Ca^{2+} channels were advantageous because the information acquired from one family of ion channels was relevant to other families. My studies contributed to the growing knowledge about ion channels by offering structural information and suggesting mechanisms for the action of drugs.

ACKNOWLEDGEMENTS

Foremost, I would like to thank my supervisor Dr. Boris Zhorov for his guidance, inspiration, and patience. You have been a positive role model with your kind and encouraging attitude. You have made me enthusiastic about molecular modelling and ion channels! It has been a pleasure working with you. I hope that I have lived up to all expectations as your first graduate student in Canada.

Over the years, I have received continuous help, constructive comments, and interest in my studies from my committee members. Thank you, Dr. Murray Junop and Dr. Daniel Yang.

I would like to thank my family and friends. Particularly, my mother for her endless love, undeniable support, and for initiating my interest in biology and chemistry; and my father for his guidance and motivation in computers, physics, and math. I appreciate the caring support I received from Manu, Vince, and Suzanne.

Members of the Biochemistry department have made my time at McMaster University enjoyable. Kevin, Daniel, Jack, Ricky, Armela, and Yulia, you have been my good and helpful friends. I appreciated all the useful discussions, particularly with Denis Tikhonov.

I would like to acknowledge the Canadian Institute of Health Research for funding my PhD studies and the Shared Hierarchical Academic Research Computing Network (www.SHARCNET.ca) for supplying powerful computer resources for my projects.

TABLE OF CONTENTS

| | Page |
|--|-----------|
| ABSTRACT | iii |
| ACKNOWLEDGEMENTS | iv |
| TABLE OF CONTENTS | v |
| LIST OF FIGURES | viii |
| LIST OF TABLES | x |
| LIST OF ABBREVIATIONS | xi |
| | |
| CHAPTER ONE - Introduction | 1 |
| GENERAL STRUCTURE OF VOLTAGE-GATED ION CHANNELS | 2 |
| X-RAY STRUCTURES OF ION CHANNELS | 3 |
| MOLECULAR MODELLING OF ION CHANNELS | 8 |
| STRUCTURE, FUNCTION, AND PHARMACOLOGY OF VOLTAGE-GATED CHANNELS | 9 |
| Voltage-gated K ⁺ channels | 10 |
| Voltage-gated Ca ²⁺ channels | 12 |
| Voltage-gated Na ⁺ channels | 13 |
| OVERVIEW | 16 |
| | |
| CHAPTER TWO - Predicting the open-state geometry of eukaryotic K⁺ channels | 17 |
| PREFACE | 18 |
| ABSTRACT | 19 |
| INTRODUCTION | 19 |
| METHODS | 21 |
| Determining dimensions of <i>Shaker</i> channel blockers | 21 |
| Modeling the Cd ²⁺ -bound <i>Shaker</i> channel | 23 |
| Simulating Cd ²⁺ ions | 23 |
| RESULTS AND DISCUSSION | 24 |
| Dimensions of the <i>Shaker</i> blockers | 24 |
| Locked-open conformations of the <i>Shaker</i> channel | 28 |
| Conformational changes at the PVP motif | 33 |
| Simulating the Cd ²⁺ block of the locked-open <i>Shaker</i> channel | 35 |
| Block by a single cadmium ion | 35 |
| Block by two cadmium ions | 36 |
| Sensitivity of results to the chosen computational methodology | 38 |
| CONCLUSIONS | 38 |

| | |
|--|-----------|
| CHAPTER THREE - The binding of nucleophilic blockers in voltage-gated K⁺ channels involves electrostatic interactions with a K⁺ ion in the selectivity filter | 40 |
| PREFACE | 41 |
| ABSTRACT | 42 |
| INTRODUCTION | 42 |
| METHODS | 44 |
| RESULTS | 47 |
| Correolide in the K _v 1.2-based model of the open K _v 1.3 | 47 |
| Chromanol 293B in the KcsA- and K _v 1.2-based model of the closed and open K _v 7.1 | 57 |
| Sensitivity of results to the chosen computational methodology | 58 |
| DISCUSSION | 62 |
| Correolide-sensing residues | 62 |
| Chromanol-sensing residues | 63 |
| Possible involvement of K ⁺ in the binding of nucleophilic ligands | 63 |
| CONCLUSION | 65 |
| | |
| CHAPTER FOUR - K_v1.2-based model of a calcium channel is consistent with available SCAM data | 66 |
| ABSTRACT | 67 |
| INTRODUCTION | 67 |
| METHODS | 68 |
| RESULTS | 71 |
| SCAM data and the cysteine-orientation concept | 71 |
| MTS-modified cysteines in pore-facing positions | 72 |
| MTS-modified cysteines in positions that do not face the pore | 76 |
| Modified cysteines in the outer helices of Ca _v 2.1 | 81 |
| Currents correlate with the distance of the MTS nitrogen from the pore axis | 81 |
| DISCUSSION | 84 |
| CONCLUSION | 88 |
| | |
| CHAPTER FIVE - Access and binding of local anaesthetics in the closed sodium channel | 89 |
| PREFACE | 90 |
| ABSTRACT | 91 |
| INTRODUCTION | 91 |
| METHODS | 94 |
| RESULTS | 97 |
| LA Binding | 97 |
| LAs in the H ₂ O-DEKA model | 97 |

| | |
|---|------------|
| LAs in the Na ⁺ -DEKA model | 106 |
| Access pathways of QX-314 | 108 |
| DISCUSSION | 112 |
| Relations between slow inactivation and binding of cationic LAs | 114 |
| LA access through the III/IV domain interface | 115 |
| Modeling limitations | 118 |
| | |
| CHAPTER SIX - Summary | 120 |
| Prokaryotic and eukaryotic K ⁺ channels are structurally similar | 121 |
| Metal ions are indispensable components to the binding of ligands in K ⁺ channels | 123 |
| Ca ²⁺ channels and K ⁺ channels are structurally similar | 124 |
| Local anaesthetics in the closed Na ⁺ channel | 124 |
| Extracellular access pathway of LAs into the closed Na ⁺ channel is located between repeats III and IV | 125 |
| | |
| REFERENCES | 127 |

LIST OF FIGURES

| | Page |
|---|------|
| CHAPTER ONE | |
| Figure 1.1 - General membrane topology of voltage-gated ion channels | 5 |
| Figure 1.2 - The pore-forming domains of prokaryotic K ⁺ channel X-ray structures | 7 |
| CHAPTER TWO | |
| Figure 2.1 - Structure of correolide | 25 |
| Figure 2.2 - Dimensions of the <i>Shaker</i> channel intracellular blockers | 26 |
| Figure 2.3 - The 10 Å-ring of methane molecules vs. correolide and KvAP-based model of the <i>Shaker</i> channel | 27 |
| Figure 2.4 - Convergence of the <i>Shaker</i> models from the X-ray based starting structures to conformations with coordinating bonds $C^{i24}_S^{\gamma} \cdots Cd^{2+} \cdots N^{\epsilon 2}_H^{i34}$ | 29 |
| Figure 2.5 - KvAP-based models of the <i>Shaker</i> channel | 31 |
| Figure 2.6 - KvAP-based model of the <i>Shaker</i> inner-helices bundle obtained by MC-minimization without using the advantage of the channel four-fold symmetry | 34 |
| Figure 2.7 - Pulling a K ⁺ ion through the locked-open mutant V ⁱ²² C/V ⁱ²⁴ C blocked by two Cd ²⁺ ions | 37 |
| CHAPTER THREE | |
| Figure 3.1 - Structure of ligands | 45 |
| Figure 3.2 - Random search for the energetically optimal binding site of correolide in model 2/4 | 49 |
| Figure 3.3 - Systematic search for the energetically optimal binding site of correolide in model 2/4 | 51 |
| Figure 3.4 - Correolide in model 1/3/5 of K _v 1.3 | 54 |
| Figure 3.5 - Random search for the energetically optimal binding site of chromanol in the open and closed K _v 7.1 models | 59 |
| Figure 3.6 - K _v 1.3:correolide models calculated with different settings | 61 |
| Figure 3.7 - The extracellular view at the inner-helices bundle in the open K _v 1.3 | 64 |
| CHAPTER FOUR | |
| Figure 4.1 - The extracellular and cytoplasmic views of the inner and outer helices of the K _v 1.2 X-ray structure | 73 |

| | |
|---|----|
| Figure 4.2 - The top and side views of the lowest-energy orientations of ${}^m\text{C}^{1i15}$ and ${}^m\text{C}^{1i19}$ in the open $\text{Ca}_v2.1$ channel | 74 |
| Figure 4.3 - Orientations of ${}^m\text{C}^{i18}$ in $\text{Ca}_v2.1$ | 75 |
| Figure 4.4 - The top view of MTS-modified cysteines in position <i>1i22</i> , <i>2i22</i> , <i>3i22</i> , and <i>4i22</i> | 77 |
| Figure 4.5 - Preferable orientations of MTS-modified cysteine in non-pore facing residues in the open $\text{Ca}_v2.1$ channel | 78 |
| Figure 4.6 - The top view of the lowest-energy orientations of ${}^m\text{C}^{2o10}$, ${}^m\text{C}^{3o10}$, and ${}^m\text{C}^{4o10}$ | 82 |
| Figure 4.7 - Distance of MTS nitrogen and C^β from the pore axis | 83 |

CHAPTER FIVE

| | |
|--|-----|
| Figure 5.1 - Chemical structures of LAs that are used in calculations | 99 |
| Figure 5.2 - Searching for energetically favourable binding modes of QX-314 in the closed $\text{Na}_v1.5$ with a water molecule in the selectivity filter | 100 |
| Figure 5.3 - Searching for energetically favourable binding modes of cocaine in the closed $\text{Na}_v1.5$ with a water molecule or Na^+ ion in the DEKA locus | 102 |
| Figure 5.4 - Searching for energetically favourable binding modes of tetracaine in the closed $\text{Na}_v1.5$ channel with a water molecule in the DEKA locus | 104 |
| Figure 5.5 - All-atom model of the closed $\text{Na}_v1.5$ with a water molecule in the DEKA locus and QX-314 in the inner pore | 107 |
| Figure 5.6 - Exploring hypothetical access pathways of QX-314 | 109 |
| Figure 5.7 - Pulling QX-314 through the sidewalk, between segments IIIP, IIIS6, and IVS6 | 110 |
| Figure 5.8 - The MC-minimized energy profile of QX-314 pulled through the sidewalk | 111 |
| Figure 5.9 - A scheme of coupled movement of Na^+ and a LA molecule in the closed Na^+ channel | 117 |

CHAPTER SIX

| | |
|---|-----|
| Figure 6.1 - The comparison of our KvAP-based model of the locked-open <i>Shaker</i> channel to two open X-ray structures | 122 |
|---|-----|

LIST OF TABLES

| | Page |
|--|------|
| CHAPTER ONE | |
| Table 1.1 - Sequence alignment between voltage-gated K ⁺ , Na ⁺ , and Ca ²⁺ channels | 6 |
| CHAPTER TWO | |
| Table 2.1 - Alignment of K ⁺ channels | 21 |
| Table 2.2 - Comparison of the <i>Shaker</i> channel models | 30 |
| CHAPTER THREE | |
| Table 3.1 - Sequence alignment of K ⁺ channels | 46 |
| Table 3.2 - Correolide-sensing residues in the inner helices and their energy contributions (kcal/mol) to correolide binding | 56 |
| Table 3.3 - Energy components (kcal/mol) of the most energetically favourable complexes of chromanol inside K _v 7.1 | 60 |
| Table 3.4 - Ligand-receptor energy predicted with various methodological setup | 61 |
| CHAPTER FOUR | |
| Table 4.1 - Sequence alignment between K ⁺ , Na ⁺ , and Ca ²⁺ channels and effects of MTS reagents on Cys mutant channels | 69 |
| Table 4.2 - Proposed inner helix alignments between K ⁺ , Na ⁺ , and Ca ²⁺ channels | 86 |
| CHAPTER FIVE | |
| Table 5.1 - Sequences of ion channels and effect of mutations in Na ⁺ channels | 95 |
| Table 5.2 - Energetically favourable binding modes of LAs in the closed Na _v 1.5 with the DEKA locus loaded by either H ₂ O or Na ⁺ | 105 |
| Table 5.3 - Interaction energy (kcal/mol) of QX-314 with the all-atom Na _v 1.5 model | 107 |
| CHAPTER SIX | |
| Table 6.1 - The C ^α RMSD (Å) of the K _v 1.2 X-ray, the KvAP X-ray, and the KvAP-based model of the locked-open <i>Shaker</i> channel | 122 |

LIST OF ABBREVIATIONS

| | |
|-----------------------|--|
| 1/3/5 | K _v 1.3 model in which K ⁺ binding sites 1, 3, and 5 are loaded with K ⁺ ions |
| 2/4 | K _v 1.3 model in which K ⁺ binding sites 2 and 4 are loaded with K ⁺ ions |
| BTZ | benzothiazepine |
| Ca _v 2.1 | PQ-type voltage-gated Ca ²⁺ channel |
| CTX | Conotoxin |
| DEKA | Asp-Glu-Lys-Ala residues forming the selectivity filter of Na ⁺ channels |
| DHP | 1,4-dihydropyridine |
| EEEE | four glutamate residues forming the selectivity filter of Ca ²⁺ channels |
| GYGD | main chain carbonyls of this sequence form the K ⁺ channel selectivity filter |
| H ₂ O-DEKA | water molecule occupying the DEKA locus in the Na ⁺ channel model |
| IC ₅₀ | half maximal inhibitory concentration |
| KcsA | proton-gated K ⁺ channel crystallized in the closed state |
| KirBac | inward rectifier K ⁺ channel crystallized in the closed state |
| K _v | voltage-gated K ⁺ channels |
| K _v 1.2 | subtype of the <i>Shaker</i> K ⁺ channels crystallized in the open state |
| K _v 1.3 | subtype of the <i>Shaker</i> K ⁺ channels expressed in T-lymphocytes |
| K _v 7.1 | subtype of voltage-gated K ⁺ channels, also known as KCNQ1 |
| KvAP | voltage-gated K ⁺ channel crystallized in the open state |
| LAs | local anaesthetics |
| ^m C | MTS-modified cysteine |
| MC | Monte Carlo |
| MCM | Monte Carlo-energy minimization |
| MthK | Ca ²⁺ -gated K ⁺ channel crystallized in the open state |
| MTS | methanethiosulfonate derivative |
| MTSEA | methanethiosulfonate ethylammonium |
| MTSET | methanethiosulfonate ethyltrimethylammonium |
| Na ⁺ -DEKA | Na ⁺ ion occupying the DEKA locus in the Na ⁺ channel model |
| Na _v 1.4 | muscle voltage-gated Na ⁺ channel |
| Na _v 1.5 | cardiac voltage-gated Na ⁺ channel |
| P | membrane re-entrant loop between S5 and S6 |
| PAA | phenylalkylamine |
| PVP | Pro-Val-Pro motif in the <i>Shaker</i> channel |
| RMSD | root mean square deviation |
| S1-S6 | six transmembrane α -helices of voltage-gated ion channels |
| S5 | outer helix of the pore-forming domain |
| S6 | inner helix of the pore-forming domain |
| SCAM | substituted-cysteine accessibility method |
| TBA | tetrabutylammonium |
| TTX | tetrodotoxin |

CHAPTER ONE

INTRODUCTION

Ion channels are membrane proteins that regulate the flow of ions through a pore across the lipid bilayer. The channels form a large superfamily with different structural, functional, and pharmacological properties. Ion channels are classified based on their primary permeating ion, such as K^+ , Na^+ , Ca^{2+} and Cl^- channels, or group of permeating ions, such as cation channels. Depending on the type of activation stimulus, ion channels are categorized as voltage-gated or ligand-gated (Hille, 2001). Structurally, ion channels are composed of multiple domains forming hetero- or homo-multimers with numerous transmembrane helices. In this thesis, I will focus on voltage-gated K^+ , Na^+ , Ca^{2+} channels, which are structurally similar tetrameric ion channels containing six transmembrane helices per monomer.

Voltage-gated K^+ , Na^+ , and Ca^{2+} channels are found in excitable cells, such as neuron, heart, muscle, and endocrine cells (Hille, 2001). These channels work in concert to control the electrical activity of excitable cells. They are responsible for the maintenance of the resting membrane potential, the generation and propagation of action potentials, and the regulation of intracellular concentration of Ca^{2+} , which play an important role as a second messenger. Voltage-gated Na^+ channels are responsible for the rapid upstroke and propagation of the action potential. Voltage-gated K^+ channels shape the action potential, return the membrane voltage to its negative resting value after an action potential, and set the action potential firing rate. Voltage-gated Ca^{2+} channels shape action potentials in heart cells and help translate electrical signals into chemical signals by controlling the concentration of intracellular Ca^{2+} . Thus, voltage-gated ion channels are involved in muscle contraction, flow of information in the nervous system, the pace of the heart, the secretion of hormones and neurotransmitters and other physiological functions (Hille, 2001). Non-surprisingly, these channels are targets for natural toxins and chemically diverse drugs used for the treatment of pain, cardiovascular diseases, epilepsy, migraines, and other disorders (Zhorov and Tikhonov, 2004).

In the past, ion channels have been given various names corresponding to their gene products causing confusing nomenclatures. Currently, a unified nomenclature is used for mammalian K^+ (Chandy and Gutman, 1993), Na^+ (Goldin et al., 2000), and Ca^{2+} (Ertel et al., 2000) channels. Ion channels are named using the chemical symbol of the primary permeating ion (K, Na, or Ca) with the principal physiological regulator (voltage or ligand) indicated as a subscript (K_v , K_{Ca}). A numerical identifier follows, which corresponds to the subfamily and the order of discovery within that subfamily ($K_v1.3$, $Ca_v2.1$).

GENERAL STRUCTURE OF VOLTAGE-GATED ION CHANNELS

Structural determinants of major physiological characteristics, namely ion selectivity, gating, and ligand binding are localized in the α subunit (Striessnig et al., 1998; Kaczorowski and Garcia, 1999; Catterall, 2000a). The pore-forming α subunit is sufficient for functional expression, but auxiliary subunits can modify the kinetics and

voltage dependence of channel gating (Isom et al., 1994). Most K^+ channels are homotetramers consisting of four identical α subunits symmetrically folded around a central pore (Figure 1.1). In some cases, four related, but not identical subunits associate to form a heterotetrameric K^+ channel. Na^+ and Ca^{2+} channels are composed of one polypeptide chain with four homologous but diverse repeats, which fold similarly as K^+ channels (Sato et al., 2001). Each K^+ channel subunit and each Na^+ and Ca^{2+} channel repeat contain six transmembrane helices (S1-S6). Ion permeation and selectivity is controlled by the pore-forming domain, whereas gating is controlled by the voltage-sensor domain. The pore-forming domain consists of four structural motifs, each comprising of two transmembrane helices, an outer (S5) and inner (S6) helix, which are separated by a membrane re-entrant loop (P-loop) (Figure 1.1). Due to this common structural motif, K^+ , Na^+ , and Ca^{2+} channels, along with glutamate receptors and cyclic nucleotide-gated channels are referred to as P-loop ion channels. The P-loop forms the selectivity filter to allow selective passage of ions. In K^+ channels, the selectivity filter is formed by the backbone of a conserved TVGYGD sequence from four subunits (Heginbotham et al., 1994) (Table 1.1). The selectivity region of Ca^{2+} channels contains a highly conserved pattern of four glutamates, the EEEE locus, while in the Na^+ channels it is the DEKA locus (Heinemann et al., 1992; Yang et al., 1993; Stea et al., 1994). The voltage-sensor domain is composed of four transmembrane helices (S1-S4), which control the gating of the pore-forming domain through the S4-S5 linker. Of particular importance is the S4 segment, which moves upon membrane depolarization due to several positively charged residues (Tombola et al., 2006). All the members of the voltage-gated superfamily have voltage-dependent gates that open in response to membrane depolarization. The gates shut rapidly after repolarization. Ion channels exist in different states: closed (resting), open (activated), fast-inactivated (C-type inactivated), and slow-inactivated (N-type inactivated). Only in the open state can ions pass through the channel.

X-RAY STRUCTURES OF ION CHANNELS

The X-ray structures of K^+ channels explained a large body of experimental data, such as K^+ ion selectivity, channel gating, and channel block. The first K^+ channel X-ray structure, the proton-gated KcsA channel, provided important insights into K^+ selectivity and the ion conduction process (Doyle et al., 1998). In K^+ channels, K^+ is at least 10,000 times more permeable than Na^+ despite the atomic radius of Na^+ (0.95 Å) is smaller than K^+ (1.33 Å). The X-ray structure of the K^+ channel revealed that the selectivity filter is a hydrophilic tunnel created by the main chain carbonyls of four highly conserved amino residues (GYGD), see Figure 1.2. This tunnel has a diameter exactly matching that of a dehydrated K^+ ion. It is energetically unfavourable for a Na^+ ion to dehydrate in order to pass through a tunnel wider than its diameter (Doyle et al., 1998). Further crystallographic studies with KcsA assisted in explaining the mechanism of fast inactivation and suggested structural rearrangement upon slow inactivation of K^+ channels (Zhou et al., 2001a; Cordero-Morales et al., 2007).

In the closed KcsA channel, the inner helices are straight with their C-ends sloped into a hydrophobic bundle, which functions as a gate. A water-filled cavity (referred to as the inner pore) is located between the gate and the selectivity filter, where organic compounds bind as seen in the X-ray structure of KcsA with tetrabutylammonium (Zhou et al., 2001a). The X-ray structures show that the inner helices obstruct the cytoplasmic entrance in the closed channel KcsA, but diverge in widely open channels as seen in the X-ray structures of Ca²⁺-gated K⁺ channel MthK (Jiang et al., 2002b; Jiang et al., 2002a) and voltage-gated K⁺ channel KvAP (Jiang et al., 2003a; Jiang et al., 2003b) (Figure 1.2). The open-state X-ray structures explain the gating of bacterial K⁺ channels by suggesting a gating-hinge role for a conserved glycine in the inner helix (Jiang et al., 2002b). The inner helices bend opening the inner pore to the cytoplasm. This open pore is the target for a variety of drugs, which enter the inner pore from the cytoplasm and block ion permeation.

Voltage-gated K⁺ channels, KvAP and Kv1.2, were crystallized in the open state, which included both the pore-forming domain and the voltage-sensor domain (Jiang et al., 2003b; Long et al., 2005b). Doubts were raised with the first X-ray structure of KvAP, because its S4 helices were in a horizontal orientation relative to the pore and located outside the membrane (Jiang et al., 2003a). Subsequent crystallization of KvAP demonstrated that the voltage-sensor domain was in a non-native conformation, possibly because the voltage sensors do not adhere tightly to the pore-forming domain and thus would require an intact lipid membrane for stability (Lee et al., 2005). Kv1.2 was crystallized with a cytoplasmic T1 multimerization domain that helps maintain a native conformation of the voltage sensor (Long et al., 2005a). The full-length structure revealed that the voltage sensors (S1-S4) are independent domains inside the membrane with minimal contact with the pore-forming domain. S4 contains four arginines, two of which are lipid-facing, whereas the other two are buried in the protein forming salt-bridges with negatively charged residues in S1 and S2 (Long et al., 2005b). Upon membrane depolarization the arginines cause the S4 helix to move and/or rotate influencing the pore to open through the S4-S5 linker. Several models have been proposed for the mechanism of voltage-dependent gating (Guy and Seetharamulu, 1986; Jiang et al., 2003b; Chanda et al., 2005; Ruta et al., 2005; Tombola et al., 2006), but without the X-ray structure of a closed K_v channel, the gating mechanism is still unclear.

The prokaryotic non-selective sodium-potassium channel NaK (Shi et al., 2006; Alam and Jiang, 2009a; Alam and Jiang, 2009b) has been crystallized in both the conducting (open) and non-conducting (closed) states. However, this channel functions and behaves differently than eukaryotic Na⁺ and Ca²⁺ channels. An ideal candidate for crystallizing a voltage-gated Na⁺ channel is the NaChBac channel, mainly due to its high expression in bacteria and identical four-fold symmetry. NaChBac is the first functionally characterized bacterial voltage-gated sodium-selective channel cloned from *Bacillus halodurans* (Ren et al., 2001). Unlike mammalian voltage-gated Na⁺ channels, NaChBac contains a single polypeptide with six transmembrane helices, which self-assembles to

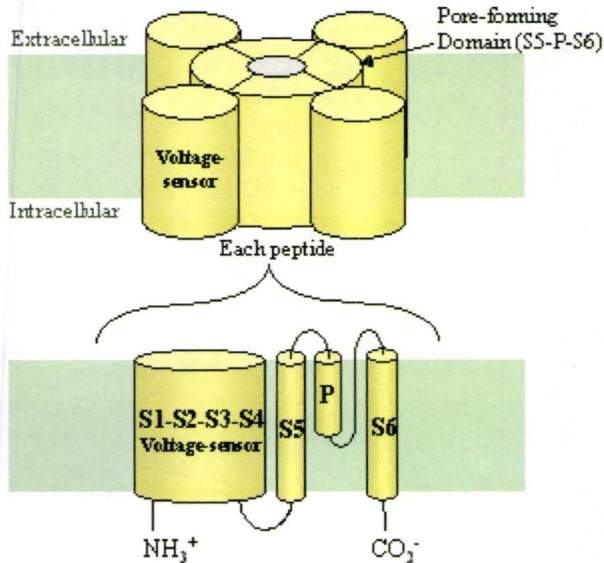
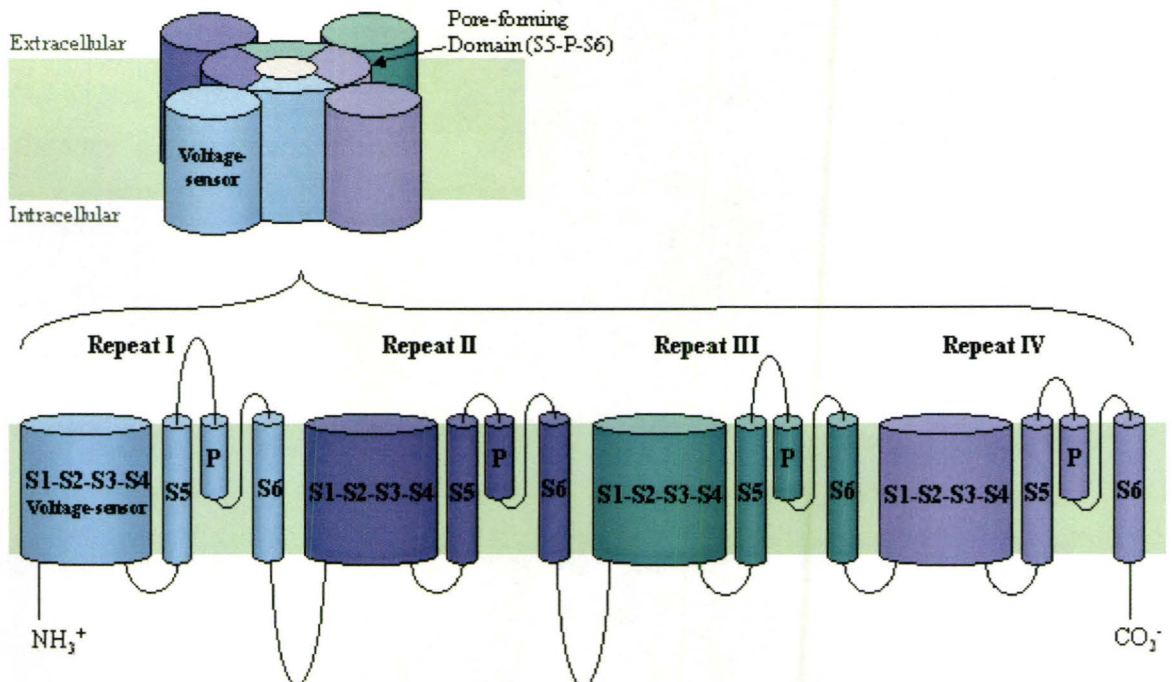
Voltage-gated K^+ channels – homotetramers, 4 identical peptides**Voltage-gated Na^+ and Ca^{2+} channels – heterotetramers, 1 peptide with 4 homologous repeats**

Figure 1.1. General membrane topology of voltage-gated ion channels. Channels are tetramers, composed of four monomers symmetrically folded around a central pore. Each monomer consists of six transmembrane helices (S1-S6) and a pore-forming region (P). The P-region, located between the S5 and S6 helices, forms the ion selectivity filter.

Table 1.1. Sequence alignment between voltage-gated K⁺, Na⁺, and Ca²⁺ channels^a

| Channel | Segment ^b | # ^b | 1 | 11 | 21 ^c |
|---------------------|----------------------|----------------|------------------------------------|--|--|
| K _v 1.2 | S5 o | 322 | KASMREL L GLL | IFF L FIGVIL | FSSAVYFAEA |
| Ca _v 1.2 | IS5 1o | 292 | IKAMVPLLHI | ALLVLFV ^{III} | YAIIGLELFM |
| | IIS5 2o | 675 | LNSVRSIASL | LLLLFLF ^{III} | FSLLGMQ ^L FG |
| | IIIS5 3o | 1053 | FVAIRTIGNI | VIV T TL LQ FM | FACIGVQ ^L FK |
| | IVS5 4o | 1384 | IKSFQALPYV | ALLIVMLFFI | YAVIGMQ ^V FG |
| Na _v 1.4 | IS5 1o | 244 | IQSVKKLSDV | MILTVFCLSV | FALVGLQ ^L FM |
| | IIS5 2o | 688 | GNSVGALGNL | TLVLAIIVFI | FAVVGMQ ^L FG |
| | IIIS5 3o | 1147 | LGAIPSIMNV | LLVCLIFWLI | FSIMGVN ^L FA |
| | IVS5 4o | 1469 | MMSLPALFNI | GLLLFLVMFI | YSIFGMS ^N FA |
| | | | 33 | 41 | 51^c |
| K _v 1.2 | P p | 358 | FPSIPDAF | WWAVVSM T TV | YGDM VP T |
| Ca _v 1.2 | IP 1p | 376 | FDNFAFAM | LT V FQ CIT ME | G W T D V L Y W |
| | IIP 2p | 719 | FDNFPQSL | LT V FQ I L T GE | D W N S V M Y D |
| | IIIP 3p | 1128 | FDNVLAAM | MAL F T V S T FE | G W P E L L Y R |
| | IVP 4p | 1429 | FQ T F P Q AV | L L L F R C A T GE | A W Q D I M L A |
| Na _v 1.4 | IP 1p | 383 | YDTFSWAF | LAL F R L M T Q D | Y W E N L F Q L |
| | IIP 2p | 738 | MNDFFHSF | LIV F R I L C GE | W I E T M W D C |
| | IIIP 3p | 1220 | YDNVGLGY | L S L L Q V A T FK | G W M D I M Y A |
| | IVP 4p | 1512 | FETFGNSI | I C L F E I T T S A | G W D G L L N P |
| | | | 1 | 11 | 21^c |
| K _v 1.2 | S6 i | 385 | IGGKIVGSLC | A I A G V L T I A L | P V P V I V S N F N |
| Ca _v 1.2 | IS6 1i | 409 | ELPWVYFVSL | VIFGSFFV L N | LVLGVLS G E F |
| | IIS6 2i | 757 | MLVCIYFIIL | FISPNYILL N | LFLAIAV D N L |
| | IIIS6 3i | 1170 | VEISIFFII Y | I III I A F F M M N | I F V G F V I V T F |
| | IVS6 4i | 1480 | SFAVFYFISF | Y M L C A F L I I N | L F V A V I M D N F |
| Na _v 1.4 | IS6 1i | 415 | KTYMIFVVI | I F L G S F Y L I N | L I L A V V A M A Y |
| | IIS6 2i | 770 | AMCLTVFLMV | MVIGNL V V L N | L F L A L L L S S F |
| | IIIS6 3i | 1262 | LYMYLFVIF | I I F G S F F T L N | L F I G V I I D N F |
| | IVS6 4i | 1565 | SIGICFFCSY | I I I S F L I V V N | M Y I A I I L E N F |

^a The outer and inner helices were aligned according to Huber et al. (2000) and Zhorov et al. (2001), respectively. Selectivity filter residues are highlighted yellow. The prokaryotic gating hinge (Gly) is highlighted green. The Asn residues conserved in all four repeats of Na⁺ and Ca²⁺ channels are highlighted grey. Bold-typed are residues affecting the binding of correolide in K_v1 channels (Hanner et al., 2001), DHPs in Ca_v1 channels (Bodi et al., 1997; Peterson et al., 1997), and LAs in Na⁺ channels (Wang et al., 2001; Yarov-Yarovoy et al., 2001).

^b The standard segment name includes the repeat number (I-IV) and symbols S5, S6, or P. An alternative segment name is used for labelling residues, which includes the repeat number (1-4) and symbols o, i, and p for the outer helices, inner helices, and P-loops, respectively. Absolute numbers (#) of the first residue in each segment.

^c Relative numbers of residues (see text).

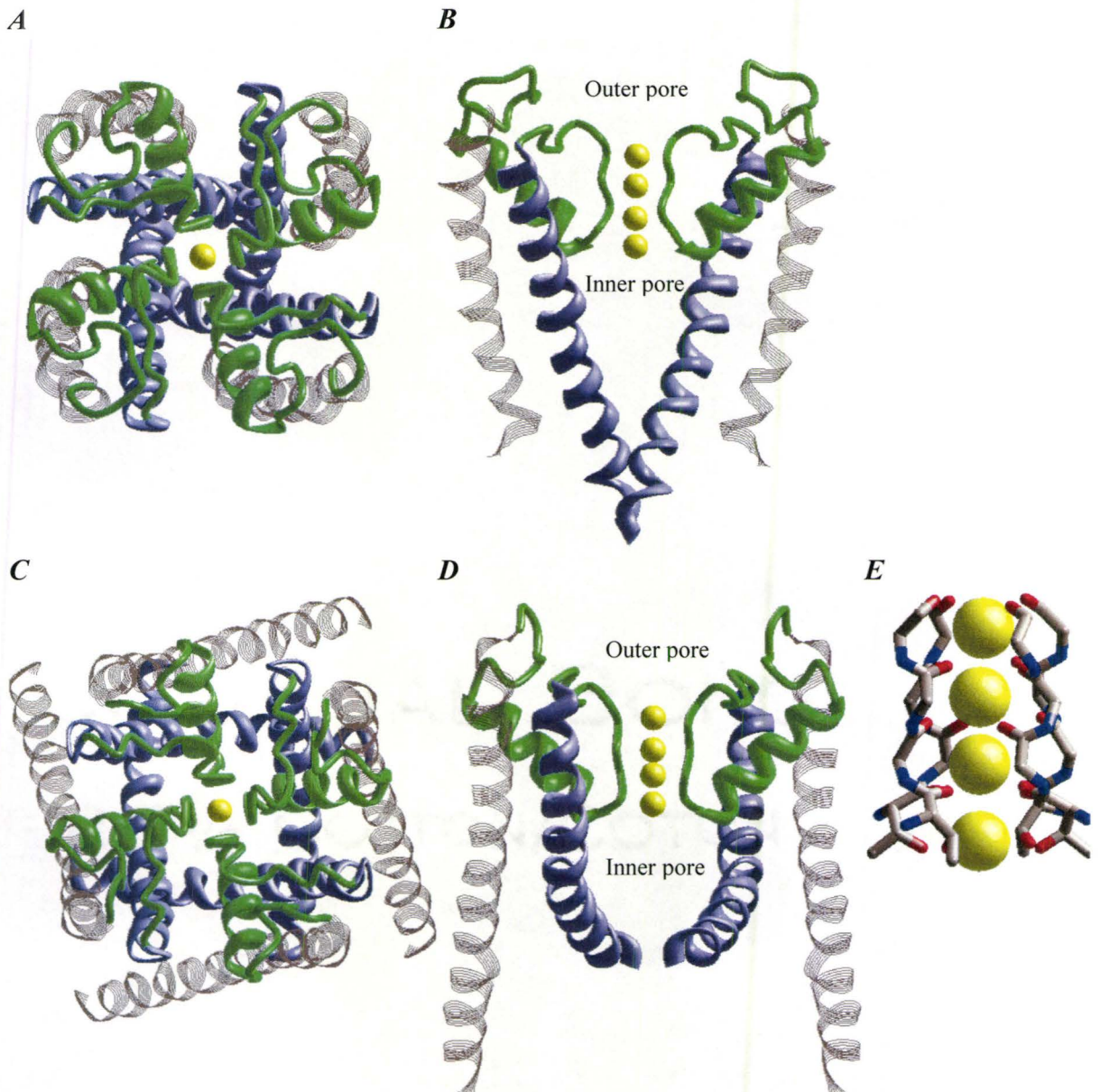


Figure 1.2. The pore-forming domains of prokaryotic K⁺ channel X-ray structures. *A* and *B*, The cytoplasmic and side views of the closed-state KcsA X-ray structure. *C* and *D*, The cytoplasmic and side views of the open-state KvAP X-ray structure. The following colouring scheme is used: outer helices (S5) - grey strands; inner helices (S6) - violet ribbons; pore helices (P) - green ribbons; the selectivity-filter region and extracellular segments - green strings; K⁺ ions - yellow spheres. For clarity, only the opposing domains are shown in the side views. *E*, A closer view of the K⁺ channel selectivity filter. The selectivity filter is formed by four backbone carbonyls and one side chain oxygen per domain.

form a homotetramic channel. Currently the X-ray structures of Na⁺ and Ca²⁺ channels are unavailable.

MOLECULAR MODELLING OF ION CHANNELS

Electrophysiological and crystallographic studies have provided valuable information about the structure-function relationship of ion channels. However, currently there are only a few published X-ray structures of ligand-channel complexes and no X-ray structures of Na⁺ and Ca²⁺ channels. Atomic-resolution structures of ion channels and their complexes with ligands are necessary to understand the mechanisms of the action of ligands, an important step towards developing new potent and selective drugs. In the absence of experimental data on three-dimensional structures of ion channels, molecular modelling is a valuable tool to predict the atomic-level structures of ion channels with drugs.

Molecular modelling has been used for many years to predict low energy conformations of small molecules and peptides. Early modelling was limited to small systems. The advances in molecular modelling algorithms and computer technology enabled the simulation of larger systems, including ion channels.

Only a few three-dimensional structures of the pore-forming domain of ion channels have been solved. Using an approach called homology modelling, we can build an atomic-resolution model of a target ion channel using the X-ray structure of a related homologous ion channel as a template. The energy of the homology model is calculated using a force field, in particular we use AMBER, which includes energy functions for both bonded and non-bonded interactions (Weiner et al., 1984; Weiner et al., 1986). We and several other groups use Monte Carlo (MC) energy minimization to find energetically optimal conformations of a model (Li and Scheraga, 1987), an effective methodology for ligand docking. Many other groups use molecular dynamics simulations. To maintain the folding of the template protein, during MC-minimization the backbone C^α atoms of the model are allowed to move up to 1 Å from their corresponding positions in the template and for further deviations an energy penalty is applied. Dehydration energy is calculated using an implicit solvent method (Lazaridis and Karplus, 1999a), a valuable alternative to using explicit water molecules. Without imposing any bias, the optimal positions and orientations of ligands are searched from thousands of random starting points. The area of the random search usually covers the entire pore-forming domain. The energetically most favourable conformations are collected and further MC-minimized with both the ligand and protein flexible. The above methodology is integrated in the ZMM program (<http://www.zmmsoft.com>), which I have used for all my molecular simulations. Other molecular modelling programs, ICM (<http://www.molsoft.com>) and Rosetta (<http://www.rosettacommons.org>), use a similar approach.

The most common source of error in homology modelling is an incorrect sequence alignment between the target and the template. The inner helices of K^+ channels align at a conserved Gly residue, which was proposed to be the gating hinge for prokaryotic K^+ channels (Jiang et al., 2002a). The inner helices of Na^+ and Ca^{2+} channels align at an Asn residue, which is conserved among all four repeats (Table 1.1). Sequence analysis suggests that Na^+ and Ca^{2+} channels have evolved from K^+ channels by the processes of successive gene duplication, mutation, and selection from common ancestral channels (Anderson and Greenberg, 2001). However, the alignment between K^+ , Na^+ , and Ca^{2+} channels is not obvious. Automatic alignment algorithms do not work; instead a knowledge-based approach is used, in which sequences of K^+ , Na^+ , and Ca^{2+} channels are manually aligned taking into consideration various experimental data. Several different alignments have been proposed for the inner helices. We use the alignment, which was previously proposed for inner (Zhorov et al., 2001) and outer (Huber et al., 2000) helices (Table 1.1). Using this alignment, homology models of Na^+ and Ca^{2+} channels were built from the X-ray structures of K^+ channels. The models explained the drug action of benzothiazepines (Tikhonov and Zhorov, 2008), batrachotoxin (Wang et al., 2006), local anaesthetics (Tikhonov et al., 2006), and tetrodotoxin and saxotoxin (Tikhonov and Zhorov, 2005a). In comparison to the inner helix alignment in Table 1.1 (Zhorov et al., 2001), other research groups propose a shifted alignment position (Huber et al., 2000; Lipkind and Fozzard, 2000; Lipkind and Fozzard, 2003) or suggest an insertion in Ca^{2+} channels (Stary et al., 2008). Assuming that all ligand-sensitive residues should face the pore, Lipkind and Fozzard aligned Na^+ and Ca^{2+} channels with the conserved Asn residues of different domains not appearing in matching positions (Lipkind and Fozzard, 2000; Lipkind and Fozzard, 2001; Lipkind and Fozzard, 2003). Currently, the alignment between K^+ , Na^+ , and Ca^{2+} channels is still disputed.

STRUCTURE, FUNCTION, AND PHARMACOLOGY OF VOLTAGE-GATED CHANNELS

In the following sections I review the structure, function, and pharmacology of voltage-gated K^+ , Ca^{2+} , and Na^+ channels and how molecular modelling has advanced our knowledge of ion channels and the action of ligands. A universal residue-labelling scheme is used (Zhorov and Tikhonov, 2004), since a variety of ion channels are discussed in this thesis, each having different residue numbering. A residue label includes the domain (repeat) number (1-4), segment type (*o*, the outer helix, *p*, P-loop; *i*, the inner helix), and relative number of the residue in the segment (see Table 1.1). For the transmembrane segments, the relative numbers are counted from the beginnings of the respective KcsA helices as seen in the X-ray structure (Doyle et al., 1998). Relative numbers of residues in P-loop are counted from the EEEE- and DEKA-locus, whose residues are assigned number 50 to avoid negative numbers for residues in P-helices.

Voltage-gated K⁺ channels

Potassium channels are considered the largest and the most ancient group of ion channels, which allow the selective passage of K⁺ ions across the cell membrane. K⁺ channels regulate neuronal and cardiac electrical patterns, release of neurotransmitters, muscle contraction, and hormone secretion. K⁺ channels can be gated by voltage, the binding of intracellular ligand, or by both types of stimulus. The α subunit of K⁺ channels is associated with a variety of accessory proteins, including β subunits, calmodulin, and MinK (Gutman et al., 2005). Voltage-gated and Ca²⁺-activated channels contain six transmembrane segments, while inward rectifiers, K_{ATP} channels, and the G protein-coupled channels possess two transmembrane segments (Doupnik et al., 1995). Voltage-gated K⁺ channels (K_v) are the most diverse consisting of twelve families, K_v1 – K_v12 (Gutman et al., 2005). The best studied are voltage-gated K⁺ channels derived from the *Drosophila* gene, K_v1, K_v2, K_v3, and K_v4, also referred to as *Shaker*, *Shab*, *Shaw*, and *Shal*, respectively.

Crystallographic studies of prokaryotic K⁺ channels have significantly advanced our understanding of ion channels; however, upon starting my graduate studies, there were no X-ray structures of eukaryotic channels. Structural similarity between prokaryotic and eukaryotic voltage-gated K⁺ channels was questioned by controversial interpretations of experiments. On one hand, substituting the prokaryotic pore into the eukaryotic *Shaker* K⁺ channel suggests the conservation of the pore domain between the channels (MacKinnon et al., 1998; Lu et al., 2001). On the other hand, experiments on Cd²⁺ action to the *Shaker* channel with engineered cysteines (Holmgren et al., 1998; del Camino et al., 2000) imply structural differences between prokaryotic and eukaryotic K⁺ channels. Webster et al. (2004) introduced Cys at or near the Pro-Val-Pro (PVP) motif on the S6 helices. They demonstrated that Cys mutant channel gets locked in the open state by a Cd²⁺ bridge between the engineered Cys and a native His residue. A double Cys mutant was able to lock open and then blocked by Cd²⁺ ions. They proposed that eukaryotic K⁺ channels have a different gating mechanism than prokaryotic channels, suggesting that the PVP motif of the eukaryotic *Shaker* K⁺ channel is a gating swivel that causes a kink at the inner helix (Webster et al., 2004). The authors proposed that the open pore size of the eukaryotic potassium *Shaker* channels is narrower (approximately 8 Å wide) compared to the prokaryotic X-ray structures, which are 10-12 Å wide. Webster et al. (2004) suggested that the structure of eukaryotic K⁺ channels is significantly different from the X-ray structures of prokaryotic K⁺ channels. This suggests that the available X-ray structures of prokaryotic K⁺ channels could not be used as a template to molecular model eukaryotic K⁺, Na⁺, nor Ca²⁺ channels.

The above controversy is addressed in Chapter 2, where we modelled the wild type *Shaker* channel and its mutants with Cd²⁺ ions (Bruhova and Zhorov, 2005). Our study showed that the open *Shaker* channel should be as wide as in the X-ray structure of KvAP to accommodate correolide, a large open *Shaker* channel blocker (Felix et al., 1999). Simulating Cd²⁺ experiments of Webster et al. (2004), we found that the Cd²⁺

bridge between the engineered Cys and native His residues can be formed in the KvAP-based model of the *Shaker* channel. The locked-open KvAP-based model was easily blocked by two Cd²⁺ ions coordinated by two pairs of Cys residues, which caused the system to be electrically balanced and did not involve large conformational changes. This study infers the suitability of the KvAP structure for modelling eukaryotic K⁺ channels. Upon publishing our KvAP-based locked-open model of the *Shaker* channel, months later the first eukaryotic K⁺ channel X-ray structure was released of the open voltage-gated Kv1.2 *Shaker* channel (Long et al., 2005a; Long et al., 2005b). This structure confirmed our predictions and finally resolved the dispute to show that prokaryotic and eukaryotic K⁺ channels are indeed structurally similar.

A variety of K_v channel inhibitors have been characterized (Kaczorowski and Garcia, 1999). Peptides from the venom of scorpions, spiders, snakes, and sea snails inhibit K_v channels. These neurotoxic peptides have been used as probes to understand the structure and function of K_v channels. The outer pore was probed using charybdotoxin, a 37 amino acid peptide blocker isolated from scorpion venom, which blocks K_v1 channels with nanomolar affinity (MacKinnon et al., 1990). Tetraethylammonium and 4-aminopyridine are small-molecule inhibitors of K_v channels, however, they lack subtype selectivity, and thus are less effective for pharmacological studies. In order to develop effective drugs, selective low-molecular-weight inhibitors are necessary. Thus, several K_v channels, particularly ones that are pharmacologically important drug targets, have been screened for small-molecule blockers. Correolide was the first natural product found to selectively inhibit K_v1.3 channels, a target for the development of novel immunosuppressants (Goetz et al., 1998; Felix et al., 1999; Chandy et al., 2001). Mutational studies were performed with [³H]dihydrocorreolide to locate its binding site (Hanner et al., 1999; Hanner et al., 2001), nevertheless, structural aspects of correolide binding to K_v1.3 channels remain unclear. Another drug found through drug screening was chromanol 293B, which could potentially treat cardiac arrhythmia by selectively inhibiting cardiac K_v7.1 (also known as KCNQ1) channels (Gerlach et al., 2001). Dr. Seeböhm's group identified two inner helix residues to be involved in chromanol binding and when mutated dramatically lowered the potency of chromanol block (Lerche et al., 2007). Both correolide and chromanol possess several nucleophilic groups, but the inner pore of the K_v channel is predominantly lined with hydrophobic residues, which raises questions regarding the nature of ligand-channel interactions.

Binding of correolide and chromanol 293B to eukaryotic K_v channels was simulated in Chapter 3. Thousands of orientations of correolide and chromanol were randomly sampled in the closed and open models of K_v1.3 and K_v7.1, respectively. Both, correolide and chromanol bind favourably inside the open channel but experience steric clashes or ligand strain in the closed channel. In the most energetically favourable orientation of correolide and chromanol, two of their oxygen atoms coordinate the K⁺ ion in the selectivity filter. The electrostatic interaction between the ligand and the K⁺ ion contributes to the stronger binding energy. Residues identified from mutational analysis to effect correolide (Hanner et al., 2001) and chromanol (Lerche et al., 2007) binding,

where explained in our models to either directly contact the ligand or affect the pore geometry. Our study suggests that a K^+ ion at the selectivity filter is a critical determinant for correolide and chromanol binding and possibly other nucleophilic blockers.

Voltage-gated Ca^{2+} channels

Voltage-gated Ca^{2+} channels are activated by membrane depolarization and mediate the selective entry of Ca^{2+} ions into excitable cells. Ca^{2+} channels are formed of complexes consisting of the pore-forming domain α_1 subunit, transmembrane $\alpha_2\delta$ subunit, intracellular β subunit, and transmembrane γ subunit (Catterall, 2000b). Ca^{2+} channels are categorized as L-type, P/Q-type, N-type, R-type, and T-type, reviewed in (Catterall et al., 2005). Of all the channel types, one of the most intensely studied are L-type Ca^{2+} channels ($Ca_v1.1$ - $Ca_v1.4$), which are expressed broadly in neurons, muscles (skeletal and cardiac), and glands. These channels mediate contraction in smooth and cardiac muscles, hormone secretion, and transcriptional events supporting learning and memory. L-type Ca^{2+} channels are selectively sensitive to 1,4-dihydropyridines (DHPs), phenylalkylamines (PAAs), and benzothiazepines (BTZs), reviewed in (Striessnig et al., 1998). Members of these classes of drugs, particularly, verapamil, diltiazem, and nifedipine, are clinically used to treat hypertension and cardiac arrhythmia. P/Q-type, N-type, and R-type Ca^{2+} channels ($Ca_v2.1$ - $Ca_v2.3$) are expressed in neurons, where they initiate neurotransmission at synapses and mediate calcium entry. They are insensitive to L-type Ca^{2+} channel blockers, but are specifically blocked with high affinity by peptide toxins from spiders and marine snails, such as ω -agatoxin and ω -conotoxin, reviewed in (Doering and Zamponi, 2003). T-type Ca^{2+} channels ($Ca_v3.1$ - $Ca_v3.3$) are insensitive to both blockers of the Ca_v1 and Ca_v2 subfamily. They are located in a variety of cell types, such as the neurons, heart and muscle, where they are involved in shaping the action potential and controlling repetitive firing.

Mutational studies of the Ca_v1 channels revealed residues in helices IIS5, IIS6, and IVS6 are involved in the binding of all three classes of drugs (Hockerman et al., 1997). DHPs, PAAs, and BTZs are believed to bind at three separate receptor sites, however located in close proximity to each other by binding to different faces of the inner helices in domains III and IV. PAAs and BTZs are protonated at physiological pH and are believed to block LCC by occluding the inner pore. However, DHPs are generally neutral at physiological pH and interestingly can act as antagonist and agonist depending on its chemical substituents and geometry (Hockerman et al., 1997). Experiments with quaternary derivatives show that PAAs block the channel from the intracellular side, whereas DHPs and BTZs block from the extracellular side (Kass et al., 1991; Hering et al., 1993; Seydl et al., 1993; Kwan et al., 1995). Homology models of Ca^{2+} channels have been built to explain the action of DHPs (Huber et al., 2000; Zhorov et al., 2001; Lipkind and Fozzard, 2003; Tikhonov and Zhorov, 2009), PAAs (Lipkind and Fozzard, 2003), and BTZs (Tikhonov and Zhorov, 2008), however ambiguous alignments between Ca^{2+} and K^+ channels shed doubts on these models.

The substituted-cysteine accessibility method (SCAM) is a valuable technique to identify pore-lining residues in ion channels, which could potentially aid in resolving the disputed alignment between K^+ and Ca^{2+} channels. Zhen et al. (2005) used SCAM to identify pore-lining residues in $Ca_v2.1$; however, paradoxically, the SCAM data of $Ca_v2.1$ did not agree with the pore-lining residues of K^+ channels. Methanethiosulfonate reagents (e.g. MTSET) did not block $Ca_v2.1$ with cysteine substitutions at positions critical for PAA and local anaesthetic binding, which were presumed to be pore-lining residues. The $Ca_v2.1$ inner pore is asymmetric, because identical positions from different repeats experience various degrees of MTSET modification. Unexpectedly, MTSET blocked $Ca_v2.1$ with cysteine substitutions at seemingly distant outer helix positions (Zhen et al., 2005). Zhen et al. (2005) concluded that their results are inconsistent with published sequence alignments between Ca^{2+} and K^+ channels. This conclusion casts doubts on homology models of Ca^{2+} channels.

In Chapter 4, we modelled MTSET-substituted cysteine mutants of $Ca_v2.1$ based on $K_v1.2$ using the alignment proposed by Huber et al. (2000) and Zhorov et al. (2001) for outer and inner helices, respectively. We demonstrated that certain pore-facing residues of $Ca_v2.1$ are surrounded by large hydrophobic residues, which would prevent cysteine ionization and hence reaction with MTSET. Using Monte-Carlo minimization, we searched for energetically favourable orientations of MTSET-modified cysteines, which can be considered as long flexible tethered ligands that can adopt a variety of orientations in the channel. MTSET-modified cysteines at pore-facing positions can occlude the inner pore or protrude into the domain interface. Depending on the surrounding residues, MTSET-modified cysteines can adopt distinct binding modes even when located at the same relative position in the inner helix of different repeats. MTSET-modified cysteines at outer helix positions can extend its ammonium group toward the periphery of the inner pore. Our calculations rationalize the SCAM data of $Ca_v2.1$ obtained in a meticulous experimental study by Zhen et al. (2005), validate the reported alignment between Ca^{2+} and K^+ channels, and suggest similar dispositions of transmembrane helices in these channel types.

Voltage-gated Na^+ channels

Na^+ channels play an essential role in initiating and propagating action potentials in excitable cells. Unlike voltage-gated K^+ and Ca^{2+} channels, the family of Na^+ channels is less diverse, likely appearing relatively recently in evolution, and share similar functional properties (Catterall, 2000a). The α subunit of Na^+ channels is associated with auxiliary β subunits which have been found to be involved in channel localization (Catterall et al., 2005). Nine isoforms of mammalian Na^+ channels ($Na_v1.1$ - $Na_v1.9$) have been identified, which have a sequence identity greater than 60% (Catterall et al., 2005). The most closely related group with sequence similarity over 80% are $Na_v1.1$, $Na_v1.2$, $Na_v1.3$, and $Na_v1.7$, which are primarily expressed in neurons. These four channels along

with the skeletal muscle $\text{Na}_v1.4$ and central nervous system $\text{Na}_v1.6$ isoforms are highly sensitive to tetrodotoxin (TTX, affinities ranging $\sim 1\text{-}12\text{nM}$). A single amino acid change from a Phe or Tyr side chain to Cys in domain I cause $\text{Na}_v1.5$, $\text{Na}_v1.8$, and $\text{Na}_v1.9$ channels to be resistant to TTX (affinities ranging $\sim 1\text{-}40\text{mM}$) (Backx et al., 1992; Satin et al., 1992). The latter channels are highly expressed in the heart and dorsal root ganglion neurons. $\text{Na}_v1.1\text{-}\text{Na}_v1.3$ are potential targets for anti-epileptic drugs, while $\text{Na}_v1.6\text{-}\text{Na}_v1.9$ are targets for analgesic drugs (Catterall et al., 2005). Point mutations in $\text{Na}_v1.4$ cause hyperkalemic periodic paralysis and paramyotonia congenita (Cannon, 1997). In $\text{Na}_v1.5$, point mutations and deletions cause long QT syndrome and idiopathic ventricular fibrillation (Keating and Sanguinetti, 2001).

Before X-ray structures of K^+ channels were available, two groups (Guy and Seetharamulu, 1986; Oiki et al., 1990) modelled the Na^+ channel and correctly predicted the transmembrane folding pattern. The model predicted six transmembrane α -helices and a re-entrant loop between segments S5 and S6 that dipped into the transmembrane region of the protein. After the first K^+ channel X-ray structure was released, Lipkind and Fozzard (2000) modelled the closed-state Na^+ channel with the S5 and S6 helices arranged exactly as in the KcsA X-ray structure. The selectivity filter DEKA locus of the Na^+ channel was modelled with side-chains facing the pore, unlike the main-chain carbonyls that face the pore in K^+ channels.

Tetrodotoxin and saxitoxin are highly potent Na^+ channels blockers, which are known to plug the outer pore by forming multiple contacts with the Na^+ channel selectivity-filter region (Kirsch et al., 1994; Penzotti et al., 2001; Choudhary et al., 2003). Tikhonov and Zhorov (2005a) modelled the P-loop domain of $\text{Na}_v1.4$ having the pore helices arranged as in the MthK K^+ channel X-ray structure. The conformation of the selectivity-filter region was shaped around TTX and saxitoxin using experimentally known data contacts between the toxins and Na^+ channel outer pore (Tikhonov and Zhorov, 2005a). The docking of another class of peptide Na^+ channels blockers, such as μ -conotoxin (μ -CTX) (Olivera et al., 1987), into this Na^+ channel model, was consistent with experimentally known data (Stephan et al., 1994; Li et al., 1997).

Another group of neurotoxins cause the activation of Na^+ channels. The group includes batrachotoxin, veratridine, aconitine, and grayanotoxin, which have been isolated from frog or plant species. Ligand-binding residues are found in the pore-lining inner helices of all four repeats suggesting that the activators could bind inside the pore (Wang et al., 2001). Paradoxically, these activators share similar structure, size, and receptor site as Na^+ channel blockers. The comparison of their three-dimensional structures reveals that activators have polar groups lined on one side of the molecule and hydrophobic groups on the opposite side, whereas in blockers the hydrophilic groups are sparse (Tikhonov and Zhorov, 2005b). Activators can fit in the inner pore of the Na^+ channel model and interact with all four inner helices as in agreement with mutational experiments. Activators bind near the channel gate stabilizing the open state, thus explaining the easier and longer opening of activator-modified channels. Ions are able to

permeate through a narrow hydrophilic pathway shaped by the polar groups of the activator inside the channel (Tikhonov and Zhorov, 2005b).

Local anaesthetics (LAs) block Na^+ channels and are clinically used to reduce pain. The receptor for both toxin activators and LA blockers is in the inner pore (Ragsdale et al., 1994; Wright et al., 1998). LAs can bind to the closed, open and inactivated states of the channel, but generally have a stronger potency to open or inactivated channels compared to closed channels (Hille, 1977; Ragsdale et al., 1994; Wright et al., 1997). Inner helix residues in repeat IV were found to be critical for the use-dependent block by LAs (Ragsdale et al., 1994; O'Leary and Chahine, 2002). Interestingly, the mutation of residues critical for use-dependent block by LAs had different effects on the closed channel block (Wright et al., 1998; Li et al., 1999). Thus, the mechanisms of LA action on the closed and open channels are still unresolved.

Quaternary analogs of LAs, such as QX-222 and QX-314, cannot cross the membrane and therefore are used as probes for exploring the access pathways into the channels. When applied intracellularly, the quaternary LAs can only block the open Na^+ channels (Hille, 1977). In the open channel, LAs can reach their binding site through the open intracellular gate along the ion conduction pathway. In the closed state, the straight inner helices converge at the cytoplasmic side and obstruct ion permeation (Doyle et al., 1998). Interestingly, closed cardiac $\text{Na}_v1.5$ channels, but not $\text{Na}_v1.2$ and $\text{Na}_v1.4$, are sensitive to externally applied quaternary LAs (Alpert et al., 1989; Qu et al., 1995) suggesting an extracellular access pathway for LAs. TTX-binding studies and mutations at the selectivity filter suggest that extracellular LAs can reach their binding site through the outer pore (Qu et al., 1995; Sunami et al., 2000; Sasaki et al., 2004). On the other hand, μ -CTX-binding studies and inner helices mutations in domain IV suggest the involvement of the inner helices in the extracellular pathway of LAs (Wang et al., 1998; Sunami et al., 2001).

In Chapter 5, I docked three structurally different LAs into the closed $\text{Na}_v1.5$ model and explored various hypothetical extracellular access pathways for LAs into the closed channel (Bruhova et al., 2008). Our study predicts that the LA molecules can favourably adopt two binding modes in the closed state: a vertical and horizontal binding mode. The horizontal binding mode is consistent with the closed channel block, whereas the vertical mode is consistent with open channel block. The energetically most favourable pathway for the LA molecule to and from the closed channel is the interface between domains III and IV, whereas the selectivity filter and the closed activation gate impose large energy barriers for LAs. Finally, we propose that the occupancy of the pore with a Na^+ ion affects both access and binding of LAs.

OVERVIEW

During my graduate studies, the focus of my research was the geometry of the pore-forming domain of voltage-gated ion channels and their complexes with metal ions and small molecules. I used experimental data as constraints in my models to resolve the controversy regarding the dimensions of the open pore in eukaryotic and prokaryotic K^+ channels (Chapter 2). The prediction that the pore dimensions are similar between these channels allowed us to model eukaryotic K^+ channels based on the X-ray structures of prokaryotic K^+ channels. We predicted that metal ions in the selectivity filter are important determinants for the binding of nucleophilic K^+ channel blockers, such as correolide and chromanol (Chapter 3). The next problem was to model Ca^{2+} and Na^+ channels using the X-ray structures of their distant K^+ channel relatives. Our model of $Ca_v2.1$ based on the X-ray structure of $K_v1.2$ explained SCAM observations, thus validating a previously proposed alignment between K^+ , Na^+ , and Ca^{2+} channels (Chapter 4). This is an important justification that homology models of Na^+ and Ca^{2+} channels can be based on the X-ray structures of K^+ channels. We predicted a binding site and access route of local anaesthetics in the closed cardiac Na^+ channel. This model helped clarify a large body of experimental data. We proposed that Na^+ deficiency in the outer pore of the slow-inactivated Na^+ channels stabilizes the binding and facilitates access of local anaesthetics (Chapter 5). I hope my studies have contributed to the expanding literature on the structure of eukaryotic voltage-gated ion channels and their complexes with drugs.

CHAPTER TWO

PREDICTING THE OPEN-STATE GEOMETRY OF EUKARYOTIC K⁺ CHANNELS

CHAPTER TWO PREFACE

The work presented in this chapter was previously published in:

Bruhova I and Zhorov BS (2005) KvAP-based model of the pore region of *Shaker* potassium channel is consistent with cadmium- and ligand-binding experiments. *Biophysical Journal* **89**:1020-9.

Permission has been granted from the publisher to reproduce the material here.

I conducted all of the experiments described in this chapter.

ABSTRACT

Potassium channels play fundamental roles in excitable cells. X-ray structures of bacterial potassium channels show that the pore-lining inner helices obstruct the cytoplasmic entrance to the closed channel KcsA, but diverge in widely open channels MthK and KvAP, suggesting a gating-hinge role for a conserved Gly in the inner helix. A different location of the gating hinge and a narrower open pore were proposed for voltage-gated *Shaker* potassium channels that have the Proⁱ²¹-Val-Pro (PVP) motif. Two major observations back the proposal: cadmium ions lock mutant Vⁱ²⁴C in the open state by bridging Cⁱ²⁴ and Hⁱ³⁴ in adjacent helices, and cadmium blocks the locked-open double mutant Vⁱ²²C/Vⁱ²⁴C by binding to Cⁱ²² residues. Here we used molecular modeling to show that the open *Shaker* should be as wide as KvAP to accommodate an open-channel blocker, correolide. We further built KvAP-, MthK-, and KcsA-based models of the *Shaker* mutants and Monte Carlo-minimized them with constraints Cⁱ²⁴---Cd²⁺---Hⁱ³⁴. The latter were consistent with the KvAP-based model causing a small bend N-terminal to the PVP motif. The constraints significantly distorted the MthK-based structure, making it similar to KvAP. The KcsA structure resisted the constraints. Two Cd²⁺ ions easily block the locked-open KvAP-based model at Cⁱ²² residues, while constraining a single cadmium ion to four Cⁱ²² caused large conformational changes and electrostatic imbalance. While mutual disposition of the voltage-sensor and pore domains in the KvAP X-ray structure is currently disputed, our results suggest that the pore-region domain retains a native-like conformation in the crystal.

INTRODUCTION

Voltage-gated K⁺ channels (K_v channels) are involved in the electrical impulse generation in nerve, muscle, endocrine, and other excitable cells. The landmark crystallographic structures of bacterial K⁺ channels show that the pore-lining inner helices obstruct the cytoplasmic entrance to the closed channel KcsA (Doyle et al., 1998), but diverge in widely open channels MthK (Jiang et al., 2002b) and KvAP (Jiang et al., 2003a), suggesting a gating-hinge role for conserved glycine in the inner helix (Jiang et al., 2002a). The X-ray structures of bacterial channels helped to explain a large body of experimental data on eukaryotic channels and have been used as templates to build homology models of pharmacologically important voltage-gated potassium (Laine et al., 2003; Luzhkov et al., 2003; Durell et al., 2004), sodium (Lipkind and Fozzard, 2000; Tikhonov and Zhorov, 2005b), and calcium (Lipkind and Fozzard, 2001; Zhorov et al., 2001) channels, as well as channels gated by glutamate (Tikhonov et al., 2002) and cyclic nucleotides (Flynn and Zagotta, 2003). However, the reliability of the homology models is questioned by controversial interpretations of experiments addressing structural similarity between prokaryotic and eukaryotic K⁺ channels.

In the absence of high-resolution structures of eukaryotic channels, information on their geometry is deduced from experiments such as chemical cross-linking, metal

binding, ligand binding, and cysteine scanning. These experiments do not provide direct data on the channel geometry, but determine distance constraints between individual atoms and residues. The emerging picture of the pore architecture of K_v channels generally agrees with the structure of bacterial K^+ channels. However, K_v channels have important structural peculiarities within the pore domain. The inner helices of K_v channels include a highly conserved Pro-X-Pro motif between the conserved glycine, which is N-terminal to the motif, and C-terminal residues whose crossover forms the activation gate in bacterial channels. In *Shaker* channels, the Pro-X-Pro motif includes residues P^{i21} , V^{i22} , and P^{i23} referred to as the PVP motif. Lu et al. (2001) substituted the pore of a prokaryotic channel into an eukaryotic voltage-gated channel and showed that the resulting chimera retained the hallmark functional properties of eukaryotic channels, indicating that the ion conduction pore is conserved among K^+ channels.

A different conclusion regarding the similarity between prokaryotic and eukaryotic K^+ channels has been proposed by Yellen and coworkers. In particular, del Camino et al. (2000) demonstrated that intracellularly applied blockers prevent chemical modification of engineered cysteines in the inner helices C-terminal to the PVP motif, but not at the positions N-terminal to it. To explain this fact, the authors hypothesized that, unlike prokaryotic channels, the *Shaker* channels have a sharp bend at the PVP motif. This hypothesis is supported by the similar studies of Cd^{2+} action on *Shaker* mutants (Holmgren et al., 1998; Webster et al., 2004), which provided valuable distance constraints between certain residues in the inner helices of the open *Shaker* channel. The authors found that (i) Cd^{2+} ions lock mutant $V^{i24}C$ in the open state by bridging C^{i24} and H^{i34} in adjacent helices and (ii) Cd^{2+} blocks the locked-open double mutant $V^{i22}C/V^{i24}C$ by coordinating C^{i22} residues. Current structural interpretation of these constraints is visualized in a conceptual model, in which the N-terminal halves of the inner helices are disposed as in KcsA, whereas the C-terminal halves kink significantly at the PVP motif to form a rather narrow open pore (Swartz, 2004; Webster et al., 2004).

The consistency of the constraints by Webster et al. (2004) with the available X-ray structures has not yet been tested in a molecular modeling study. Such study is necessary, in particular, because the current interpretation of the Cd^{2+} -binding experiments involves certain ambiguity. On one hand, the fact that Cd^{2+} blocks the double mutant $V^{i22}C/V^{i24}C$ suggests that the pore lumen should be as small as the diameter of Cd^{2+} ion. On the other hand, the open pore should be wide enough to accommodate flexible quaternary ammonium blockers and permeate hydrated K^+ ions. To compromise these observations, Webster et al. (2004) proposed that the width of the open pore may vary from ~ 3 to $\sim 8-9$ Å.

The upper estimate of the pore dimension proposed by Webster et al. (2004) is deduced from the size of flexible ligands that block the channel. The interpretation of data on flexible drugs binding in terms of the pore dimensions requires analysis of conformation-activity relationships (Zhorov et al., 1991). More rigid open-channel blockers may provide direct estimates of the minimal width of the cytoplasmic pore

entrance. One such blocker is correolide, a nortriterpene alkaloid isolated from the Costa Rican tree *Spachea correa* (Felix et al., 1999). Correolide prevents T-cell activation and attenuates immune responses by selectively blocking open (or C-type-inactivated) $K_v1.3$ channels in T-cells (Koo et al., 1999). Besides $K_v1.3$, the drug blocks other members of the *Shaker* subfamily (Hanner et al., 1999). Correolide interacts with several residues in the inner helix, suggesting that the binding site is located inside the pore (Hanner et al., 2001). Correolide has a semirigid hexacyclic core, which makes the drug an ideal candidate to probe the dimensions of the open *Shaker* channel.

In this work we use molecular modeling to explore whether available experimental data on the dimensions of the *Shaker* open pore are consistent with available crystallographic structures of bacterial K^+ channels. We first calculate the cross-sectional dimensions of correolide and demonstrate that it matches the width of KvAP at the level of the cytoplasmic entrance to the open pore. We further build KcsA-, MthK-, and KvAP-based models of the *Shaker* mutant $V^{i24}C$ and apply distance constraints $C^{i24} \cdots Cd^{2+} \cdots H^{i34}$ to impose the locked-open conformations. The KvAP-based model readily accommodates the constraints, whereas KcsA- and MthK-based models seem inconsistent with the Cd^{2+} -binding data. Finally, we create the KvAP-based model of the double mutant $V^{i22}C/V^{i24}C$ in the locked-open conformation and simulate Cd^{2+} block at the level of engineered C^{i22} . The model readily accommodates two but not one Cd^{2+} ion at this site. Our study shows that experimental constraints of Webster et al. (2004) are consistent with the X-ray structure of KvAP. These data imply that the geometry of the pore region of the open *Shaker* is similar to that of KvAP.

METHODS

Energy calculations were performed using the Monte Carlo minimization (MCM) method (Li and Scheraga, 1987), AMBER force field (Weiner et al., 1984), and the ZMM program (www.zmmsoft.com) as described in Chapter 1. Ionizable residues were kept in their neutral forms, except for the Cd^{2+} -bound cysteines, which were modeled in the deprotonated forms. The homology models of the *Shaker* channel and its $V^{i22}C$ and $V^{i24}C$ mutants were built using the alignment shown in Table 2.1. The starting KcsA-, MthK-, and KvAP-based models of the *Shaker* channel and its $V^{i24}C$ mutants were built and MC-minimized using the approach described elsewhere (Tikhonov and Zhorov, 2004).

Determining dimensions of *Shaker* channel blockers

The dimensions of correolide and tetrabutylammonium (TBA) were determined by computing plots of MC-minimized energy of the drug pulled through variable-diameter rings of methane molecules. The epoxy oxygen of correolide was constrained to a movable plain P_O , which is parallel to the ring plane. Plane P_O was translated with a step of 0.5 Å at each step the energy was MC-minimized. The translational position of correolide at the plots corresponds to the displacement of plane P_O from the ring plane.

Table 2.1. Alignment of K⁺ channels^a

| Outer helices | | 1 | 11 | 21^b | |
|----------------------|-----|------------|-------------------|-----------------------|-----------|
| KcsA | 23 | ALHWRAAGAA | TVLLVIVLLA | GSYLAVLAE | |
| MthK | 14 | RVLKVPATRI | LLLVLAVIIY | GTAGFHFIE | |
| KvAP | 144 | AADKIRFYHL | FGAVMLTVLY | GAFAIYIVE | |
| <i>Shaker</i> | 390 | KASMRELGLL | IFFLFIGVVL | FSSAVYFAE | |
| Inner helices | | | | | |
| | | 1 | 11 | 21 | 31 |
| KcsA | 86 | LWGRLVAVVV | MVAGITSFGL | VTAALATWFV | GREQ |
| MthK | 70 | PLGMYFTVTL | IVLGIGTFAV | AVERLLEFLI | NREQ |
| KvAP | 207 | PIGKVIGIAV | MLTGISALTL | LIGTVSNMEQ | KILV |
| <i>Shaker</i> | 453 | VWGKIVGSLC | AIAGVLTIAL | PVPVIVSNFN | YFYH |

^a Correolide-sensing residues in the inner helices of Kv1.3 (Hanner et al., 2001) are bold-typed.

^b Relative numbering as described in Chapter 1.

To prevent the flip-flop of correolide during MC-minimizations, an atom in the seven-membered ring of correolide was constrained not to occur ahead of plane P_O .

Modeling the Cd^{2+} -bound *Shaker* channel

The locked-open conformations of the channel were built to satisfy distance constraints between C^{i24} and H^{i34} residues (Webster et al., 2004). In the starting KcsA-, MthK-, and KvAP-based models, the distances between C^{i24} and H^{i34} residues were too large to form Cd^{2+} bridges described by Webster et al. (2004). The lengths of coordinating bonds $\text{S}-\text{Cd}^{2+}$ and $\text{N}-\text{Cd}^{2+}$ are known from the crystal structures of small molecules with Cd^{2+} . Applying the lengths of the coordinating bonds as fixed distance constraints $\text{C}^{i24}-\text{S}^{\gamma}-\text{Cd}^{2+}-\text{N}^{\epsilon 2}-\text{H}^{i34}$ to the X-ray based models of the *Shaker* caused abrupt conformational changes and bad contacts, which were difficult to relax in a reasonable computational time. Therefore, each X-ray based model of the *Shaker* was modified in a series of MCM trajectories with variable, gradually diminishing constraints (Tikhonov and Zhorov, 2004). The starting values of the variable distance constraints $\text{S}-\text{Cd}^{2+}$ and $\text{N}-\text{Cd}^{2+}$ were calculated in the MCM trajectory in which the protein backbones were kept rigid while distances between Cd^{2+} ions, $\text{S}^{\gamma}-\text{C}^{i24}$, and $\text{N}^{\epsilon 2}-\text{H}^{i34}$ were minimized. The experimental lengths of the coordinating bonds $\text{S}-\text{Cd}^{2+}$ and $\text{N}-\text{Cd}^{2+}$ were used as the target values for the variable distance constraints. In the subsequent series of MCM trajectories, the variable constraints were diminished with the step of 0.5 Å. At each step, the energy was MC-minimized starting from the optimal structure found at the previous step.

In the constraints-driven MCM trajectories, the alpha carbons in the P-loops and extracellular halves of the inner and outer helices were constrained to the respective crystallographic positions using pins, flat-bottom energy functions with the bottom width of 1 Å. The secondary structure of the C-terminal parts of the inner helices (S^{i27} through H^{i34}) was preserved by constraining α -helical H-bonds between CO and NH groups. MCM trajectories were terminated when the last 2000 consecutive energy minimizations did not decrease the lowest energy found. At the last stage of simulating the locked-open conformations of the *Shaker* channel, all constraints were removed and an additional MCM trajectory was run. This protocol ensured smooth conformational changes that yielded a compromise between the starting X-ray based structure of the *Shaker* channel and the experimental $\text{S}-\text{Cd}^{2+}$ and $\text{N}-\text{Cd}^{2+}$ constraints. The same methodology was also used to simulate the Cd^{2+} block of the locked-open *Shaker* channel.

Simulating Cd^{2+} ions

Classical force-field parameters for Cd^{2+} do not reproduce experimental geometry of Cd^{2+} -Cys complexes (Berweger et al., 2000) and quantum-chemical methods are impractical for large systems. Therefore, we simulated Cd^{2+} using AMBER parameters for Mg^{2+} . This approximation had little effect on calculations, in which bonds with Cd^{2+} were constrained. In the non-constrained trajectories, the strong electrostatic attraction of

the divalent cation to electronegative atoms influenced the formation of coordinating bonds. Too close coordination of the divalent cation with the electronegative atoms was precluded by flat-bottom penalty functions with no upper-distance limit and lower-distance limits of 2.65, 2.3, and 2.47 Å, which are seen in the X-ray structures of Cd²⁺ coordinated to sulfur (Stalhandske et al., 1997), nitrogen (Bebout et al., 1999), and oxygen (Stalhandske et al., 1997), respectively. Subsequent removal of the flat-bottom penalty functions and additional energy minimizations did not noticeably change the complexes found. Test calculations with Ca²⁺ and Zn²⁺ in place of Cd²⁺ resulted in practically the same conformations as with Mg²⁺.

RESULTS AND DISCUSSION

Dimensions of the *Shaker* blockers

The dimensions of semirigid open-channel blockers may provide direct estimates of the minimal width of the cytoplasmic pore entrance. Correolide has a flattened-ellipsoid shape with a hexacyclic core decorated with six acetoxy groups (Figure 2.1). The maximal length of correolide, measured between oxygen atoms at the ellipsoid poles, is 13.6 Å. The dimensions of correolide in directions normal to the long axis depend on orientations of acetoxy groups. To determine these dimensions, we created circular constructs of 14 – 18 methane molecules of variable inner diameter $d_i = d_c - 4 \text{ Å}$, where d_c is the diameter of the circle drawn via centers of carbon atoms and 4 Å is an approximate van der Waals diameter of methane. The number of methane molecules increased with the ring diameter to sustain the distance of $\sim 3 \text{ Å}$ between adjacent carbons. The drug was pulled through the rings with the step of 0.5 Å and at each position the energy was optimized using the MCM protocol (Figure 2.2 A, B). Large energy barriers were obtained for correolide pulled through rings with $d_i < 10 \text{ Å}$ (Figure 2.2 A). The 10 Å-ring is also smaller than the minimal-profile projection of correolide in the energetically optimal conformation (Figure 2.3 A). However, the drug can pass through this ring by adopting more compact conformations. (A pore entrance in an open channel may experience rare fluctuations during which the cross-sectional dimensions could increase. However, short-lived fluctuations are unlikely to contribute to the high-affinity binding of bulky drugs as discussed in a later section). Analogous calculations show that TBA could pass through a ring as small as 7-8 Å (Figure 2.2 C, D).

Pi²³ residues form the narrowest level at the cytoplasmic entrance to the pore of the KvAP-based model of the *Shaker* channel (Figure 2.3 B, C). The distance of 14.4 Å between diagonally opposed atoms C^y Pⁱ²³ remarkably matches the ring of $d_c = 14 \text{ Å}$ ($d_i = 10 \text{ Å}$). Several correolide-sensing residues line the pore (Hanner et al., 2001) suggesting that correolide binds between the entrance and the selectivity filter. Figure 2.3B shows Pⁱ²³ residues aligned with the ring of $d_i = 10 \text{ Å}$. The latter embraces correolide molecules in which the epoxy oxygen is displaced 0 - 8 Å from the ring plane. In the topmost position, the drug's pole would reach the selectivity filter, whereas part of the drug would

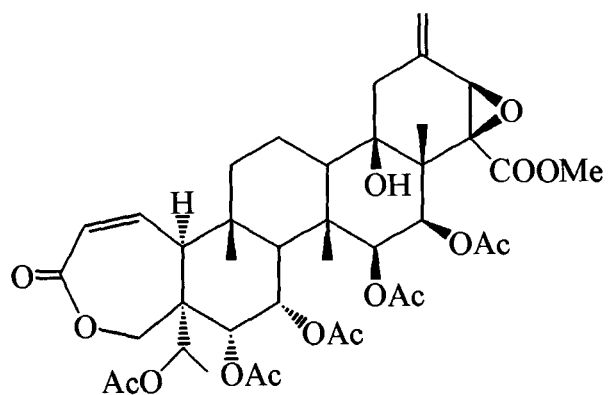


Figure 2.1. Structure of correolide.

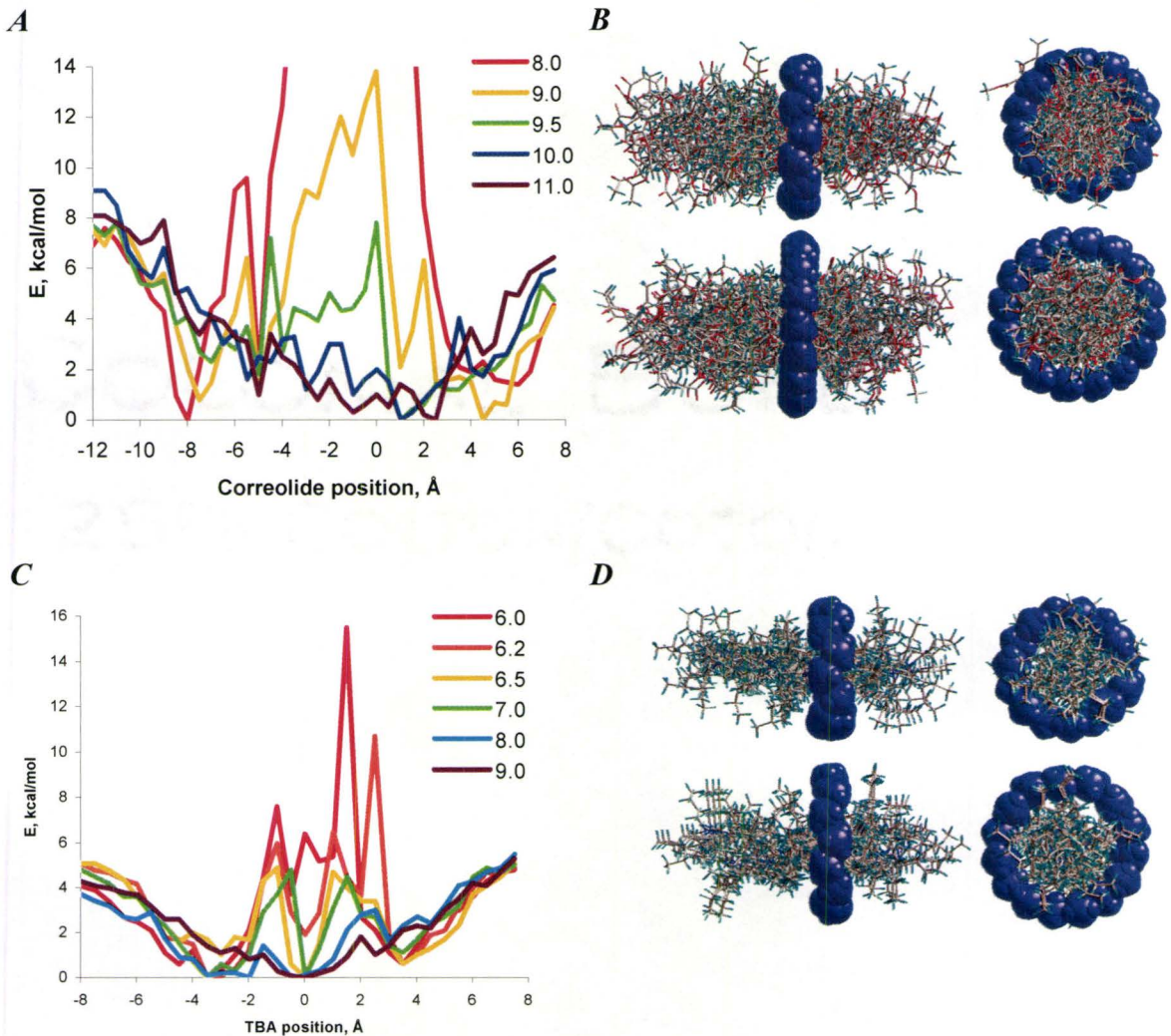


Figure 2.2. Dimensions of the *Shaker* channel intracellular blockers. **A**, Plots of MC-minimized energy of correolide pulled via the variable-diameter rings of methane molecules. The zero position corresponds to the epoxy group of correolide in the plane of the ring. The energy barrier increases sharply as the diameter decreases from 10 to 9.5 Å. **B**, The superposition of MC-minimized structures of correolide pulled through the rings with the inner diameter d_i of 8 and 10 Å. Large deformations of correolide in the smaller ring explain the high energy barrier shown in **A**. MC-minimization caused some methane molecules of the smaller ring to violate in-plane constraints to avoid strong repulsions with their neighbours. **C**, Plots of MC-minimized energy of TBA pulled via the variable-diameter rings of methane molecules. The zero position corresponds to the nitrogen atom in the plane of the ring. Barrier increases sharply as the diameter decreases from 6.5 to 6 Å. **D**, The superposition of MC-minimized structures of TBA pulled through the rings with the inner diameter d_i of 6 and 8 Å.

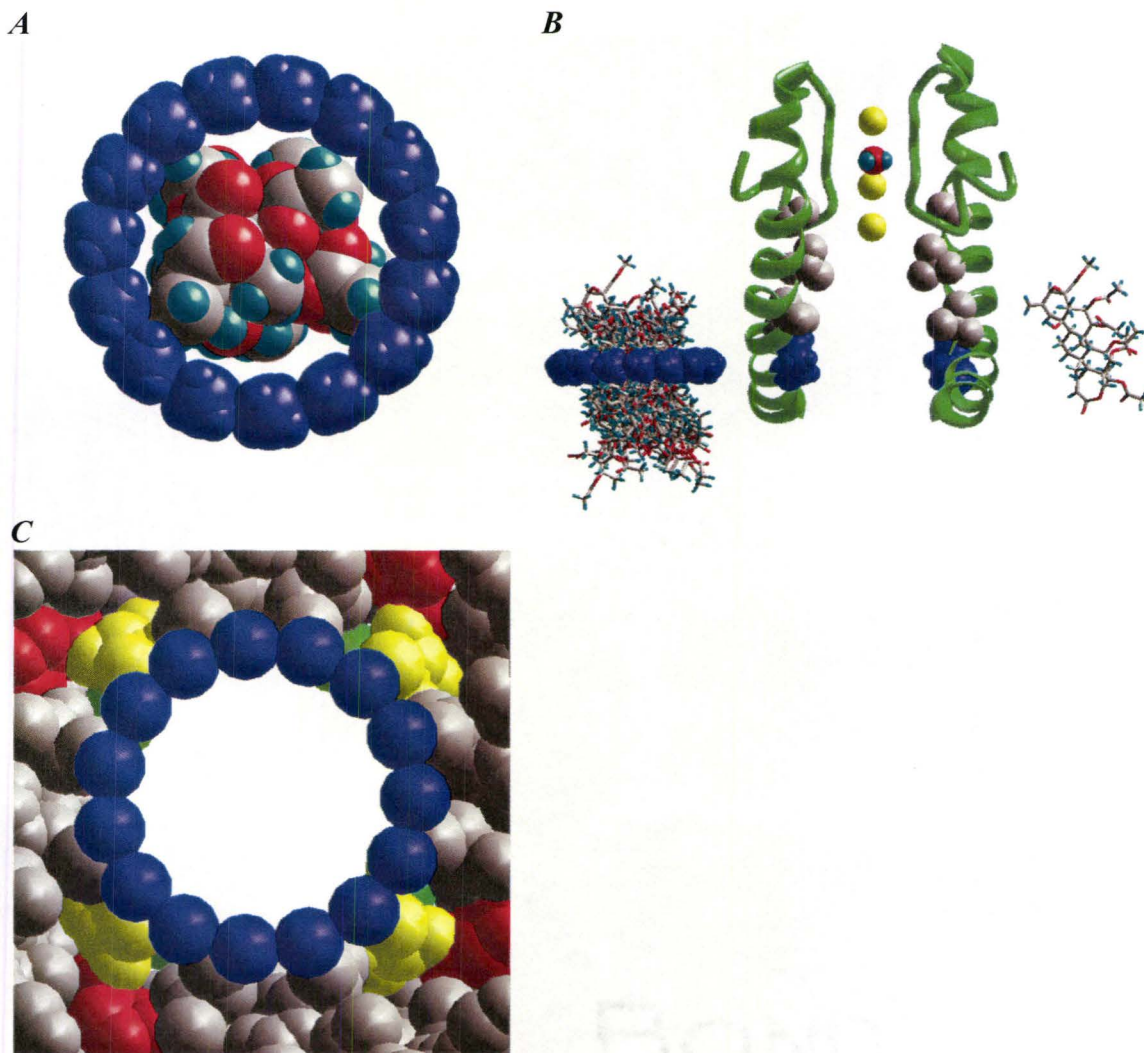


Figure 2.3. The 10 Å-ring of methane molecules vs. correolide and KvAP-based model of the *Shaker* channel. *A*, Space-filled model of correolide viewed via the ring. *B*, The side view of the *Shaker* model. The inner helices in two opposite domains are shown as ribbons. C-terminal parts of the pore helices and the selectivity-filter region are shown as rods. Correolide-sensing residues A^{i11} , V^{i15} , A^{i19} , V^{i22} , and P^{i23} are space-filled. Blue-coloured P^{i23} at the cytoplasmic entrance is aligned with the 10 Å-ring embracing correolide molecules in positions 0 through 8 Å from the ring plane (left pane). In the latter position (right pane), correolide would occur between the selectivity filter and the cytoplasmic entrance to the pore, which should be at least 10 Å wide to enable high-affinity binding of the drug. *C*, Space-filled model of the KvAP-based model of the *Shaker* channel viewed via the 10 Å-ring. P^{i21} , V^{i22} , and P^{i23} are coloured red, yellow, and green, respectively. Hydrogen atoms are not shown. Note a perfect match in the dimensions of the ring and the cytoplasmic entrance to the pore.

remain outside the entrance (Figure 2.3 B), suggesting that the entrance narrower than 10 Å would not accommodate correolide. In T-lymphocytes, the development of the K⁺ current block by correolide is slow (Koo et al., 1999), but intracellular application results in a faster block (Wunderler et al., 1999). In the KvAP-based model, the correolide-binding site has a cylindrical shape (Figure 2.3 B). The energy barrier for a drug entering such a site should inversely correlate with the binding energy. Correolide binds with a high affinity (Koo et al., 1999), suggesting that the native conformation of the *Shaker* open pore is wide enough to accommodate the drug.

Locked-open conformations of the *Shaker* channel

To explore the consistency of the data on Cd²⁺ locking the open *Shaker* with crystallographic structures of bacterial K⁺ channels, we created KvAP-, MthK-, and KcsA-based models of the *Shaker* mutant Vⁱ²⁴C. When α-carbons were constrained (pinned) to the corresponding X-ray templates, the models failed to form Cⁱ²⁴_S^γ---Cd²⁺---N^{ε2}_Hⁱ³⁴ bridges, indicating the necessity of backbone deformations. Current theories suggest that such deformations would occur at the gating-hinge Gⁱ¹⁴ (Jiang et al., 2002a) or the PVP motif (Webster et al., 2004) or at both. To test these theories, we removed all pins at the intracellular half of the channel and ran series of consecutive MCM trajectories, in which distance constraints Cⁱ²⁴_S^γ---Cd²⁺---N^{ε2}_Hⁱ³⁴ were gradually introduced to yield locked-open conformations.

The KvAP-based model converged to the energetically preferable structure, which was similar to the starting X-ray structure (Figure 2.4; Table 2.2). In the KvAP-based model of the locked-open *Shaker*, each Cd²⁺ ion coordinates the side chains of Cⁱ²⁴ and Hⁱ³⁴ in the inner helices and E^{o6} in the outer helix (Figure 2.5 A, B). Interestingly, no constraints were imposed between Cd²⁺ and E^{o6}, which was kept neutral in the model. Despite that, the coordinating bonds Cd²⁺---E^{o6} were formed, exemplifying the notion that Cys, His, and Asp form Cd²⁺ binding sites in proteins (Paul-Soto et al., 1999; Heinz et al., 2003). This finding is experimentally testable. If proven, it would serve as a strong argument in favour of the proposed alignment of the outer helices (Table 2.1). Both electrostatic and van der Waals interactions are more favourable in the locked-open conformation than in the starting conformation. Superimposing the 10Å-ring of methane molecules with the locked-open KvAP-based model of *Shaker* shows a remarkable match in the pore diameter, which is minimally required to accommodate correolide (Figure 2.3 C).

The KcsA-based model underwent small deformations to accommodate Cⁱ²⁴_S^γ---Cd²⁺---N^{ε2}_Hⁱ³⁴ constraints, but at the expense of a large energy increase. The resultant model cannot be categorized as the locked-open channel, since the pore remained in the closed conformation (Figure 2.4). MCM trajectories of the MthK-based model with the locking-open constraints converged to an energetically favourable conformation, but it was significantly different from the starting structure (Figure 2.4; Table 2.2).

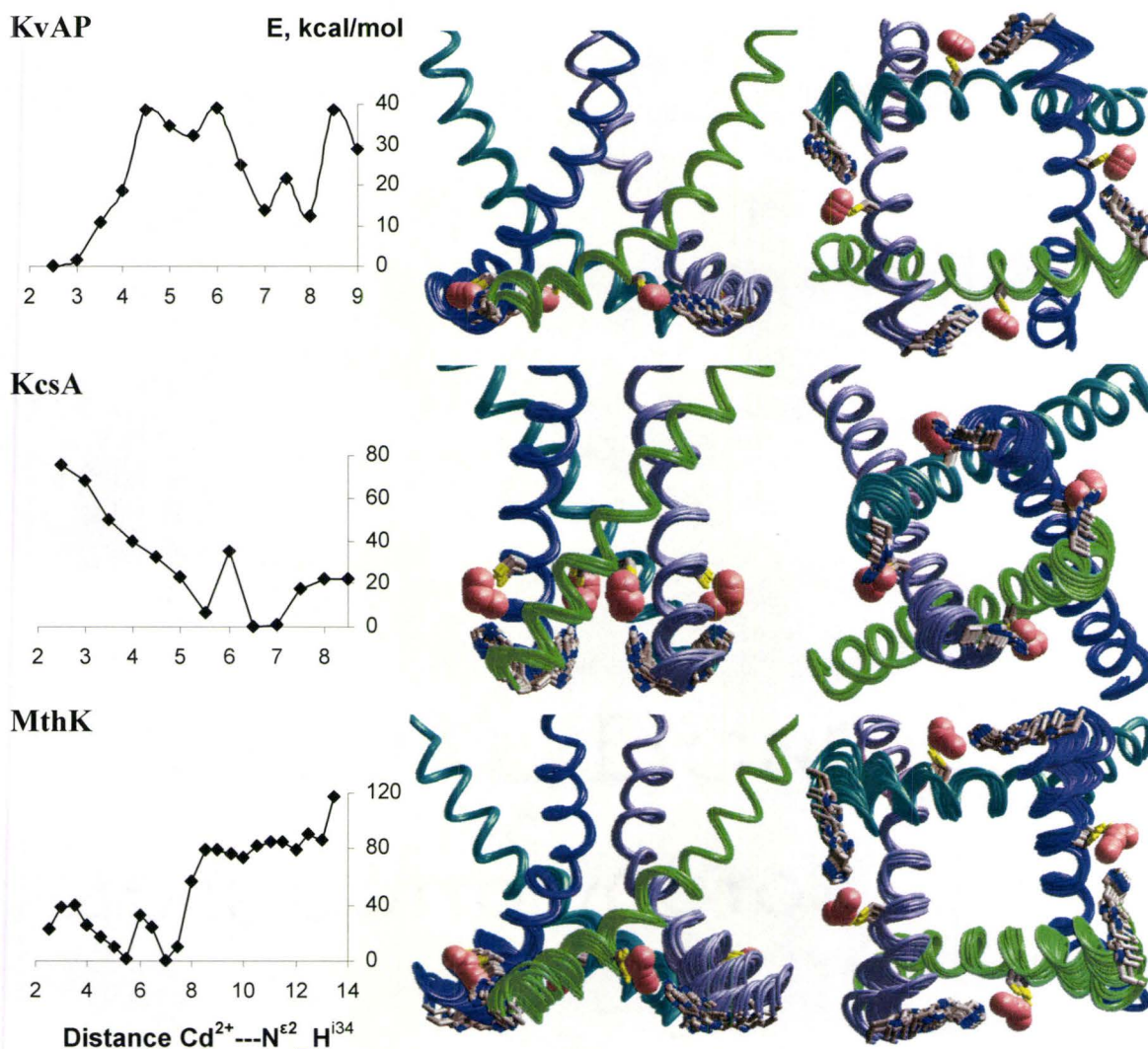


Figure 2.4. Convergence of the *Shaker* models from the X-ray based starting structures to conformations with coordinating bonds $C^{i24}_S \gamma \text{---} Cd^{2+} \text{---} N^{\epsilon 2}_H i^{34}$. Cd^{2+} ions were constrained to $S^{\gamma}_C i^{24}$ at the distance of 2.65 Å. Distance constraints $Cd^{2+} \text{---} N^{\epsilon 2}_H i^{34}$ were decreased with the step 0.5 Å from the starting values found in the X-ray based structures. At each step, the energy was MC-minimized until the distances of ~ 2.3 Å were achieved. In the plots of MC-minimized energy against the imposed distance $Cd^{2+} \text{---} N^{\epsilon 2}_H i^{34}$, the energy is shown relative to the lowest-energy structure found. The locked-open conformations are more preferable energetically than the starting KvAP- and MthK-based structures. KcsA-based conformation with coordinating bonds $C^{i24}_S \gamma \text{---} Cd^{2+} \text{---} N^{\epsilon 2}_H i^{34}$ has higher energy than the starting structure. Superposed MC-minimized structures are right to the respective energy plots. In the side and cytoplasmic views, only the inner helices are shown for clarity. Cys and His are shown as sticks and Cd^{2+} ions as magenta spheres. Locking open the KvAP-based structure is energetically preferable and requires minimal structural deformations.

Table 2.2. Comparison of the *Shaker* channel models

| Compared models | RMSD (Å) of C ^α atoms in the inner-helix residues ^a | | | | |
|--|---|-------|-------|-------------------|-------------------|
| | 1-13 | 14-20 | 21-24 | 25-34 | 1-34 |
| X-ray KvAP vs. locked-open KvAP-based | 1.06 | 1.21 | 1.40 | 4.19 | 2.48 |
| X-ray KcsA vs. constrained KcsA-based ^b | 0.95 | 2.03 | 2.44 | 3.95 | 2.55 |
| X-ray MthK vs. locked-open MthK-based | 1.17 | 1.24 | 2.01 | 4.84 ^c | 3.39 ^c |
| X-ray MthK vs. X-ray KvAP | 1.86 | 2.54 | 3.53 | 6.20 ^c | 3.37 ^c |
| Locked-open MthK-based vs. locked-open KvAP-based | 2.77 | 2.58 | 2.52 | 2.55 ^c | 2.65 ^c |

^a Relative residue numbers, see Table 2.1

^b MC-minimization with constraints Cⁱ²⁴---Cd²⁺---Hⁱ³⁴ did not produce the open conformation of the channel.

^c The inner helix ends at residue *i29*, which is the last residue in the MthK X-ray structure.

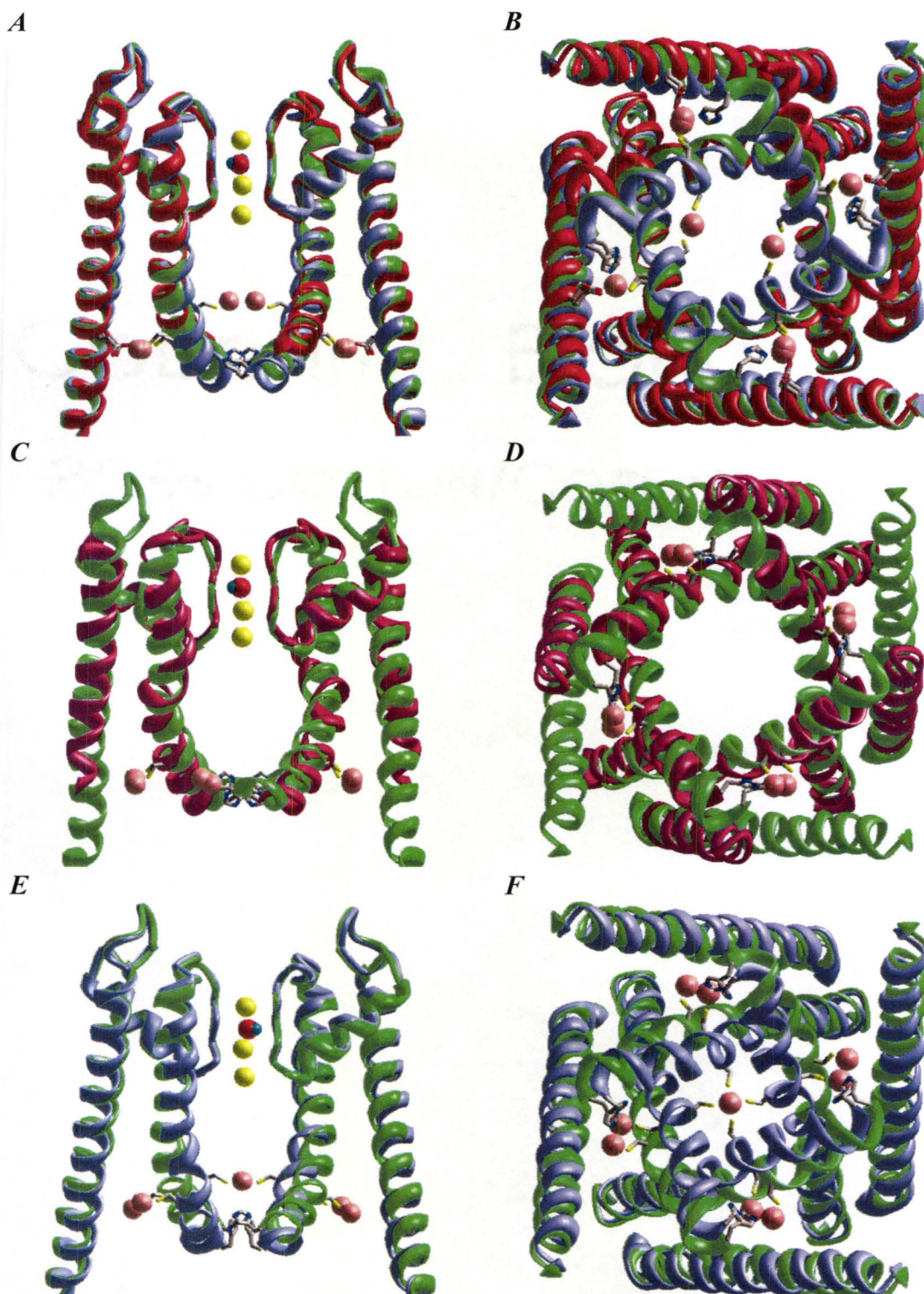


Figure 2.5. KvAP-based models of the *Shaker* channel. *A* and *B*, Side and cytoplasmic views of the superposition of the X-ray based structure (red), the locked-open mutant Vⁱ²⁴C (green), and locked-open mutant Vⁱ²²C/Vⁱ²⁴C (violet) blocked by two Cd²⁺ ions.

The side chains of E⁰⁶, Cⁱ²⁴, and Hⁱ³⁴ are shown as sticks, Cd²⁺ ions as magenta spheres, and K⁺ ions as yellow spheres. The involvement of E⁰⁶ in the Cd²⁺ coordination sphere was an unexpected result of MC-minimization. The coordination occurred despite E⁰⁶ was not ionized in the model. In the cell, negative charges at E⁰⁶ and Cⁱ²² would facilitate Cd²⁺ binding. **C and D**, The superposition of the locked-open conformations obtained from KvAP (green) and MthK (magenta) starting structures. The conformations are similar despite starting structures are essentially different, especially at the C-termini (Table 2.2). For clarity, only two opposed domains are shown in the side views and only inner and outer helices are shown in cytoplasmic views. **E and F**, The superposition of the locked-open model (green) and the locked-open model blocked by a single Cd²⁺ ion (violet). Constraining a single Cd²⁺ ion to four Cⁱ²² residues caused large conformational deformations, which are inconsistent with the experimentally observed easiness of the Cd²⁺ block of the locked-open channel.

Unexpectedly and importantly, the final locked-open conformation occurred rather similar to the KvAP-based locked-open conformation (Figure 2.5 C, D; Table 2.2).

Thus, among the three X-ray structures tested, only the KvAP-based model readily accommodated $C^{i24}_S \text{---} Cd^{2+} \text{---} N^{\epsilon 2}_H^{i34}$ constraints, producing a locked-open conformation. The opening of the Ca^{2+} -gated channel MthK is driven by the inner helices linked to the cytoplasmic Ca^{2+} binding domains. The opening of the voltage-gated channel KvAP is driven by the outer helices linked to the voltage-sensing domains. The different mechanisms of activation may account for the different pore geometry observed in the crystal structures of these channels. The consistency of the KvAP-based model of the *Shaker* channel with Cd^{2+} - and correolide-binding experiments suggests that the pore region of KvAP retains a native-like conformation in the crystal.

Conformational changes at the PVP motif

In all the locked-open models, the inner helices did not kink at the PVP motif, but bent at residues N-terminal to it. This result agrees with the conclusion from the statistical analysis of crystallographic structures of proline-containing transmembrane helices that kinks occur not at prolines *per se*, but at residues three to four positions N-terminal to the prolines (Cordes et al., 2002). In the *Shaker* channel, P^{i21} and P^{i23} deprive backbone carbonyls between T^{i16} and L^{i20} of H-bond donors, thus increasing the flexibility of residues C-terminal to G^{i14} , which aligns with the gating hinge in prokaryotic K^+ channels. This region also undergoes the largest conformational changes during *in-silico* activation of KcsA by lateral forces applied to the C-termini of inner helices (Tikhonov and Zhorov, 2004). Our calculations show that Cd^{2+} binding causes conformational changes between the conserved Gly and the PVP motif (Figure 2.6), but the latter does not show substantial kinks.

Another argument in favour of a sharp bend at the *Shaker* PVP motif was raised by del Camino et al. (2000), who studied how the open-channel blockers protect engineered cysteines in the inner helices from the chemical modification by methanethiosulfonate reagents. The authors demonstrated, in particular, that TBA protects engineered cysteines in positions *i18*, *i22*, and *i26*, but not in positions *i24*, *i30*, and *i31*. Despite the fact that our model does not include the kink at the PVP motif, it agrees with the experimental observations of del Camino et al. (2000) as well as with their prediction that side chains in positions *i18*, *i22*, and *i26* face the pore, position *i24* faces away from the pore, and positions *i30* and *i31* are far from the pore axis.

Calculations of the full-fledged models of the *Shaker* channel were performed taking advantage of the four-fold symmetry of the channel. As a control, we ran a series of constrained MC-minimizations of the KvAP-based inner-helices without employing the symmetry operations. The search yielded a slightly asymmetric locked-open structure (Figure 2.6 A, B), in which disposition of the inner helices is very similar to that in the symmetric model (Figure 2.5 A, B). The comparison of torsions in the starting and locked-open structures shows that major changes occur at I^{i18} , one helical turn upstream to the PVP motif. (Figure 2.6 C, D). To increase the probability of backbone deformations

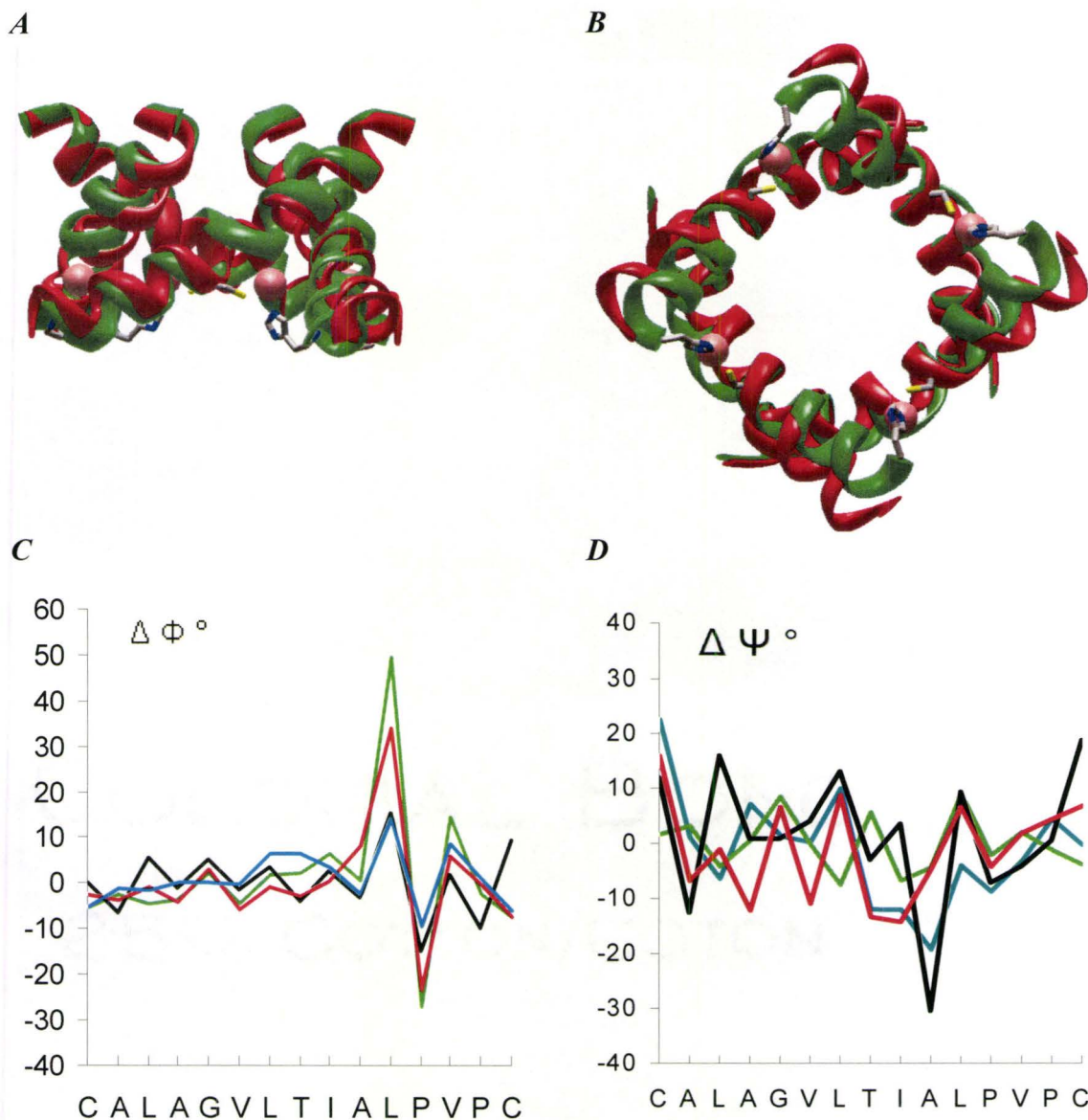


Figure 2.6. KvAP-based model of the *Shaker* inner-helices bundle obtained by MC-minimization without using the advantage of the channel four-fold symmetry. *A* and *B*, Side and cytoplasmic views of superposition of KvAP X-ray structure (red) and locked-open *Shaker* mutant Vⁱ²⁴C (green). The side chains of Cⁱ²⁴ and Hⁱ³⁴ are shown as sticks. K⁺ and Cd²⁺ ions are shown as spheres. The inner helices bend smoothly at residues N-terminal to the PVP motif. *C* and *D*, Changes of backbone torsions in four subunits observed during the simulated locking the open channel starting from KvAP-based conformation. Largest changes of Φ are at Lⁱ²⁰ and Pⁱ²¹ and moderate changes are in segments both N- and C-terminal to the PVP motif. Largest changes of Ψ are at Aⁱ¹⁹ whose backbone oxygen lacks the helical H-bond. Changes at Iⁱ²⁶ through Hⁱ³⁴ are not shown because torsions were restrained in alpha-helical conformation. Changes at Lⁱ⁹ are not shown because this residue was constrained at conformation seen in KvAP.

at the PVP motif, additional simulations of the locked-open conformations were performed with elastic bond angles varied in the PVP residues. Calculations with rigid and elastic bond angles at the PVP motif gave similar results.

Thus, the KvAP-based model of the *Shaker* channel is consistent with experimental observations that were interpreted in favour of a sharp kink at the PVP motif. However, instead of a sharp kink, the model shows a smooth bend of the inner helices between the conserved Gly and the PVP motif. If the PVP motif does not cause a kink, why is it conserved in *Shaker* channels? A possible reason is an increased flexibility of the inner helices, which may be important for the gating of the *Shaker* channel (Labro et al., 2003) and possibly for its regulation.

Simulating the Cd²⁺ block of the locked-open *Shaker* channel

Block by a single cadmium ion

The observation that Cd²⁺ blocks the locked-open *Shaker* double mutant Vⁱ²²C/Vⁱ²⁴C by coordinating Cⁱ²² implies that the pore lumen at the level of S^γ-Cⁱ²² could be as small as the diameter of a Cd²⁺ ion (Webster et al., 2004). A much wider lumen is needed to accommodate hydrated K⁺ and certain blockers (Webster et al., 2004), implying that Cd²⁺ block would cause essential conformational changes of the locked-open *Shaker*. To evaluate these changes, we built the KvAP-based model of the *Shaker* double mutant, retained the eight locking-open constraints with the four Cd²⁺ ions, and imposed constraints between the fifth Cd²⁺ ion and four Cⁱ²² residues. The constrained MCM trajectories were run to yield the Cd²⁺-blocked locked-open conformations. The KvAP-based model blocked by a single Cd²⁺ deviated significantly from the starting locked-open conformation (Figure 2.5 C, D).

The variable diameter of the locked-open *Shaker* was proposed to explain different dimensions of organic and inorganic blockers acting at the same region of the open pore (Webster et al., 2004). However, large deformations that would be caused by the Cd²⁺ coordination to three or four Cⁱ²² residues are inconsistent with the observed easiness with which the *Shaker* double mutant assumes a Cd²⁺-blocked conformation from the locked-open state (Webster et al., 2004). The problem arises from the assumption that at least three Cⁱ²² residues should coordinate Cd²⁺ simultaneously (Webster et al., 2004). This assumption is backed by the observation that channels with four Cⁱ²² bind Cd²⁺ irreversibly, whereas channels with two Cⁱ²² bind Cd²⁺ reversibly (Liu et al., 1997). It should be noted that the channels with two Cⁱ²² were expressed as tandems of two dimers with a Cⁱ²² mutation only in the first protomer (Liu et al., 1997). In such tandems, Cⁱ²² are at the opposite inner helices and cannot coordinate Cd²⁺ simultaneously in the open channel.

Block by two cadmium ions

In an alternative model, two pairs of the negatively charged residues would chelate two divalent cations. Such a pattern was proposed in the selectivity-filter models of Ca^{2+} channels (Zhorov and Ananthanarayanan, 1996; Zhorov et al., 2001) and is seen in the X-ray structure of a Ca^{2+} pump (Toyoshima et al., 2000). MC-minimization of the locked-open KvAP-based model of *Shaker* blocked by two Cd^{2+} ions at C^{i22} residues caused only small backbone deformations (Figure 2.5 A, B). In terms of the coordination number, the model with two Cd^{2+} ions seems less preferable than the model, in which Cd^{2+} is tetra-coordinated by four C^{i22} residues. However, the coordination stereochemistry of Cd^{2+} is known to be unusually variable, including coordination numbers from two to eight (Andersen, 1984). Coordination of Cd^{2+} by two Cys residues was demonstrated in the *Shaker* channel (Webster et al., 2004). Another advantage of the model blocked by two Cd^{2+} ions is an electrostatic balance between positive charges at Cd^{2+} ions and negative charges at C^{i22} residues.

Two Cd^{2+} ions chelated by C^{i22} residues do not physically occlude the pore, raising the question about the mechanism of the K^+ current block. To address this question, we estimated the energy barrier of a hydrated K^+ ion pulled via the *Shaker* double mutant $\text{V}^{i24}\text{C}/\text{V}^{i22}\text{C}$ using methodology described elsewhere (Zhorov and Bregestovski, 2000). The hydration shell of the K^+ ion included eight water molecules. The solvation shell of each Cd^{2+} ion included five water molecules in addition to two sulfur atoms from C^{i22} residues. The oxygen atom of each water molecule was constrained to the respective cation via a distance penalty function that prevented oxygen-metal separation by more than 3 Å. These constraints were necessary because the model did not include water molecules beyond the first hydration shells, which in a real system would substitute a water molecule abandoning a cation. We did not consider an unlikely scenario of sharing a water molecule between the first hydration shells of two closely spaced cations.

The hydrated K^+ ion was constrained to a plane normal to the pore axis. The plane was translated with a step of 0.5 Å and at each step the energy of the entire system was MC-minimized. The calculations predicted that the hydrated K^+ pulled from the cytoplasm through the level of C^{i22} with two Cd^{2+} ions would encounter an energy barrier of 36.2 kcal/mol (Figure 2.7 A). The barrier has two major components: (i) electrostatic energy of K^+ , whose repulsion from Cd^{2+} ions is stronger than the attraction to ionized C^{i22} residues, and (ii) energy of the K^+ hydration shell in which some hydrogen atoms would occur too close to the Cd^{2+} ions (Figure 2.7 B). These simple calculations suggest that K^+ permeation via the *Shaker* double mutant blocked by two Cd^{2+} ions is hardly possible. Thus, the KvAP-based model of the *Shaker* channel is consistent with the distance constraints known from the action of Cd^{2+} ions and organic blockers. Our results indicate that the pore region is structurally conserved between prokaryotic and eukaryotic K^+ channels.

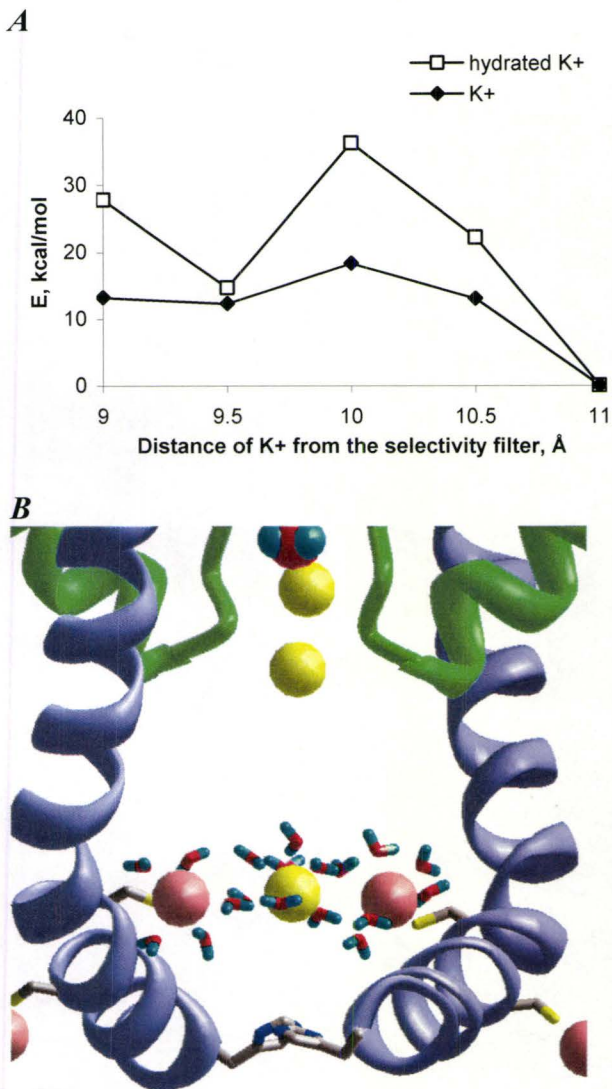


Figure 2.7. Pulling a K^+ ion through the locked-open mutant $V^{i22}C/V^{i24}C$ blocked by two Cd^{2+} ions. **A**, The energy of a K^+ ion (\blacklozenge) and the same ion with the first hydration shell comprising eight water molecules (\square) pulled via the *Shaker* locked-open double mutant $V^{i22}C/V^{i24}C$ blocked by two Cd^{2+} ions. The pulling was accomplished by constraining K^+ to the plane, which was translated normally to the pore axis. Abscissa (d) is the distance between the plane and K^+ ion bound to Thr residues in the selectivity-filter sequence TVGYG. The energy values are partitioned from the structures MC-minimized at each position of the K^+ -constraining plane. The energies are given relative to the point $d = 11$ Å. Note that at position $d = 10$ Å, K^+ contributes $\sim 50\%$ to the energy barrier, and eight water molecules contribute remaining $\sim 50\%$. **B**, MC-minimized structure with hydrated K^+ constrained at the level of $d = 10$ Å. In addition to electrostatic repulsion between the closely spaced cations, the system is destabilized by the unfavourable orientation of water molecules, some of which cannot avoid exposure of their hydrogen atoms towards alien Cd^{2+} ions.

Sensitivity of results to the chosen computational methodology

Experimental data on the binding of correolide and Cd^{2+} ions to *Shaker* channels provide seemingly conflicting constraints on the open pore geometry. Cd^{2+} -binding constraints are not consistent with available X-ray structures, and their interpretation requires the modeling of the backbone deformations. For this goal, we applied the methodology of MC-minimization in the space of generalized coordinates, which was recently used for the simulations of large-scale conformational transitions in KcsA (Tikhonov and Zhorov, 2004). Three X-ray structures of K^+ channels were used as the starting points. The KvAP structure underwent minimal conformational deformations to accommodate the distance constraints from experiments on the *Shaker* V^{i24}C mutant locked-open by Cd^{2+} ions, but the pore remained wide enough to accommodate a large molecule of correolide.

Results of molecular simulations are not always confirmed by subsequent experiments. Therefore, the sensitivity of our results to the chosen computational methodology should be discussed. Pulling correolide through the rings of methane molecules predicts energy barriers that rule out correolide binding in rings smaller than 10 Å. The barriers are determined by repulsive forces, which are similar in different force fields. Entropy was ignored, but its inclusion would increase rather than decrease the free energy barrier at the critical diameter of the ring, which is matched by one of many possible conformations of correolide. Our simulations of the *Shaker* channel in different states depend on the applied constraints, starting geometry, energy optimization method, and force fields. The constraints used are defined in experiments. Three different X-ray structures of K^+ channels were tested as starting approximations and the KvAP structure was found to be most consistent with the constraints. The MCM protocol is a highly efficient method of non-local conformational search (Li and Scheraga, 1987). Force field parameters can be questioned in any computational work. However, these parameters are less critical in our study, which does not explore relative probabilities of various structures, but addresses consistency of the available X-ray structures of K^+ channels with experiments on Cd^{2+} binding to the *Shaker* mutants.

CONCLUSIONS

X-ray structures of bacterial K^+ channels are widely used for homology modeling of eukaryotic channels. However, the reliability of the models is questioned by controversial interpretations of experiments addressing structural similarity between eukaryotic and prokaryotic K^+ channels. On one hand, substituting the prokaryotic pore into the *Shaker* channel suggests conservation of the pore domain between the channels (Lu et al., 2001). On the other hand, experiments providing insights on the pore structure using cadmium block of *Shaker* channels with engineered cysteines (Holmgren et al., 1998; del Camino et al., 2000; Webster et al., 2004) imply structural differences between eukaryotic and prokaryotic K^+ channels.

In this work, we have shown that the distance constraints derived from the experiments on locking-open the *Shaker* mutants (Webster et al., 2004), as well as the seemingly paradoxical ability of large correolide (Hanner et al., 2001) and small Cd^{2+} ions (Webster et al., 2004) to block the open *Shaker* in the same region of the pore, are consistent with the KvAP structure. These data imply a structural conservation between the pore regions in prokaryotic and eukaryotic voltage-gated potassium channels.

A possibility that the antibody in the KvAP crystal structure distorts the mutual disposition of the voltage-sensor and pore domains is disputed (Mackinnon, 2004). Distortion of the pore domain *per se*, which is stabilized by multiple intra-domain contacts and does not form direct contacts with the antibody, seems less likely. Our finding that the KvAP-based structure is consistent with the distance constraints derived from cadmium- and ligand-binding experiments on the open *Shaker* channel can be explained in two ways. One possibility could be that both antibody binding to KvAP and Cd^{2+} binding to the *Shaker* mutant induce similar distortions in the native conformations of the proteins. However, the fact that the KvAP-like structure was obtained upon locking-open the MthK-based starting conformation supports a more likely possibility that the KvAP pore domain retains the native conformation in the crystal.

CHAPTER THREE

THE BINDING OF NUCLEOPHILIC BLOCKERS IN VOLTAGE-GATED K⁺ CHANNELS INVOLVES ELECTROSTATIC INTERACTIONS WITH A K⁺ ION IN THE SELECTIVITY FILTER

CHAPTER FOUR PREFACE

The work presented in this chapter was previously published in:

Bruhova I and Zhorov BS (2007) Monte Carlo-energy minimization of correolide in the $K_v1.3$ channel: Possible role of potassium ion in ligand-receptor interactions. *BMC Struct Biol* 7:5.

and

Lerche C, Bruhova I, Lerche H, Steinmeyer K, Wei AD, Strutz-Seebohm N, Lang F, Busch AE, Zhorov BS and Seebohm G (2007) Chromanol 293B binding in KCNQ1 ($K_v7.1$) channels involves electrostatic interactions with a potassium ion in the selectivity filter. *Molecular pharmacology* 71:1503-11.

Permission has been granted from the publishers to reproduce the material here.

I conducted all of the molecular modelling simulations described in this chapter.

ABSTRACT

Mutational studies identified that the pore of voltage-gated potassium (K_v) channels is a target for nucleophilic drugs. The pore-lining helices in K_v channels are predominantly hydrophobic raising questions about the nature of drug-channel interactions. Two such examples are correolide and chromanol 293B. Correolide, a nortriterpene isolated from the Costa Rican tree *Spachea correa*, is a novel immunosuppressant, which blocks $K_v1.3$ channels in human T lymphocytes. Chromanol 293B is a lead compound to potentially treat cardiac arrhythmia that blocks $K_v7.1$ channels. We employed the method of Monte Carlo (MC) with energy minimization to search for optimal complexes of correolide in $K_v1.2$ -based models of the open $K_v1.3$ with potassium binding sites 2/4 or 1/3/5 loaded with K^+ ions. Chromanol 293B was docked into the closed KcsA-based and opened $K_v1.2$ -based model of the $K_v7.1$ channel with K^+ ions loaded in the 2/4 sites. The energy was MC-minimized from many randomly generated starting positions and orientations of the ligand. In all the predicted low-energy complexes, oxygen atoms of the ligand chelate a K^+ ion. Ligand-sensing residues known from mutational analysis along with the ligand-bound K^+ ion provide major contributions to the ligand-binding energy. Deficiency of K^+ ions in the selectivity filter of C-type inactivated $K_v1.3$ would stabilize K^+ -bound correolide in the inner pore. The open model accommodates chromanol 293B more favourably than the closed model. Our study explains the paradox that cationic and nucleophilic ligands bind to the same region in the inner pore of K^+ channels and suggests that a K^+ ion is an important determinant of the correolide and chromanol receptor and possibly receptors of other nucleophilic blockers of the inner pore of K^+ channels.

INTRODUCTION

Numerous naturally occurring and synthetic compounds block K_v channels (Kaczorowski and Garcia, 1999). Classical low molecular weight blockers such as hydrophobic cations tetraethylammonium and tetrabutylammonium (TBA) are non-selective drugs, which bind to various subtypes of K^+ channels. Low molecular weight blockers that selectively target K_v channels have great potential as pharmaceuticals. Two of such drugs are correolide and chromanol 293B. Correolide blocks the members of the K_v1 family, but the highest binding affinity is observed for $K_v1.3$ and $K_v1.4$ channels (Felix et al., 1999; Hanner et al., 1999). Correolide prevents the activation of T-cells by selectively blocking the open or C-type inactivated $K_v1.3$ channels (Koo et al., 1999). Correolide and its derivatives are candidates for the development of novel immunosuppressant drugs for the treatment of graft rejection and autoimmune diseases (Matko, 2003). The chromanol 293B is a lead compound of potential class III antiarrhythmics that inhibit cardiac $K_v7.1$ (KCNQ1) channels. Since closely related neuronal $K_v7.2$ channels are insensitive to chromanol, $K_v7.1/K_v7.2$ chimeras were used to identify the binding site of the inhibitor. The binding site of chromanol was located to the central cavity, particularly the selectivity region and the inner helices (Seeböhm et al.,

2003). Mapping of correolide and chromanol 293B receptor in K_v channels may aid in the design of new and more specific K^+ channel pharmaceuticals.

Mutational and ligand-binding studies predicted that dihydrocorreolide (henceforth referred to as correolide) binds in the central pore of $K_v1.3$ (Hanner et al., 2001). Earlier we have built the KvAP-based model of the *Shaker* channel, which provides a basis for interpreting Cd^{2+} -binding experiments (Holmgren et al., 1998; del Camino et al., 2000; Webster et al., 2004) and seemingly paradoxical observations that large correolide and small Cd^{2+} ions block the open channel at the same level of the pore (Bruhova and Zhorov, 2005), see Chapter 2. The structure of $K_v1.2$ (Long et al., 2005a) confirmed major predictions of the model (Bruhova and Zhorov, 2005), but demonstrated that the open pore of $K_v1.2$ is ~ 1 Å narrower than that in KvAP. The 9 Å-wide pore of $K_v1.2$ is consistent with the correolide dimensions predicted to be 9 - 10 Å (Bruhova and Zhorov, 2005). Mapping of the correolide receptor in the $K_v1.2$ -based model of $K_v1.3$ is now warranted to rationalize mutational studies (Hanner et al., 2001) and provide information for possible design of simpler drugs targeting $K_v1.3$ channels.

Several theoretical and experimental studies predicted the involvement of metal ions in ligand-receptor interactions in ion channels (Ananthanarayanan, 1991; Zhorov and Ananthanarayanan, 1996; Zhorov et al., 2001; Tikhonov and Zhorov, 2005b). However, no direct experimental data on the structure of the ternary complex is available yet. In this regard, the complex of K_v channel with correolide and chromanol seems to be a promising probe to provide insights into the K^+ channels structure using computational approaches. Due to the large semirigid and nucleophilic structure of correolide (Figure 3.1A), the ligand should adopt a limited number of binding modes in the pore. Chromanol 293B is also nucleophilic (Figure 3.1C), but smaller in size, thus could adopt a variety of binding modes in the pore. The X-ray structures of K^+ channels show that the K^+ ion bound to Thr residues in the four TVGYG motifs (position 4 according to ref. (Zhou and MacKinnon, 2003)) may be accessible from the cytoplasmic side by ligands. A metal ion in the focus of macrodipoles of the pore helices (position 5) also may interact with nucleophilic ligands (Tikhonov et al., 2006).

In this work, we have built $K_v1.2$ -based models of the open $K_v1.3$ and $K_v7.1$ with potassium binding sites 2/4 or 1/3/5 loaded by K^+ ions. The respective models are named 2/4 and 1/3/5. The KcsA-based model of $K_v7.1$ was built to determine whether chromanol could favourably bind in the closed state. We further searched for the energetically optimal positions and orientations of correolide and chromanol by launching Monte Carlo-energy minimization (MCM) trajectories from a large number of random starting points. To explore whether the bulky correolide can reach the selectivity filter from the cytoplasm, we also computed profiles of MC-minimized energy of the drug pulled through the inner pore of model 2/4. Calculations predict that correolide can bind inside the pore in both models 2/4 and 1/3/5 and chelate a K^+ ion in position 4 or 5, respectively. Chromanol 293B chelates the internal-most K^+ ion in the open channel but experience ligand strain in the closed channel. Most of the experimentally detected correolide- and

chromanol-sensing residues directly interact with the drug. A large contribution to the ligand binding energy provided by a potassium ion suggests that it is an indispensable part of the correolide and chromanol receptor.

METHODS

Homology models of the pore domain of K_v1.3 and K_v7.1 that incorporate the outer helices, P-loops, and the inner helices (Table 3.1). The X-ray structure of K_v1.2 (Protein Data Bank code 2A79) was used as the template for the open state, while the X-ray structure of KcsA was the template for the closed state. All-*trans* starting conformations were assigned for those side chains that were not resolved in the crystal structures. The X-ray structure of correolide (Goetz et al., 1998) was used as a starting approximation.

The molecular modelling techniques used in this study have been previously described in Chapter 1. Hydration energy was calculated using the implicit-solvent method (Lazaridis and Karplus, 1999b). Hydration of the membrane-exposed residues of the outer helices is a methodological inadequacy. However, this does not affect results of ligand docking in the inner pore because the lipid-facing residues are rather far from the ligand, while the channel folding remained unchanged in this work. Electrostatic energy was calculated using the distance-dependent dielectric (Weiner et al., 1986). All ionizable residues in the pore domain of the K_v channels are located at the water-accessible intracellular and extracellular faces, far from ligand-sensing residues identified experimentally (Hanner et al., 2001; Lerche et al., 2007). Since these residues may be counterbalanced by counterions, they were considered in their neutral (non-ionized) forms, the approach used in other studies with the implicit solvent (Lazaridis and Karplus, 1999b; Bradley et al., 2005). Correolide and chromanol atomic charges were calculated by the AM1 method (Dewar et al., 1985) using MOPAC. Both torsional and bond angles of correolide and chromanol were allowed to vary during energy minimizations. The homology models were initially MC-minimized starting from the X-ray structures of K_v1.2 or KcsA. Following Zhou and MacKinnon (2003), the binding sites for K⁺ in the selectivity-filter region are numbered from 1 to 5 starting from the most extracellular site. In model 2/4, potassium binding sites 2 and 4 were loaded by K⁺ ions and sites 1 and 3 by water molecules. In model 1/3/5, potassium binding sites 1, 3, and 5 were loaded by K⁺ ions and sites 2 and 4 by water molecules. The above waters in potassium binding sites were the only explicit water molecules in our calculations.

The optimal positions and orientations of correolide and chromanol were searched by a random approach. In this approach, many MCM trajectories were launched starting from randomly generated positions and orientations of the drug. The area of the random search covered the entire pore region, including interfaces between domains. A systematic search was performed by computing profiles of MC-minimized energy for correolide pulled along the pore axis (Zhorov and Bregestovski, 2000). Two atom-plane

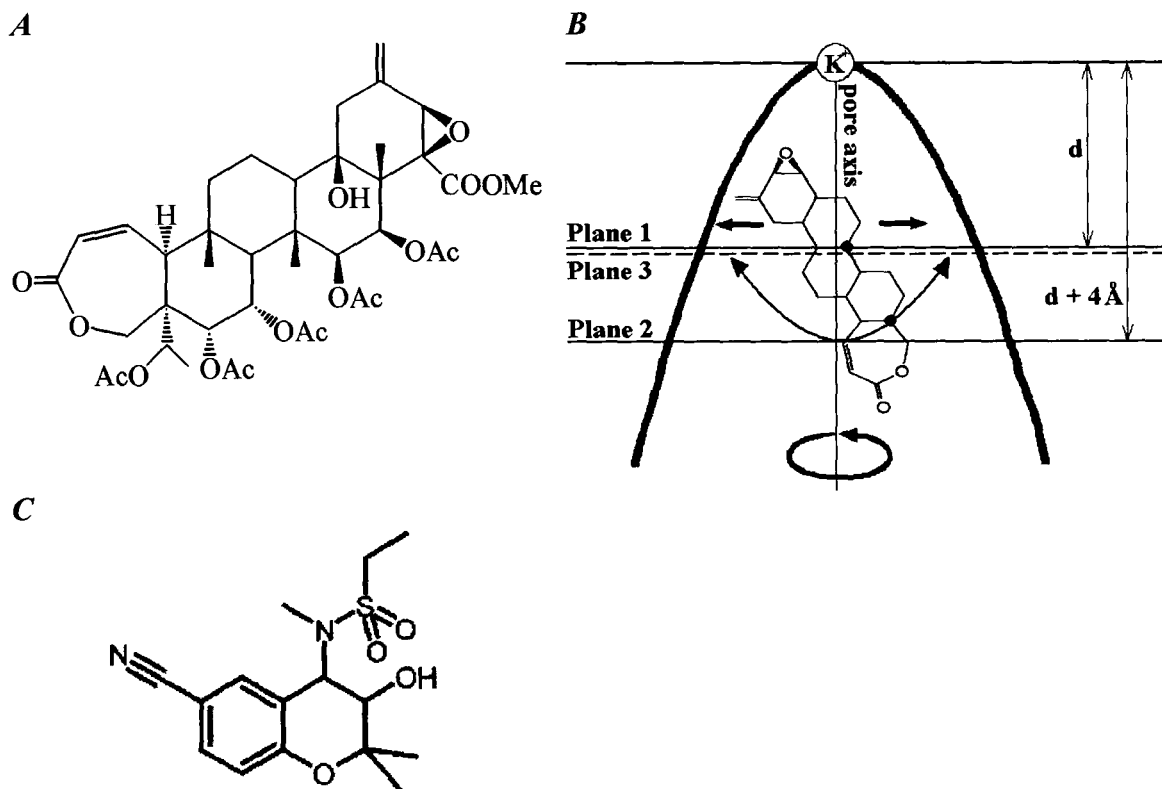


Figure 3.1. Structure of ligands. *A*, Chemical formula of correolide. *B*, Constraints used to pull correolide along the pore axis in the orientation with the epoxy group towards the selectivity filter. The inner pore is shown schematically by the thick line. K^+ ion in position 4 of the selectivity filter is shown as a sphere. A dot-designated driven atom of correolide shared by two 6-membered rings was constrained to plane 1, which is normal to the pore axis. The co-driven dot-designated atom shared by 6- and 7-membered rings was constrained between planes 2 and 3, which are farther from the selectivity filter than plane 1. All three planes were concertedly moved with the step of 0.5 \AA normally to the pore axis, and at each step the energy of the complex was MC-minimized. The driven atom retains two of the three degrees of freedom, while co-driven atom retains all three degrees of freedom, but cannot occur ahead of the driven atom. Overall, the ligand retains all internal degrees of freedom and five out of six rigid-body degrees of freedom. The curved arrows show that the ligand can turn around the pore axis and decline its long axis to the pore axis, but cannot flip-flop. A similar system of constraints was used to move correolide with its 7-membered ring towards the selectivity filter. *C*, Chemical formula of chromanol 293B. Introduction of large substituents at the sulfonyl group were reported to increase IC_{50} whereas large hydrophobic substituents at C6 of the chromane decrease the IC_{50} .

Table 3.1. Sequence alignment of K⁺ channels.

| Outer helix ^a | | 1 | 11 | 21 ^b | |
|---------------------------------|-----|------------|-------------------|------------------------|-----------|
| KcsA | 23 | ALHWRAAGAA | TVLLVIVLLA | GSYLAVLAE | |
| K _v 1.2 | 322 | KASMRELGLL | IFFLFIGVIL | FSSAVYFAE | |
| K _v 1.3 | 340 | KASMRELGLL | IFFLFIGVIL | FSSAVYFAE | |
| K _v 7.1 | 256 | FIHRQELITT | LYIGFLGLIF | SSYFVYLAE | |
| P-loop/H5 | | 33 | 41 | 51 | |
| KcsA | 59 | LITYPRAL | WWSVETATTV | GYGDLYPVT | |
| K _v 1.2 | 358 | FPSIPDAF | WWAVVSMTTV | GYGDMVPTT | |
| K _v 1.3 | 376 | FSSIPDAF | WWAVVTMTTV | GYGDMHPVT | |
| K _v 7.1 | 296 | FGSYADAL | WGWVTVTTI | GYGDKVPQT | |
| Inner helix | | 1 | 11 | 21 | 31 |
| KcsA | 86 | LWGRLVAVVV | MVAGITSEFGL | VTAALATWFBV | GREQ |
| K _v 1.2 | 385 | IGGKIVGSLC | AIAGVLTIAL | PVPVIVSNFN | YFYH |
| K _v 1.3 ^c | 403 | IGGKIVGSLC | AIAGVLTIAL | PVPVIVSNFN | YFYH |
| K _v 7.1 ^d | 323 | WVGKTIASCF | SVFAISFFAL | PAGILGSGFA | LKVQ |

^a The outer helices were aligned according to Bruhova and Zhorov (2005).

^b Relative numbering as described in Chapter 1.

^c Bold-typed are residues whose mutations change correolide binding energy by more than 1 kcal/mol (Hanner et al., 2001).

^d Chromanol-sensing residues in the inner helices of K_v7.1 are bold.

constraints were imposed to allow correolide's long axis to decline up to 90° to the pore axis, but retain the orientation of the given pole towards the selectivity filter, while the opposite pole faced the cytoplasm. For a given translational position, the driven atom was constrained to a plane normal to the pore axis and the co-driven atom between two planes normal to the pore axis (Figure 3.1B). The three planes were translated simultaneously along the pore axis with a step of 0.5 \AA , and at each step the energy was MC-minimized.

Each MCM trajectory of the ligand-channel complex was computed in two stages. In the first stage, the protein backbone and K^+ ions were fixed and energy was MC-minimized with varying protein side chains and all degrees of freedom in the ligand until the last 1000 energy minimizations did not improve the best minimum found. In the second stage, all degrees of freedom were allowed to vary, while the protein alpha carbons were constrained to the template positions using pins. A pin is a flat-bottom parabolic penalty function that allows penalty-free deviation of an atom up to 1 \AA from the corresponding position in the template and applies the force of $10 \text{ kcal mol}^{-1} \text{ \AA}^{-1}$ for further deviations. The second MCM trajectories were terminated when the last 1000 consecutive energy minimizations did not decrease the lowest energy found.

RESULTS

Correolide in the $K_v1.2$ -based model of the open $K_v1.3$

The semirigid molecule of correolide seen in the X-ray structure (Goetz et al., 1998) has the shape of a flattened ellipsoid with epoxide oxygen at one pole and carbonyl oxygen in the seven-membered ring at another. Let us define the long axis of correolide as a line drawn between the poles, which are $\sim 12 \text{ \AA}$ apart. The length of correolide is $\sim 16 \text{ \AA}$, which is defined as the distance between the most remote points at the van der Waals surfaces of the opposite poles. The length significantly exceeds the width of the open pore, which is $\sim 9 \text{ \AA}$ in $K_v1.2$. This rules out the orientation of correolide with its long axis normal to the pore axis. The molecule contains an epoxide, ester, hydroxyl, acetyl, and five acetoxo groups with a total of 16 oxygen atoms. These groups can accept up to 32 H-bonds and donate only one H-bond. This makes correolide a nucleophilic molecule. However, the nucleophilic potential of the ligand is not matched by the inner vestibule of the channel, which is predominantly lined with hydrophobic residues in the inner helices. T^{p48} and T^{p49} in the pore helices could provide H-bond donors to few oxygen atoms at the poles of correolide but not to other oxygens. The lack of chemical complementarity between correolide and the inner vestibule rules out the application of ligand-receptor constraints to bias specific orientations of the drug. Therefore, no constraints were used during the random search for the optimal binding modes of the ligand.

To predict the energetically optimal binding modes of correolide inside the 2/4 model of $K_v1.3$, 20,000 positions and orientations of the ligand were randomly generated

within a cylinder of 16 x 16 Å (Figure 3.2, *A* and *B*). From each starting point, the energy was minimized. A thousand of the lowest-energy conformations found at this stage were further MC-minimized. Six structures within 5 kcal/mol from the apparent global minimum show that correolide can adopt various positions and orientations inside the pore (Figures 3.2, *C* and *D*). The random search did not predict any low-energy complexes with the ligand in the interface between domains. In the lowest-energy complexes found, correolide interacts with the K⁺ ion in position 4, which is coordinated between the side chains and backbone oxygens of T^{p49} (Figures 3.2, *E* and *G*). Energy characteristics of the representative complexes in which correolide chelates the K⁺ ion by either the ether group in the seven-membered ring or the epoxy group are given in Table 3.2. The complexes are stabilized by van der Waals and electrostatic interactions, but do not contain intermolecular H-bonds. Table 3.1 highlights nine inner-helix residues, whose mutations affect correolide binding (Hanner et al., 2001). Seven of these residues provide contributions to the ligand-receptor energy by more than |0.4| kcal/mol (Table 3.2). In addition, T^{p48} and T^{p49} at the selectivity filter also interact with the drug, but the threonines from different domains provide either favourable or unfavourable contributions, which counterbalance each other. In the optimal complexes, oxygen atoms at the poles of the ellipsoid-shaped correolide form direct contacts with the K⁺ ion in position 4, which contributes up to -4.6 kcal/mol to the ligand-receptor energy. Several other oxygen atoms of correolide also contribute stabilizing electrostatic energy by interacting with K⁺ ions.

While docking correolide from many randomly generated starting points predicts energetically preferable binding modes, it does not allow concluding whether the binding site is reachable for correolide from the cytoplasm. Indeed, *a priori*, we could not rule out that a large energy barrier may preclude access of the bulky correolide molecule to the selectivity-filter region of K_v1.3. To address this problem, we pulled the ligand through the pore in two different orientations: with either the epoxy group or the seven-membered ring oriented towards the selectivity filter. The translational trajectories were 25 Å long to ensure a thorough sampling of the space between the cytoplasmic entry to the pore and the selectivity filter. During this search, a flat-bottom atom-plane constraint was imposed on the K⁺ ion in position 4 to allow its penalty-free displacement up to 2 Å from the level defined in the X-ray structure. Further displacements were restrained by the penalty of 10 kcal mol⁻¹ Å⁻¹. Figure 3.3*A* shows the correolide-channel energy, which was partitioned from the MC-minimized structures. As correolide moves inside the channel and makes an increasing number of favourable contacts, the ligand-receptor energy decreases (becomes more favourable). The energy reaches the minimum as the ligand binds to the K⁺ ion in position 4, which is coordinated by residues T^{p49} in the selectivity filter. Further advancement of correolide results in the energy increase due to repulsion from T^{p49}. The plots of ligand-receptor energy against correolide position in the pore do not show large energy barriers with both orientations of the drug (Figure 3.3*A*) indicating that the binding site at the selectivity filter is reachable by correolide from the cytoplasm.

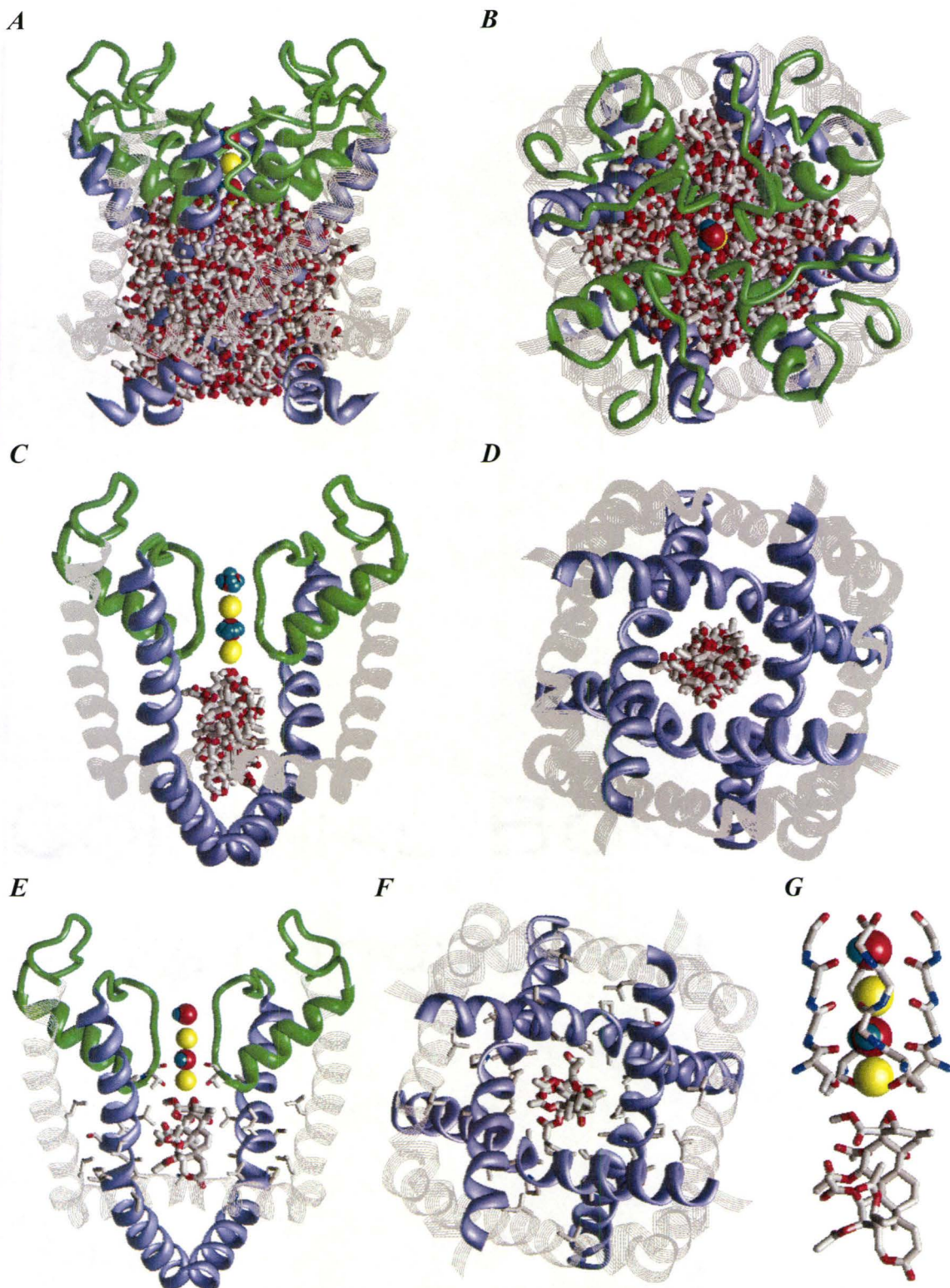


Figure 3.2. Random search for the energetically optimal binding site of correolide in model 2/4. The following colouring scheme is used: inner helices - violet ribbons; pore

helices - green ribbons; outer helices - grey strands; the selectivity-filter region and extracellular segments - green rods; K^+ ions - yellow spheres; water molecules - space filled; correolide - sticks with grey carbons and red oxygens. **A** and **B**, The side and extracellular views of 200 out of 20,000 randomly generated starting positions of correolide, in which its mass center occurred within a cylinder of 16 Å in diameter and 16 Å in length. **C** and **D**, The side and cytoplasmic views of the superposition of six lowest-energy structures found after energy minimizations from the 20,000 starting points. In the side view, only two domains are shown for clarity. In the cytoplasmic view, the P-loop domain is not shown for clarity. **E** and **F**, The structure with the most favourable ligand-receptor energy, whose characteristics are given in Table 3.2. Side chains of correolide-sensing residues found by Hanner et al. (2001) are shown as sticks. **G**, Close-up view of the complex shown at **E**. Note that two oxygen atoms of correolide, one of which from the epoxide group, bind to the K^+ ion in position 4, which is also coordinated by eight oxygen atoms from residues T^{p49}.

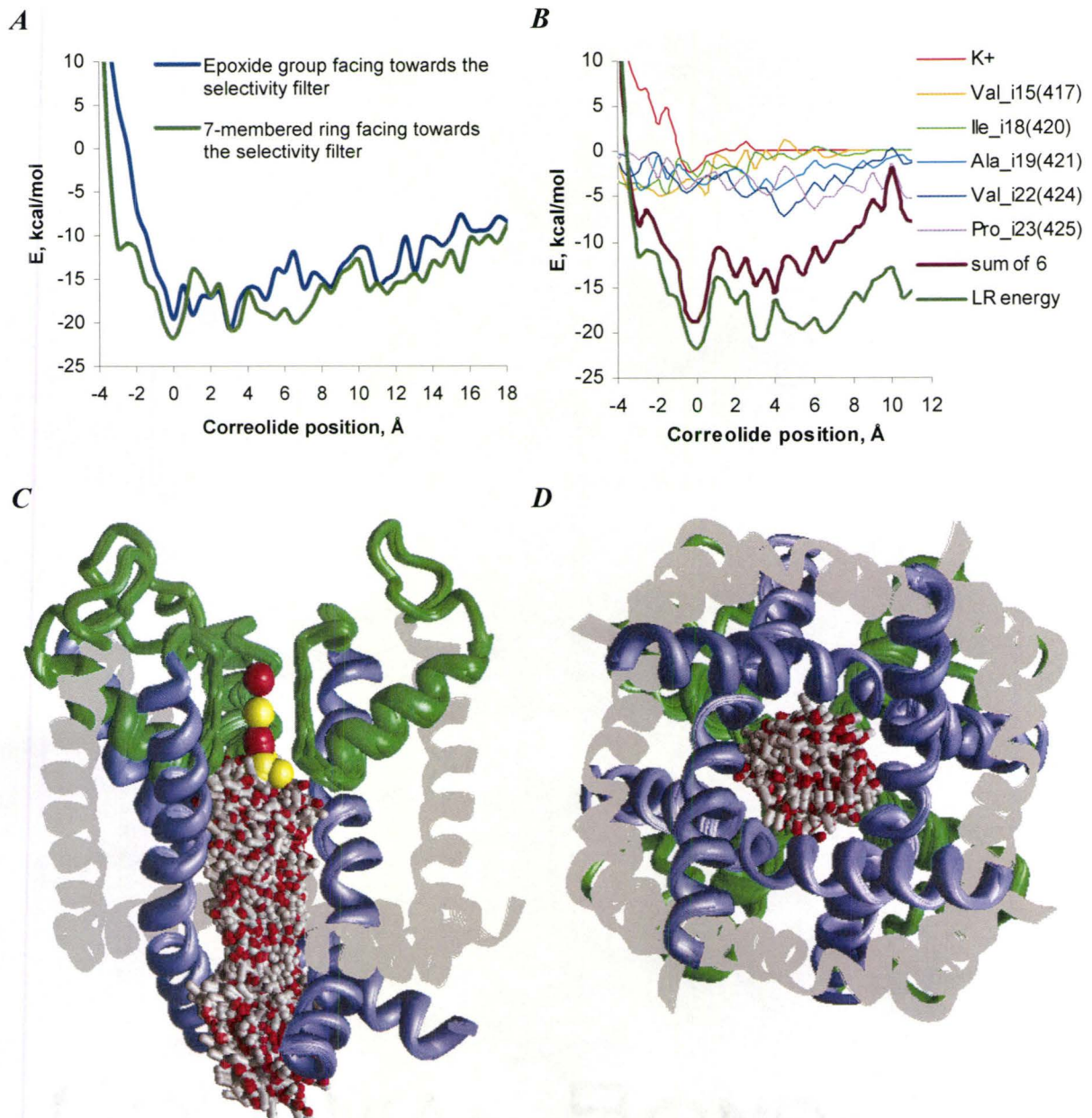


Figure 3.3. Systematic search for the energetically optimal binding site of correolide in model 2/4. *A*, Ligand-receptor energy of correolide pulled through the pore. The zero translational position is calibrated to show the complex with an oxygen atom of correolide bound to the K⁺ ion in position 4. Blue and green lines represent trajectories with the epoxy group oriented towards and away from the selectivity filter, respectively. *B*, Contributions of K⁺ ions and correolide-sensing residues revealed by Hanner et al. (2001) to the interaction energy of correolide oriented with its epoxy group away from the selectivity filter. Also included is the contribution of I¹¹⁸ whose mutation to Ala affected the channels expression. The contributions of amino acids are summed over four subunits. The energy values are partitioned from the MC-minimized structures at specific

translational positions. In most of the translational positions around the selectivity filter, the sum of six monitored contributions is close to the total ligand-receptor energy indicating that the contribution of other residues is small. At the cytoplasmic entrance to the open pore, residues Vⁱ²⁶ and Nⁱ³⁰ contribute energy to correolide binding. Residues labels include both absolute and relative numbers (Zhorov and Tikhonov, 2004). **C** and **D**, The side and cytoplasmic views of superposed MC-minimized complexes at different translational positions with the 7-membered ring facing the selectivity filter. Displacement of the K⁺ ion from the pore axis occurs at the high-energy leftmost points of the profile where correolide is forced into the selectivity filter.

As correolide approaches a residue, the stabilizing contribution of the residue to the ligand-receptor energy increases (Figure 3.3B). No inner-helix residue contributes positive energy to ligand-receptor interactions, indicating that unfavourable contacts, which are unavoidable in the starting conformations, have been relaxed in MC-minimizations. The plot of partitioned ligand-receptor energy (Figure 3.3B) shows that K⁺ ion in position 4 contributes ~ 2.5 kcal/mol to ligand-receptor energy. This energy is weaker than the contribution of -4.6 kcal/mol found during the random search because the ligand is constrained to the plane normal to the pore axis at each point of the profile and cannot establish optimal interactions with the ion. As correolide approaches the selectivity filter, the total contribution of the K⁺ ion and the pore-facing correolide-sensing residues identified in mutational experiments (Hanner et al., 2001) is close to the entire ligand-receptor energy (Figure 3.3B). L⁰⁷ and Vⁱ²⁶ stabilize correolide at the entry to the inner pore. Interestingly, L⁰⁷ was detected as a correolide-sensing residue in mutational experiments (Hanner et al., 2001).

A metal ion in the focus of macrodipoles of the pore helices (position 5) was proposed to play a crucial role in the binding of benzocaine to Na⁺ channels (Tikhonov et al., 2006). To explore a similar possibility in K_v1.3, we performed a random search of correolide binding modes in model 1/3/5. The low-energy structures are shown in Figure 3.4 and their energy characteristics are given in Table 3.2. Since K⁺ ion in position 5 does not interact directly with the channel residues, a large part of its surface is available for chelation by the ligand. Indeed, an interesting binding mode was found with three acetoxy groups chelating the K⁺ ion (Figure 3.4 C-E). In this mode, neither the epoxy group nor the seven-membered ring interacts with K⁺. Such a binding mode may explain why elimination of the above moieties does not abolish the channel-blocking activity of correolide (Bao et al., 2005). The same correolide-sensing residues that contribute to correolide binding in model 2/4 also contribute to ligand binding in model 1/3/5 (Table 3.2). The ligand-receptor energies in model 1/3/5 are only 1 – 2 kcal/mol more preferable than in model 2/4 (Table 3.2). The small energy difference does not allow us to favour model 1/3/5 over model 2/4. However, we cannot rule out that both binding modes may coexist.

Thus, our calculations predict several binding modes of correolide in K_v1.3. The population of these modes would depend on the pattern in which K⁺ binding sites are occupied by K⁺ ions and water molecules. When position 4 is occupied by K⁺, both the random and systematic MCM search predict the selectivity-filter region to be an important structural determinant of the correolide receptor (Figures 3.2 and 3.3). When position 5 is occupied by the K⁺ ion, correolide would readily bind it, providing up to three oxygens to the K⁺ coordination sphere (Figure 3.4).

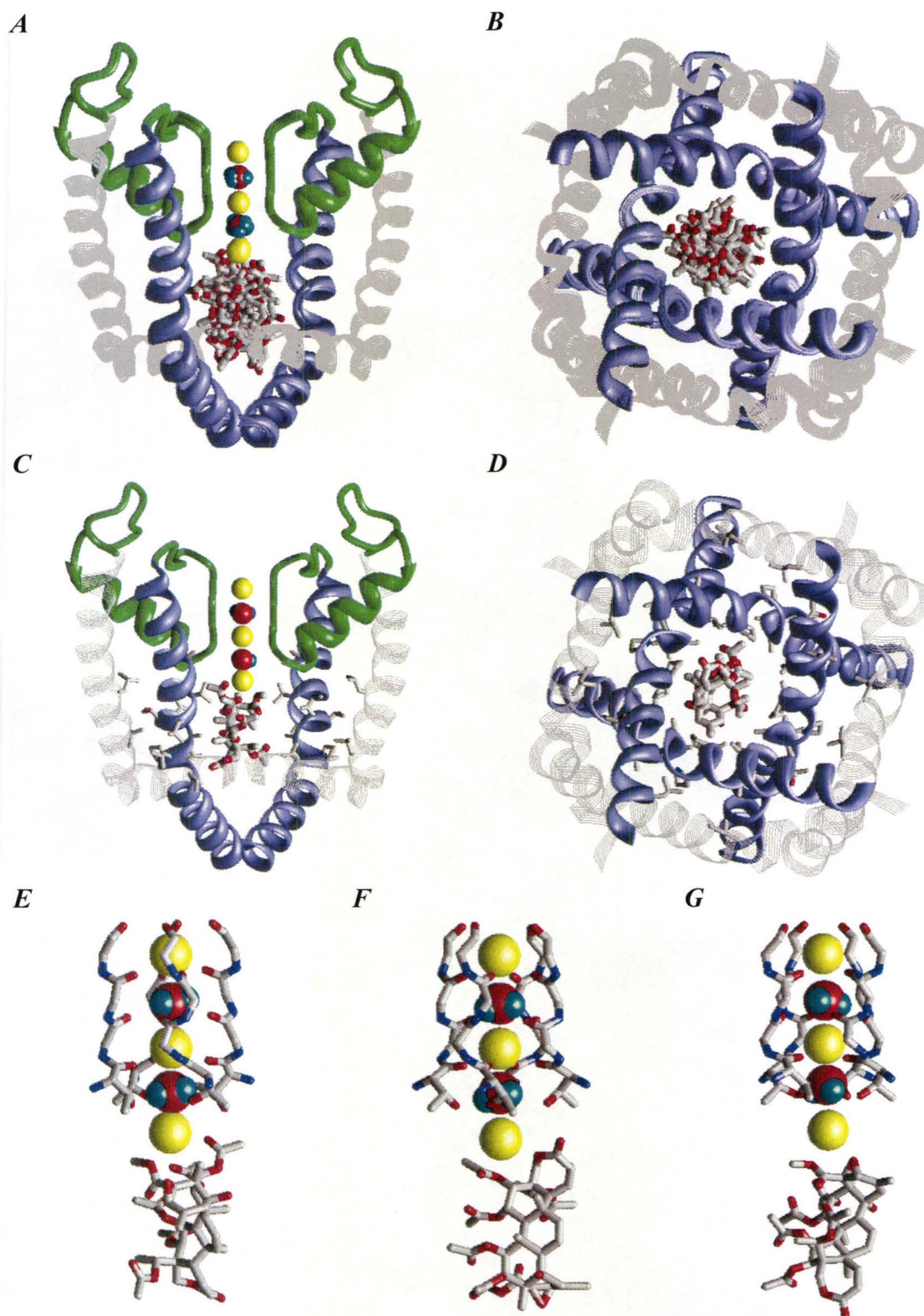


Figure 3.4. Correalide in model 1/3/5 of Kv1.3. *A* and *B*, The side and extracellular views of 12 energetically best structures obtained from 20,000 randomly generated

starting positions of correolide, in which its mass center occurred within a cylinder of 16 Å in diameter and 16 Å in length. **C** and **D**, The lowest-energy binding mode of correolide with 3 acetoxy groups chelating K⁺ ion in position 5. Side chains of correolide-sensing residues found by Hanner et al. (2001) are shown as sticks. **E-G**, The close-up view at structures with the most favourable ligand-receptor energy, whose characteristics are given in Table 3.2. The K⁺ ion in position 5 is chelated by three acetoxy groups (**E**), an acetoxy group and the ether group from the seven-membered ring (**F**), and epoxy and acetyl groups (**G**).

Table 3.2. Correolide-sensing residues in the inner helices^a and their energy contributions^b (kcal/mol) to correolide binding

| Mutations | K _v 1.3 model and K ⁺ -chelating groups of correolide | | | | |
|---|---|--------------------|-------|--------------------|----------------------|
| | 2/4 | | 1/3/5 | | |
| Inner-helix mutations affecting correolide binding ^a | Epoxy | Ether ^c | Epoxy | Ether ^c | Acetoxy ^d |
| A ⁱ¹¹ C | | | | | |
| V ⁱ¹⁵ A | -2.6 | -3.1 | -2.3 | -2.6 | -2.5 |
| L ⁱ¹⁶ A | -1.4 | -0.9 | -1.8 | -1.9 | -1.7 |
| T ⁱ¹⁷ A | | | -0.6 | -0.4 | |
| A ⁱ¹⁹ C | -4.2 | -2.5 | -1.8 | -5.0 | -2.0 |
| L ⁱ²⁰ A | -0.9 | -0.4 | 1.2 | -2.1 | -0.6 |
| P ⁱ²¹ A | | -1.0 | | -1.2 | |
| V ⁱ²² A | -2.2 | -4.7 | -4.2 | -2.8 | -4.5 |
| P ⁱ²³ A | -1.0 | -4.4 | -3.7 | -1.7 | |
| Mutations affecting channel expression ^e | | | | | |
| I ⁱ¹⁸ A | -5.1 | -1.3 | -0.6 | -0.8 | -1.8 |
| Predicted ligand-receptor energy | -20.6 | -20.3 | -19.1 | -22.4 | -21.9 |

^a Mutations that change correolide binding energy by more than 1 kcal/mol (Hanner et al., 2001).

^b A number represents interaction energy of correolide with the residue, which provides the strongest contribution among matching residues in the four domains. Contributions with the absolute energy less than 0.3 kcal/mol are not shown.

^c Ether group from the seven-membered ring

^d Three acetoxy groups (Figure 3.4E).

^e Iⁱ¹⁸ contributes to correolide binding in our models, but is not categorized as a correolide-sensing residues because its mutation results in poor expression of the channel (Hanner et al., 2001).

Chromanol 293B in the KcsA- and K_v1.2-based model of the closed and open K_v7.1

The chromanol 293B molecule possesses a chroman scaffold to which an electron withdrawing cyano group is attached at the aromatic ring, which renders the molecule highly lipophilic, thereby favouring interactions with aromatic ring systems and hydrophobic side chains. The X-ray coordinates of KcsA and K_v1.2 crystal structures were used to construct homology models of the closed and open K_v7.1 pore, respectively (based on the protein sequence alignment shown in Table 3.1), and subsequently docked chromanol 293B into the pore models. Since previous work on state-dependent binding of chromanol suggested a preferential open channel block mechanism (Seeböhm et al., 2001), we first investigated the open pore conformation. Twenty thousand orientations of the ligand were randomly sampled in the K_v1.2-based model of the open K_v7.1 channel pore (Figure 3.5, *A* and *B*). Several ligand-receptor complexes were found with the ligand-receptor energy within 5 kcal/mol from the apparent global minimum (Figure 3.5, *C* and *D*). In these energetically most favoured complexes, the largest stabilizing contribution to the binding of chromanol is provided by the K⁺ ion in position 4. In some complexes, the K⁺ ion interacts with either the SO₂ or the OH group of the ligand. In the apparent global-minimum complex, both groups chelate the K⁺ ion (Figure 3.5, *E* and *F*) that provides -14.1 kcal/mol to the binding energy. In addition to the interaction with K⁺, the ligand is stabilized by pore-facing residues Iⁱ¹⁵ and Fⁱ¹⁸ (Figure 3.5, *E* and *F*; Table 3.3). In addition, chromanol also favourably interacts with T^{p48} and T^{p49} in the selectivity filter (Table 3.3). When summed over four domains, the energy of interactions of chromanol with T^{p49} was negative (attractive), but energy contributions of residues from individual domains varied between -2.2 and +1.9 kcal/mol (Table 3.3). The repulsion between T^{p49} in two domains and chromanol is not a result of poor optimization; rather, it is caused by a strong attraction of the ligand to K⁺ in position 4.

Structure-activity relationships of chromanol analogs (Gerlach et al., 2001) revealed that replacement of the cyano group by large bulky groups produces more active compounds, showing that it is not an indispensable determinant of chromanol activity. In our model, the cyano group faces either the cytoplasmic side or the interdomain space, suggesting that its replacement with a larger alkyl group would increase van der Waals interactions without affecting the tertiary complex between the oxygen atoms of the drug, the K⁺ ion in position 4, and residues of the channel.

The docking model strongly suggests that interactions of chromanol 293B mainly take place with amino acids T^{p49}, Iⁱ¹⁵, and Fⁱ¹⁸ as well as a K⁺ ion in the selectivity filter, indicating that observed changes in chromanol blocking capability by mutation of other amino acids (amino acids *i13*, *i14*, *i16*, and *i17*) rather occurred as an indirect result from induced structural changes of the potassium channel protein.

We next explored the possibility of chromanol binding to the KcsA-based model of the closed (resting) K_v7.1 channel. Again, after randomly sampling of 20,000 orientations of the ligand, the energetically most favourable binding mode of chromanol

was found to be inside the water-lake cavity (Figure 3.5, *G* and *H*). As in the open channel pore, the largest contributions to the ligand-receptor energy are provided by the K^+ ion in position 4 and residues I^{115} and F^{118} (Table 3.3). Despite the favourable (negative) ligand-receptor energy, the ligand experienced strains inside the inner cavity, implying that the latter is too small to accommodate a chromanol molecule. However, because the overall ligand-binding energy of chromanol is negative, we cannot completely rule out the possibility that the ligand can bind inside the closed channel, although our combined results rather favour binding inside the open channel.

Sensitivity of results to the chosen computational methodology

The goals of this study were to predict the binding site for two nucleophilic ligands and to explore whether the K^+ ion could contribute to the correolide receptor. To perform the extensive search for the lowest-energy complexes between K_v channel and ligand, we used several approximations: rather small cutoff of 8 Å, implicit solvent, simple treatment of the electrostatic interactions, and neutral forms of ionizable residues. Such approximations are hardly acceptable in computational studies aimed to predict the free energy of ligand binding or simulate ion permeation. However, results of the receptor mapping are less critical to the method of energy calculation. Indeed, in the lowest-energy complexes, ligand appears to fit in the inner pore. The geometry of the tight ligand-channel complex is defined primarily by the van der Waals energy, which is reliably predicted with different force fields. Nevertheless, to assess the sensitivity of our results to variations in methodological setup, we re-evaluated the geometry and energy of the correolide complex with model 2/4 by submitting additional MCM trajectories starting from the optimal structure predicted in the random search (Figure 3.2). The additional MCM trajectories were run with a larger cutoff, ionized titrable residues, weaker electrostatics, and K^+ ion removed from position 2.

Results show that the geometry of the MC-minimized structures remains practically unchanged under different methodological setups (Figure 3.6). Among the different methodological settings that could potentially affect the ligand-receptor energy, only reduced electrostatic interactions weakened the ligand-receptor energy, which nevertheless remained preferable (Table 3.4). The involvement of a K^+ ion in correolide binding is the most important prediction, which is insensitive to the variations of methodology. Indeed, correolide does not bring charged or ionizable groups to the selectivity filter, but just replaces one to three water molecules from the cytoplasmic face of a K^+ ion at the pore axis.

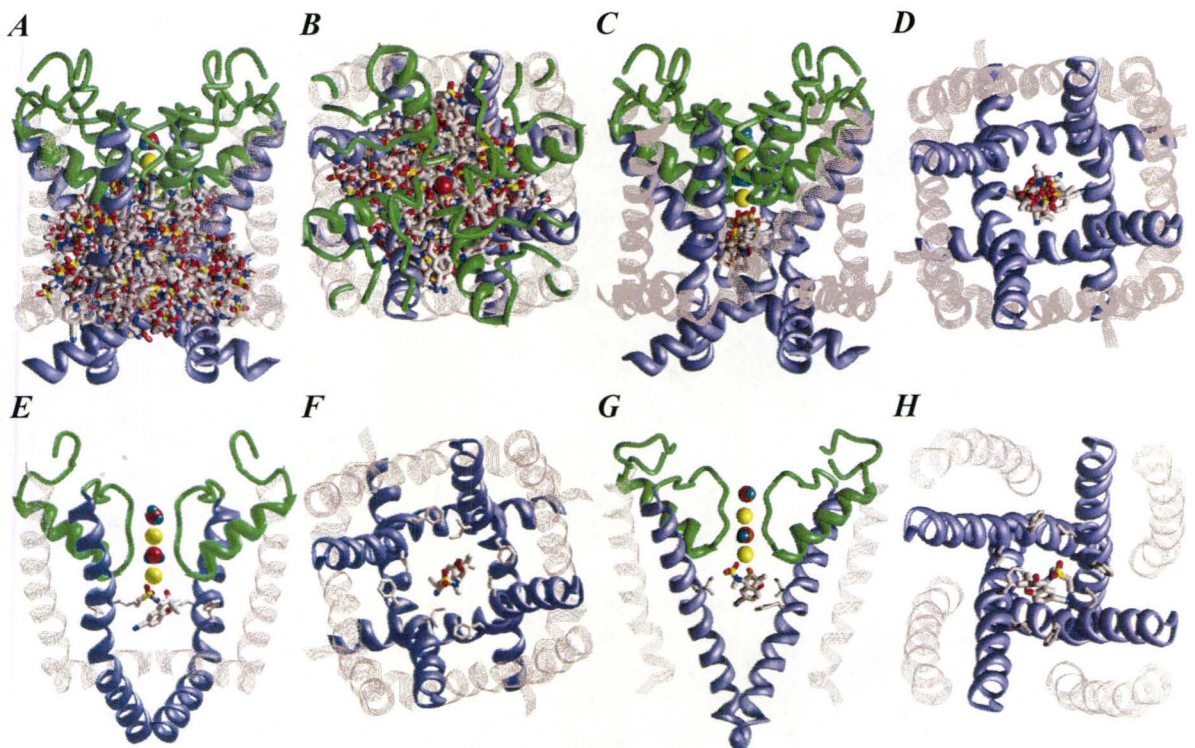


Figure 3.5. Random search for the energetically optimal binding site of chromanol in the open and closed $K_v7.1$ models. *A – F*, Open channel model of $K_v7.1$ based on the $K_v1.2$ X-ray structure. *A* and *B*, Side and top views of randomly placing chromanol inside the channel (only 200 of 20,000 positions are shown). *C* and *D*, Superposition of the five most energetically favourable binding modes of chromanol inside the $K_v7.1$ channel. *E* and *F*, Typical low-energy binding mode of chromanol inside the channel. Residues I^{115} and F^{118} are shown as sticks. *G* and *H*, Typical low-energy binding mode of chromanol inside the closed channel model of $K_v7.1$ derived from the $KcsA$ X-ray structure. For clarity, hydrogen atoms are not shown. Only inner and outer helices of two subunits are shown in *E* and *G*, and of four subunits in *F* and *H*.

Table 3.3. Energy components (kcal/mol) of the most energetically favourable complexes of chromanol inside K_v7.1

| Energy component | Open channel | Closed channel |
|---|------------------------------|------------------------------|
| Ligand-receptor components | | |
| van der Waals | -5.1 | -13.8 |
| Electrostatic | -26.7 | -30.4 |
| Solvation | 12.2 | 14.8 |
| Ligand components | | |
| Intra-ligand nonbonded ^a | -9.6 | 0.6 |
| Ligand strain ^b | 9.0 | 16.2 |
| Total | -20.2 | -12.6 |
| Major contributors to ligand binding energy ^c | | |
| K ⁺ in position 4 | -14.1 | -13.3 |
| H ₂ O in position 3 | -1.4 | -2.3 |
| T ^{p48} | -0.8 | -4.9 |
| T ^{p49} | -1.9 (-2.2/1.9) ^d | -1.8 (-4.7/4.6) ^d |
| I ⁱ¹⁵ | -2.4 | -3.6 |
| F ⁱ¹⁸ | -0.8 | -5.8 |

^a The sum of atom-atom interactions of the ligand

^b The sum of energy of deformation of bond angles plus torsional energy of the ligand.

^c The energy contribution of a residue to ligand binding is summed over four subunits.

^d The first number is the sum of contributions from the four domains. The values in brackets show the minimal and the maximal contributions from individual domains.

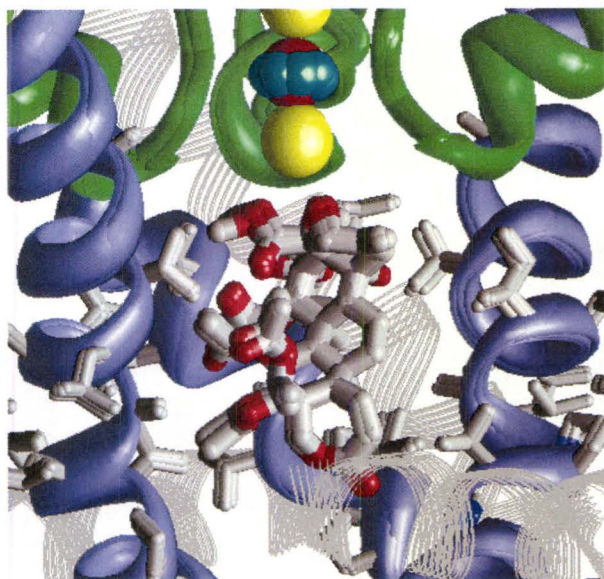


Figure 3.6. K_v1.3:correolide models calculated with different settings. Superimposed models calculated with different methodological settings (Table 3.4). Correolide-sensing residues are shown as sticks.

Table 3.4. Ligand-receptor energy predicted with various methodological setup ^a

| Variations in the methodological setup ^b | Ligand-receptor energy (kcal/mol) |
|--|-----------------------------------|
| Standard protocol (see methods) | -20.6 |
| Cutoff, 12 Å | -22.0 |
| Electrostatics, $\epsilon = 2$ d | -13.6 |
| 1,4 occupancy of selectivity-filter by K ⁺ ions | -22.1 |
| Ionized titrable residues | -23.4 |

^a Calculations were performed in the K_v1.2-based model 2/4 with correolide bound with the epoxy group towards the selectivity filter. Each value of the ligand-receptor energy was obtained in an MCM trajectory that started from the best structure found by the random search (Figure 3.2E) and terminated when the last 1000 energy minimizations did not decrease the energy of the apparent global minimum found.

^b Only deviations from the standard protocol are indicated

DISCUSSION

Various naturally occurring and synthetic compounds targeting K_v channels have been characterized (Kaczorowski and Garcia, 1999). Classical blockers of K^+ channels such as tetraethylammonium and peptidyl toxins lack selectivity to different subtypes of K^+ channels. Small-molecule blockers selectively targeting specific K_v channels are valuable tools for basic studies and have large potential as pharmaceuticals. $K_v1.3$ and $K_v7.1$ channels are important targets for drug discovery. Understanding the mechanism of correolide and chromanol block could help develop other immunosuppressants and antiarrhythmics drugs as well as selective blockers of various K_v channels.

Little structural information is available on the complexes of small-molecule ligands with P-loop channels. The crystallographic structure of a ligand-bound KcsA (Zhou et al., 2001a; Lenaeus et al., 2005) shows TBA trapped in the water-lake cavity with the center of the ammonium group being near to the focus of four macrodipoles of the pore helices. Unlike TBA, correolide and chromanol are electrically neutral ligand with numerous nucleophilic groups. Mutational studies revealed that the inner helices residues are associated with the binding of correolide (Hanner et al., 2001) and chromanol (Lerche et al., 2007), but did not explain the causes of high-affinity binding of the drug. Furthermore, all correolide-sensing residues revealed in study (Hanner et al., 2001) cannot bind simultaneously to the drug in any reasonable model of the ion channel. Therefore, the three-dimensional mapping of the receptor of correolide and chromanol was one of the aims of our study.

Correolide-sensing residues

Hanner et al. (2001) revealed nine residues in the inner helices, whose mutation changes correolide binding energy by more than 1 kcal/mol (Table 3.2). Five of these residues face the inner pore (Figure 3.7) and provide noticeable energy to correolide binding in both 2/4 and 1/3/5 models of $K_v1.3$ (Table 3.2). Why the remaining four residues in the inner helices affect correolide binding in experiments but not in the model? One of these residues is A^{i11} whose substitution with Cys affects correolide binding in mutational experiments (Hanner et al., 2001). However, A^{i11} does not contribute to correolide-binding energy (Table 3.2). The cause may be that A^{i11} approaches V^{p50} in the selectivity filter. The substitution of A^{i11} with a larger Cys may affect the selectivity filter structure and interaction of correolide with a K^+ ion at the selectivity filter. Ogielska and Aldrich (1998) found that the $A^{i11}C$ mutation in $K_v1.3$ decreases the affinity for K^+ ions, possibly due to conformational changes of residues involved in the selectivity filter. In view of our model, these data support the notion that a K^+ ion at the selectivity filter can stabilize correolide binding.

The mutation of P^{i21} in the PVP motif of the inner helix affects correolide binding, however P^{i21} does not provide noticeable contribution to the ligand-receptor energy in three ligand-binding modes characterized in Table 3.2. The substitution of P^{i21} could

decrease the flexibility of the inner helix by enabling the backbone NH group in this position to form an H-bond with carbonyl oxygens in positions *i17-i18*. This may change the orientation of Vⁱ²² and Pⁱ²³ residues that affect correolide binding in both experiments and computational models (Table 3.2).

According to our model, Iⁱ¹⁸ contributes to correolide binding (Table 3.2). However, experimental data on the involvement of Iⁱ¹⁸ in correolide binding are not available. The mutation Iⁱ¹⁸A results in the low expression of K_v1.3 (Hanner et al., 2001) indicating that large hydrophobic Ile is involved in the stabilization of the wild type channel structure. Such stabilization is more likely if the side chains of Iⁱ¹⁸ interact with other transmembrane helices rather than face the pore. Indeed, in the K_v1.2-based model, Iⁱ¹⁸ is exposed to the inter-segment interface (Figure 3.7).

Chromanol-sensing residues

Using a chimera and single-point mutational approach Seeböhm's group (Lerche et al., 2007) identify residues in the S6 transmembrane domain (Iⁱ¹⁵, Fⁱ¹⁸) and lower selectivity filter (T^{p49}) of the channel as crucial determinants of chromanol sensitivity, strongly suggesting that the chromanol receptor is located in the central pore cavity. To corroborate these experimental findings, we performed homology modeling and unbiased docking of chromanol in the closed and open K_v7.1 channels by generating a large number of starting conformations and energy-optimizing them. The obtained results confirm the mutagenesis data and propose that residues Iⁱ¹⁵ and Fⁱ¹⁸ essentially contribute to the ligand-receptor complex. It is noteworthy that nearby conservative exchanges Fⁱ¹³Y, Aⁱ¹⁴T, Sⁱ¹⁶T, and Fⁱ¹⁷Y also caused a significant reduction of chromanol sensitivity. However, we believe that these exchanges rather alter the sterical configuration of the neighbouring crucial residues Iⁱ¹⁵ and Fⁱ¹⁸, and/or hinder the access of chromanol to the binding site. To support this notion and the importance of the hydrophobic interactions with the cavity wall, we modeled the Fⁱ¹⁸A mutant and then calculated the total energy of the ligand-receptor complex in this mutated channel. The obtained ligand-receptor energy of chromanol was -17.8 kcal/mol, which indicates a significantly weaker binding as in the wild-type channel (-20.2 kcal/mol).

Possible involvement of K⁺ in the binding of nucleophilic ligands

We found that the K⁺ ion at the selectivity filter is an indispensable determinant of the binding of nucleophilic ligands, such as correolide and chromanol. This suggests the formation of a tertiary complex between the ligand, the permeating K⁺ ion, and residues facing the cavity of the channel. Correolide is much larger than chromanol 293B, but both drugs share common features that allow them to bind with high affinity to K⁺ channels. These include the ellipsoid-like shape with nucleophilic groups at the poles and hydrophobic sides. The drugs can reach the K⁺ ion bound to the cytoplasmic side of the selectivity filter by their polar groups, whereas their hydrophobic sides engage hydrophobic interactions with the predominantly hydrophobic inner helices.

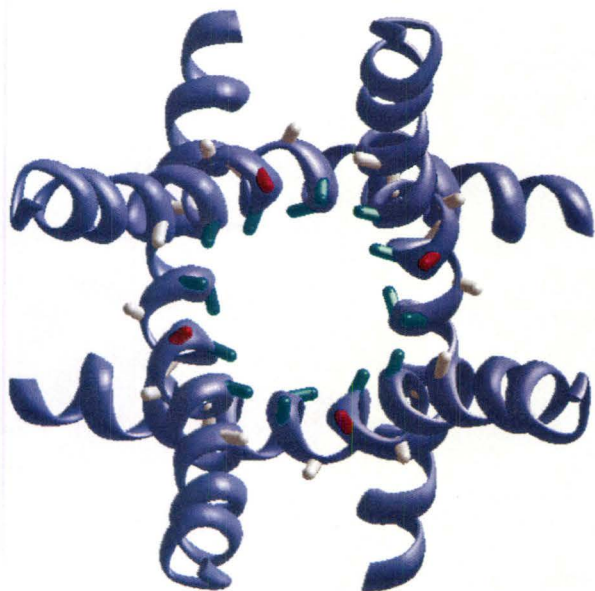


Figure 3.7. The extracellular view at the inner-helices bundle in the open K_v1.3. Bonds C^α-C^β in correolide-sensing residues (Hanner et al., 2001) are shown as either cyan sticks that face the pore or gray sticks directed away from the pore. Red sticks show bonds C^α-C^β in I¹¹⁸, the residue whose mutation to Ala results in low expression of K_v1.3 and altering the channel conformation (Hanner et al., 2001). Four correolide sensing residues face the pore, while I¹¹⁸ could stabilize the channel conformation by interacting with the outer helices, which are not shown.

The hydrophobic and electrostatic interactions of correolide and chromanol binding to the K^+ channel may ultimately disturb the coordination of the permeating potassium ions in the cavity and in the selectivity filter, which is of vital importance for ion conduction (Doyle et al., 1998; Roux and MacKinnon, 1999; Zhou and MacKinnon, 2004a; Zhou and MacKinnon, 2004b). Mutations adversely affecting chromanol block are consistently located in the inner pore or at the base of the selectivity filter. In particular, the threonines at the base of the selectivity filter (T^{p49} in $K_v7.1$) are involved in the formation of K^+ -binding site 4. Furthermore, blocking activity of (3R,4S)-chromanol mildly increased at low extracellular potassium (IC_{50} at high extracellular K^+ , $10 \pm 2 \mu M$; IC_{50} at low extracellular K^+ , $16 \pm 4 \mu M$; (Seeböhm et al., 2001)).

Correolide binds to $K_v1.3$ and $K_v1.4$ channels with a higher affinity than to other channels of the K_v1 family (Hanner et al., 1999). Since the inner and outer helices are conserved in K_v1 channels, correolide-sensing residues in these helices are unlikely to determine correolide selectivity to $K_v1.3$ and $K_v1.4$. What distinguishes the latter channels is C-type inactivation, which is less pronounced in other members of the K_v1 family. How could C-type inactivation enhance correolide binding? A recent study suggested that C-type inactivation might be caused by the rearrangement of the selectivity filter in a way that the K^+ in position 4 remains the only cation in the selectivity-filter region (Lenaeus et al., 2005). Our models 2/4 and 1/3/5 predict the strong involvement of a K^+ ion in correolide binding. In C-type inactivated channels, a deficiency of K^+ ions in positions 1 – 3 would stabilize the K^+ -bound correolide. Some analogy may be found in a ligand containing an ionizable amino group. When a proton binds to the group, the proton-ligand complex is considered as a protonated ligand, even when the proton is shared with a nucleophilic group of the receptor. Similarly, when a ligand binds K^+ , the complex may be considered as a K^+ -containing ligand that would bind stronger to the channels, in which potassium-binding sites 1 - 3 are not occupied by K^+ ions. This can explain the intriguing observations that the C-type inactivation enhances binding of both cationic and nucleophilic ligands in the inner pore of K^+ channels.

CONCLUSION

In this study we predicted that two nucleophilic K^+ channel blockers, correolide and chromanol, form a ternary complex between K^+ ion and K^+ channel. We suggested deficiency of K^+ ions at the selectivity filter would increase the affinity for chromanol and correolide binding to K^+ channels. Along these lines, we suggested a mechanism by which C-type inactivation could enhance correolide binding. The analysis of structure-activity relationships of open-channel blockers of K^+ channels shows that many blockers have nucleophilic groups whose role seems unclear given the rather hydrophobic structure of the open pore. Our study suggests that such groups can bind to the channel-bound K^+ ions, which may be important determinants of corresponding receptors.

CHAPTER FOUR

K_v1.2-BASED MODEL OF A CALCIUM CHANNEL IS CONSISTENT WITH AVAILABLE SCAM DATA

ABSTRACT

In the absence of X-ray structures of Ca^{2+} channels, their homology models can be used to interpret experimental data and design new experiments. Modeling relies on sequence alignments between Ca^{2+} and K^+ channels. Zhen et al. (2005) employed the substituted cysteine accessibility method (SCAM) to identify pore-lining residues in the $\text{Ca}_v2.1$ channel and concluded that their data are inconsistent with the symmetric architecture of the pore domain and published sequence alignments between Ca^{2+} and K^+ channels. Here we have built $\text{K}_v1.2$ -based models of $\text{Ca}_v2.1$ with MTSET-substituted engineered cysteines and used Monte Carlo-energy minimizations to predict their energetically optimal orientations. We found that depending on the sequential position of an engineered cysteine in transmembrane helices of the pore domain, the long flexible MTSET-modified side chain can orient into the inner pore, an interface between neighbouring S6 helices, or an interface between S5 and S6 helices. The predicted distances of the ammonium groups to the pore axis correlate with the reported effects of MTSET on the current. Our calculations rationalize the SCAM data, validate one of several published sequence alignments between Ca^{2+} and K^+ channels, and suggest similar spatial dispositions of S5 and S6 helices in voltage-gated K^+ and Ca^{2+} channels.

INTRODUCTION

Voltage-gated Ca^{2+} channels are membrane proteins responsible for variety of functions including shaping of action potentials and controlling intracellular concentration of Ca^{2+} (Hille, 2001). Ca^{2+} channels are targets for drugs used to treat arrhythmias, hypertension, myocardial ischemia, chronic pain, neuronal degeneration, and other disorders (Hockerman et al., 1997). In the absence of X-ray structures of voltage-gated Ca^{2+} and Na^{2+} channels, homology models based on X-ray structures of K^+ channels in the closed and open states (Doyle et al., 1998; Long et al., 2005b) are used to interpret experimental data and suggest new experiments. The homology modeling depends on the sequence alignments of K^+ channels with Na^+ and Ca^{2+} channels. Various sequence alignments have been proposed (Huber et al., 2000; Zhorov et al., 2001; Lipkind and Fozzard, 2003; Stary et al., 2008). The models of the pore-forming domain (S5-P-S6) based on these alignments have different patterns of exposure of residues to the inner pore. The substituted-cysteine accessibility method (SCAM) can be used to experimentally estimate the exposure of individual residues to the ion-permeation pathways (Karlin and Akabas, 1998). The SCAM experiments on ion channels are usually interpreted based on the cysteine-orientation concept. This is where application of the methanethiosulfonate (MTS) reagent to a channel with an engineered cysteine in a pore-facing position results in the chemical modification of the cysteine. If the ammonium group of the MTS-modified cysteine is exposed to the permeation pathway, it is expected to block the current. The orientation of the engineered cysteine towards the lipid bilayer or the protein interior is believed to suppress ionization of the thiol group and its reaction

with an MTS reagent. The current in such channels is expected to be similar to control channels with native residue in respective position.

The SCAM method was used to predict the location of the activation gate in the *Shaker* channel (Liu et al., 1997) and the major conclusions from this study were confirmed by the X-ray structures of K^+ channels. More recently, the SCAM method was used to identify pore-lining residues in the $Ca_v2.1$ channel (Zhen et al., 2005). The authors of this meticulous study interpret their results as inconsistent with known sequence alignments between K^+ and Ca^{2+} channels and suggest an asymmetric architecture of the inner pore of $Ca_v2.1$. This conclusion sheds doubts on published homology models of Ca^{2+} channels. The above interpretation of the SCAM experiments is based on the expected orientation of the modified cysteine residues, and does not consider that long flexible side chains of MTS-modified cysteines may adopt various conformations. Due to this conformational flexibility, the exposure of the MTS ammonium groups to the permeation pathway and hence the current-blocking effect of MTS may not correlate with the orientation of the C^α - C^β vector to the pore axis. Such possibilities can be explored by homology modeling of the channel with MTS-modified cysteines and energy optimization.

In this study, we have built a total of 42 $Ca_v2.1$ models with MTS-modified engineered cysteines and applied Monte Carlo minimizations to predict energetically possible orientations of MTS-modified side chains in the channels. We found that the energetically preferable positions of the ammonium groups of MTS-modified cysteines relative to the permeation pathway do not necessarily correlate with the orientation of the C^α - C^β vector to the pore axis. Instead, the distance of the ammonium nitrogen to the pore axis correlates with the observed currents in the respective channels. Our results supports the alignment between K^+ and Ca^{2+} channels used in our previous modeling studies and suggest a similar disposition of transmembrane helices in the pore-forming domains of voltage-gated K^+ and Ca^{2+} channels.

METHODS

The model of the rabbit PQ-type Ca^{2+} channel ($Ca_v2.1$, CAC1A_RABIT) includes the outer helices (S5), P-loops (P), and inner helices (S6). The alignment between K^+ , Na^+ , and Ca^{2+} proposed for the outer (Huber et al., 2000) and inner (Zhorov et al., 2001) helices is shown in Table 4.1. The S5, S6, and P-helices were built based on the X-ray structure of $K_v1.2$ (Long et al., 2005a). The ascending limbs of P-loops including the selectivity filter were built using the $Na_v1.4$ model (Tikhonov and Zhorov, 2005a) as a template. Those parts of the channel, which are far from the inner pore, were not modeled. Assuming that ionized residues are complexed with counterions, we modeled all ionizable residues, including those in the selectivity filter, in their neutral forms.

Table 4.1. Sequence alignment between K⁺, Na⁺, and Ca²⁺ channels and effects of MTS reagents on Cys mutant channels^a

| Channel | Segment ^b | | # | 1 | 11 | 21 ^c | | | |
|---------------------------|----------------------|----|------|-------------|-------------|-----------------|----|-----|----|
| KcsA | M1 | o | 23 | ALHWRAAGAA | TVLLVIVLLA | GSYLAVLAER | | | |
| K _v 1.2 | S5 | o | 322 | KASMRELGLL | IFFLFIGVIL | FSSAVYFAEA | | | |
| Ca _v 2.1 | IS5 | 1o | 220 | MKAMIPLLQI | GLLLFFAILI | FAIIGLEFYM | | | |
| | IIS5 | 2o | 608 | LNSMKSIIISL | LFLFLFIVV | FALLGMQLFG | d | | |
| | IIIS5 | 3o | 1380 | VNSLKNVFNI | LIVYMLFMFI | FAVVAVQLFK | d | | |
| | IVS5 | 4o | 1695 | VQSFKALPYV | CLLIAMLFFI | YAIIGMQVFG | d | | |
| Na _v 1.4 | IS5 | 1o | 244 | IQSVKKLSDV | MILTVFCLSV | FALVGLQLFM | | | |
| | IIS5 | 2o | 688 | GNSVGALGNL | TLVLAIIVFI | FAVVMQLFG | | | |
| | IIIS5 | 3o | 1147 | LGAIPSIMNV | LLVCLIFWLI | FSIMGVNLFA | | | |
| | IVS5 | 4o | 1469 | MMSLPALFNI | GLLLFLVMFI | YSIFGMSNFA | | | |
| Pore-facing position | | | | * | * | * | * | | |
| Channel | Segment | | # | 33 | 41 | 51 | | | |
| KcsA | P | p | 59 | LITYPRAL | WWSVETATTV | GYGDLYPV | | | |
| K _v 1.2 | P | p | 358 | FPSIPDAF | WWAVVSMTTV | GYGDMVPT | | | |
| Ca _v 2.1 | IP | 1p | 301 | FDNILFAV | LTVFQCITME | GWTDLLYN | | | |
| | IIP | 2p | 651 | FDTFPAAI | MTVFQILTGE | DWNEVMYD | | | |
| | IIIP | 3p | 1452 | YDNVLWAL | LTLFTVSTGE | GWPQVLKH | | | |
| | IVP | 4p | 1748 | FRTFFQAL | MLLFRSATGE | AWHNIMLS | | | |
| Channel | Segment | | # | 1 | 11 | 21 | | | |
| KcsA | M2 | i | 86 | LWGRLVAVVV | MVAGITSFGL | VTAALATWVF | | | |
| K _v 1.2 | S6 | i | 385 | IGGKIVGSLC | AIAGVLTIAL | PVPVIVSNFN | e | | |
| Ca _v 2.1 | IS6 | 1i | 336 | TWNWLYFIPL | IIIGSFFMLN | LVLGVLSGEF | f | | |
| | IIS6 | 2i | 690 | MVFSIYFIVL | TLFGNYTLLN | VFLAIAVDNL | f | | |
| | IIIS6 | 3i | 1485 | MEMSIFYVY | FVVFPEFFVN | IFVALIITF | f | | |
| | IVS6 | 4i | 1785 | EFAYFYFVSE | IFLCSFLMLN | LFVAVIMDNF | f | | |
| Na _v 1.4 | IS6 | 1i | 415 | KTYMIFFVVI | I FLGSFYLIN | LILAVVAMAY | | | |
| | IIS6 | 2i | 770 | AMCLTVFLMV | MVIGNLVVLN | LFLALLLSSF | | | |
| | IIIS6 | 3i | 1262 | LYMYLYFVIF | IIFGSFFTLN | LFIGVIIDNF | | | |
| | IVS6 | 4i | 1565 | SIGICFFCSY | IIISELIVVN | MYIAIILENF | g | | |
| Pore-facing position | | | | | * | * | ** | ** | ** |
| Cytoplasm-facing position | | | | | | | ** | *** | * |

^a Highlighted in yellow are positions that when mutated to Cys cause the channel to be blocked by MTS reagents significantly (30-100%) compared to the control (Zhen et al., 2005). MTS reagents blocked the current by less than 30% through cysteine mutants at positions highlighted grey. Cysteine substitutions at positions highlighted black did not produce functional channels. Highlighted and bold-typed are residues whose mutations are described under footnotes referred to in the rightmost column.

^b The standard segment name includes the domain number (I-IV) and symbols S5, S6, or P. An alternative segment name is used for labelling residues, which includes the

domain number (1-4) and symbols o, p, and i for the outer helices, inner helices, and P-loops, respectively. Absolute numbers (#) of the first residue in each segment are shown for the following sequences: KcsA, Kir2.1, Kir6.2 (IRK11_RAT), K_v1.2, K_{Ca}3.1 (KCNN4_HUMAN), Ca_v2.1 (CAC1A_RABBIT), and Na_v1.4 (SCN4A_RAT).

- ^c Relative numbers of residues in the outer and inner helices are counted based on the X-ray structure of KcsA (Doyle et al., 1998), where the first residue of the segment in the X-ray structure was assigned number 1. Relative numbers of residues in the P-loops are counted from the EEEE-locus, whose residues are assigned number 50 to avoid negative numbers for residues in P-helices.
- ^d Ca_v2.1 mutants bearing a cysteine in positions 2010, 3015, 4010, 4012, or 4017 were blocked by MTSET (Zhen et al., 2005).
- ^e Intercellular MTSET blocks current through the open *Shaker* channel when a cysteine is substituted in position i22-i27, i30-i33, or i34. MTSEA, but not MTSET, blocks the Iⁱ¹⁸C mutant (Liu et al., 1997). Instead of percentage inhibition by MTSET, modification rate was measured.
- ^f Zhen et al. (2005) investigated the inner pore of open Ca_v2.1 channel using SCAM by measuring the current upon the application of internal MTSET. The control channel with eight eliminated cysteines was blocked by MTSET by 19% (Zhen et al., 2005). The mutation N²ⁱ²⁹C increased current upon the modification by MTSET (Zhen et al., 2005). The mutants A²ⁱ²⁶C and V²ⁱ²⁷C showed a ~1000-fold faster modification rate by MTSET in the open state than in the closed state Ca_v2.1 channel (Xie et al., 2005). Cysteine in position 2i28 is modified by MTSET at a similar rate in the closed and open channel (Xie et al., 2005).
- ^g The mutation I⁴ⁱ¹¹A in Na_v1.4 exposes a cysteine that binds MTSEA, but not MTSET. The binding of MTSEA prevents external access of QX-222, a quaternary local anaesthetic (Lee et al., 2001). Mutations at C⁴ⁱ⁵L, C⁴ⁱ⁸T, or C^{4p42}A still allow MTSEA binding (Lee et al., 2001). External and internal MTSEA, but not MTSET, blocks the F⁴ⁱ¹⁵C and V⁴ⁱ¹⁹C Na_v1.4 mutants (Sunami et al., 2004). Mutations I⁴ⁱ¹¹C and Y⁴ⁱ²²C are insensitive to MTSEA and MTSET (Sunami et al., 2004).

The general molecular modelling protocols used in this work have been previously described in Chapter 1. Each model was MC-minimized until 2,000 consecutive energy minimizations did not decrease energy of the lowest-energy conformation found in the given trajectory. The multi-MCM protocol (Bruhova and Zhorov, 2007; Tikhonov and Zhorov, 2007) was employed to explore energetically possible orientations of MTS-modified cysteines (designated ^mC). The torsional angles of ^mC residues were sampled from 60,000 random starting points, and each point was optimized by a short MCM trajectory of 10 steps. The top 1,000 lowest-energy conformations were further MC-minimized during 1,000 steps. All conformations in which the interaction energy between an MTS-modified cysteine and the rest of the channel did not exceed 4 kcal/mol from the apparent global minimum were analyzed. Despite that specific energy terms were not used for π -cation interactions, these interactions were accounted for due to partial negative charges at the aromatic carbons (Bruhova et al., 2008).

To avoid channel-specific residue numbers, we use a labelling scheme, which is universal for P-loop channels (Zhorov and Tikhonov, 2004). A residue label includes the repeat number (1 – 4; that may be omitted when the side chain properties are pertinent to all four repeats/subunits), segment type (*o* - outer helix, *p* - P-loop, *i* - inner helix), and the residue relative number in the segment (Table 4.1).

To describe the interaction of an ^mC residue in a given (*mutated*) helix with its neighbours, we use the terms *anterior* and the *posterior* helices that appear shifted in clockwise and anti-clockwise directions, respectively, from the *mutated* helix viewed from the extracellular side. For example, in the case of the C^{1118} mutant, the *mutated* helix is IS6, the *anterior* helix is IIS6 and the *posterior* helix is IVS6.

RESULTS

SCAM data and the cysteine-orientation concept

In the X-ray structure of $\text{K}_v1.2$, the vectors of $\text{C}^\alpha\text{-C}^\beta$ in positions *i15*, *i18*, *i19*, *i22*, and *i23* are oriented to the pore axis, in position *i16* orients to the repeat interfaces, and in positions *i24*, *i26*, *i27*, *i28*, *i30*, and *i31* orients to the cytoplasm (Figure 4.1). $\text{C}^\alpha\text{-C}^\beta$ vectors in positions *i17*, *i20*, *i21*, *i25*, and *i29* point to neighbouring transmembrane helices. According to the cysteine-orientation concept, MTS-modified engineered cysteines in positions *i15*, *i18*, *i19*, *i22*, and *i23* should block current, whereas in positions *i17*, *i20*, *i21*, *i25*, and *i29* should not block current.

Assuming that S5 and S6 helices in $\text{Ca}_v2.1$ and $\text{K}_v1.2$ have generally similar 3D dispositions and using the sequence alignment in Table 4.1, the reported SCAM data can be divided into two categories. In agreement with the cysteine-orientation concept, the first-category data show current decrease in $^m\text{C}^{i15}$, $^m\text{C}^{i19}$, $^m\text{C}^{i23}$, $^m\text{C}^{2i18}$, and $^m\text{C}^{4i18}$

channels, where the C^α - C^β vectors of the respective positions direct to the pore axis. The second-category data disagree with the cysteine-orientation concept. These data include three groups of observations: (i) residues ${}^mC^{1i18}$, ${}^mC^{3i18}$ and ${}^mC^{i22}$ which do not block the current despite the corresponding C^α - C^β vectors point to the pore axis, (ii) residues ${}^mC^{2o10}$ and ${}^mC^{4o10}$ which decrease the current despite the corresponding outer-helix positions are far from the inner pore, and (iii) residues ${}^mC^{i16}$, ${}^mC^{2i20}$, ${}^mC^{3i20}$, ${}^mC^{3i21}$, ${}^mC^{i24}$, and ${}^mC^{2i25}$ which decrease the current despite the corresponding C^α - C^β vectors direct away from the pore axis.

Below we describe $K_v1.2$ -based homology models of $Ca_v2.1$ channels with MTSET-modified engineered cysteines and rationalize the SCAM data taking into consideration side chain conformations of these residues. When we describe the positions or orientations of a MTS-modified cysteine, we focus on the location of the ammonium group relative to the permeation pathway. We assume that the ammonium group would block the current if exposed to the pore lumen and would not block the current if it is oriented away from the permeation pathway. Unless otherwise specified, the described positions of the ammonium groups are pertinent to the majority of the low-energy conformations of the MTS-modified cysteine under consideration.

MTS-modified cysteines in pore-facing positions

In the ${}^mC^{i15}$ channels, the current is inhibited by 39.0 - 65.5%. According to our calculations, the side chains of ${}^mC^{i15}$ are exposed in the central cavity and interact with residues at the same level of the pore (*i15*) and lower levels *i18* and *i19* (Figure 4.2 *A, B*). The ${}^mC^{i15}$ ammonium group is stabilized by electrostatic interactions with the nucleophilic C-termini of P-helices (residues *p47-p49*) and with partial negative charges of the EEEE locus.

The ${}^mC^{2i18}$ and ${}^mC^{4i18}$ channels demonstrate smaller current than ${}^mC^{1i18}$ and ${}^mC^{3i18}$ channels. Calculations predict two orientations of the ${}^mC^{i18}$ side chains (Figure 4.3). In the pore orientations, the side chains are attracted to the nucleophilic C-ends of P-helices, the EEEE locus, and residues at levels *i15* and *i19*. In the repeat-interface orientation, the side chains of ${}^mC^{i18}$ s occur between the *mutated* inner helix, the *anterior* inner helix, and the outer helix of the *mutated* repeat. Hydrophobic residues in position *o10* and *anterior*-helix positions *i12* and *i16* stabilize the predicted orientations of ${}^mC^{i18}$ s, while the backbones of positions *i14*, *i17*, and *i19* of the *mutated* helix destabilize these orientations. The energetically preferable orientation of the ${}^mC^{i18}$ side chain depends on the surrounding residues, which are distinct in different repeats (Table 4.1). In agreement with the SCAM data, the pore orientation is energetically preferable for ${}^mC^{2i18}$ and ${}^mC^{4i18}$ residues, while the repeat-interface orientation is preferable for ${}^mC^{1i18}$ and ${}^mC^{3i18}$ residues.

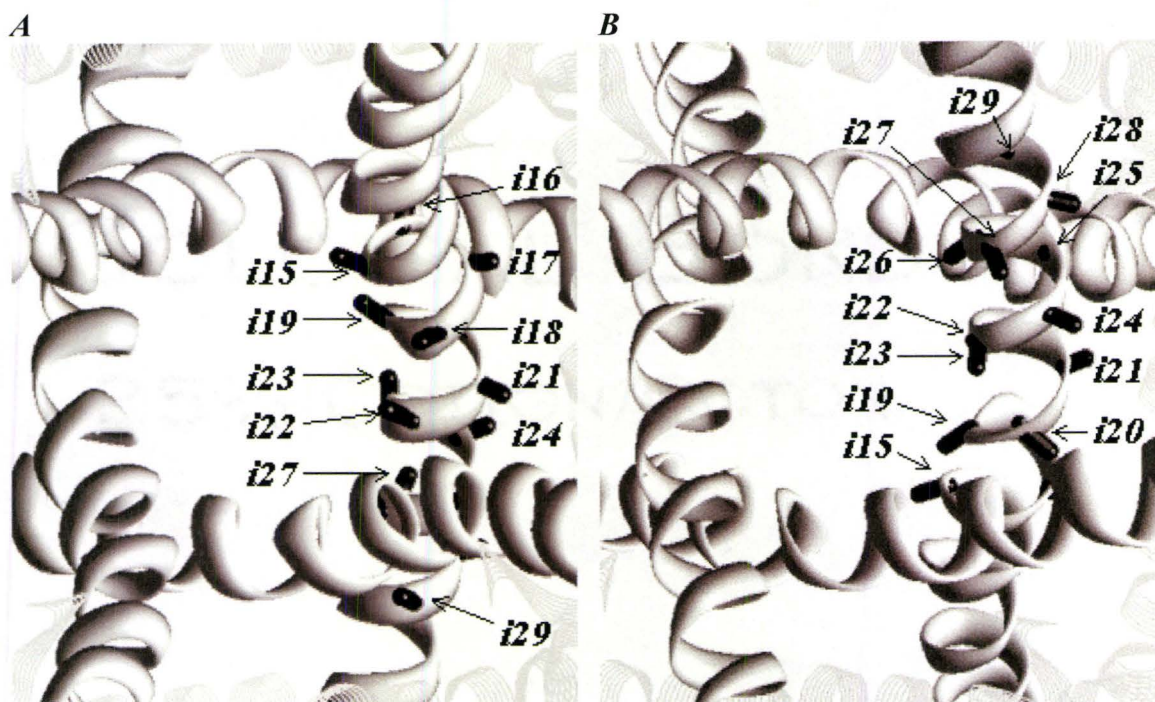


Figure 4.1. The extracellular (A) and cytoplasmic (B) views of the inner and outer helices of the Kv1.2 X-ray structure. The C^α-C^β atoms of positions *i15-i29* are shown as black sticks. The S5 and S6 helices are shown as strands and ribbons, respectively. The P-loops are not shown for clarity.

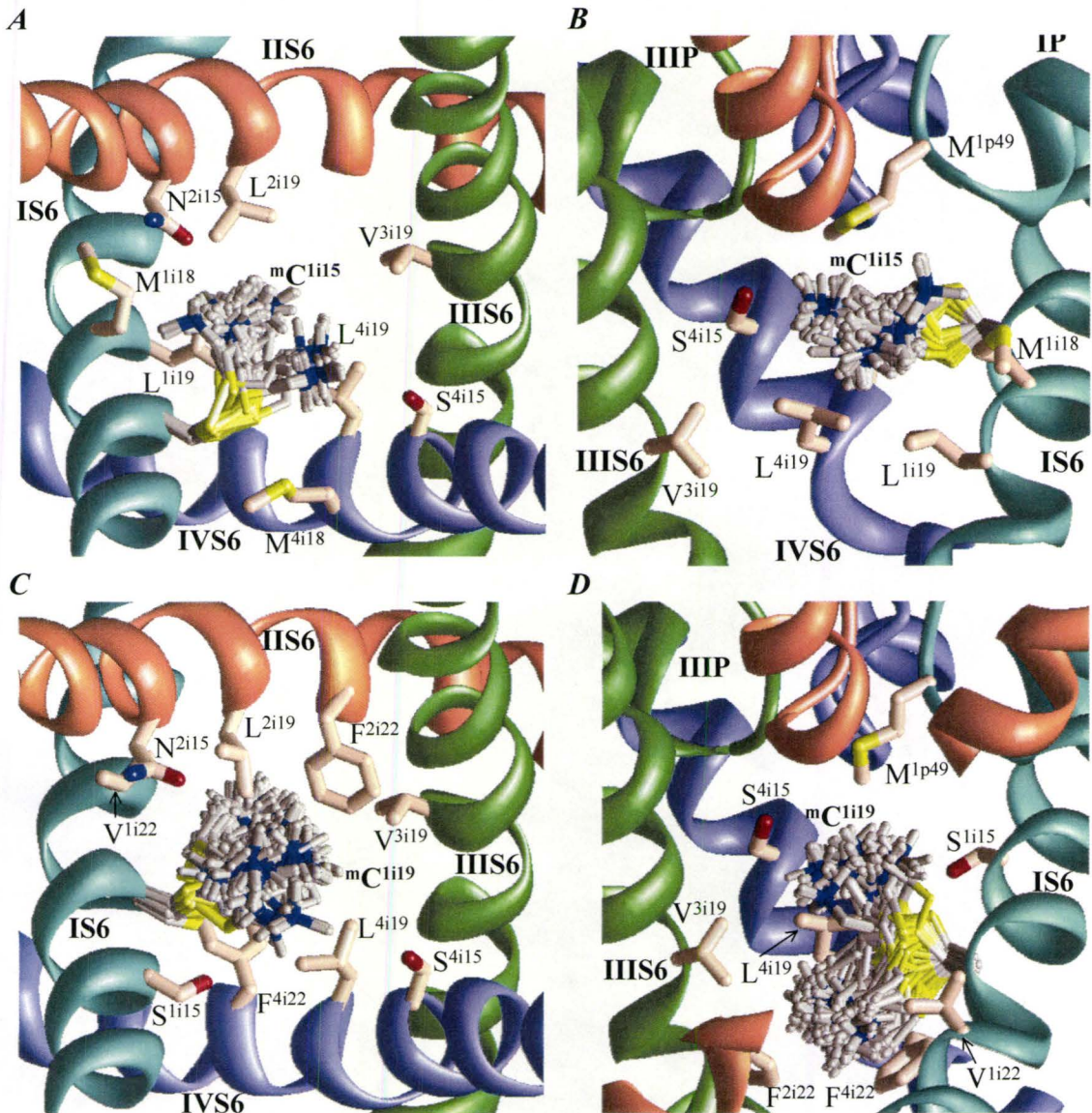


Figure 4.2. The top and side views of the lowest-energy orientations of ${}^m\text{C}^{1i15}$ (**A, B**) and ${}^m\text{C}^{1i19}$ (**C, D**) in the open $\text{Ca}_v2.1$ channel. The side chains of positions *i15*, *i18*, *i19*, and *i22* from all four repeats are shown as pale orange sticks. The P-loops and S6s in repeats I, II, III, and IV are respectively coloured cyan, orange, green, and violet. For clarity, P-loops in **A** and **C**, and S5s in all charts are not shown. **B**, ${}^m\text{C}^{1i15}$ faces the pore. For clarity, helix IIS6 is not shown. **D**, ${}^m\text{C}^{1i19}$ has two favourable orientations with the ammonium group leaning either towards the selectivity filter or the cytoplasm. Side chains of *2i12* – *2i20* are not shown for clarity.

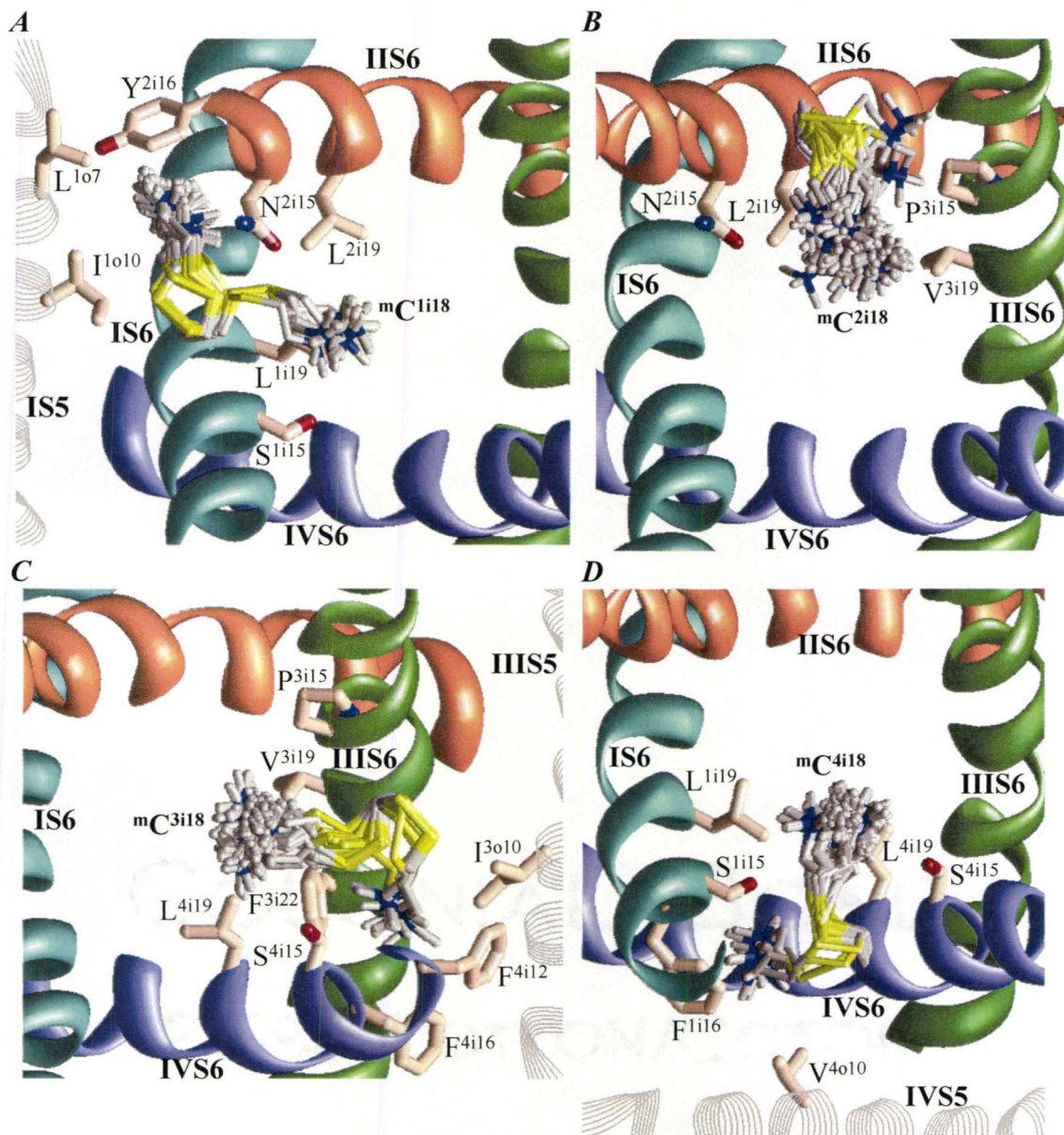


Figure 4.3. Orientations of mC^{i18} in $Ca_v2.1$. The S6s in repeats I, II, III, and IV are respectively colored cyan, orange, green, and violet; S5s are shown as gray strands. For clarity, the P-loops are not shown. **A**, Cation- π interactions with Y^{2i16} stabilize the sidewalk orientation of mC^{1i18} that does not block the current. **B**, The side chain of mC^{2i18} blocks current, because its preferable orientation is into the pore. **C**, mC^{3i18} does not block the current, because the sidewalk orientation is stabilized by cation- π interaction with F^{4i12} and F^{3i22} . **D**, mC^{4i18} partially blocks current because cation- π interactions with F^{1i16} and F^{4i22} stabilize both the pore and sidewalk orientations.

The ammonium groups of ${}^m\text{C}^{1i18}$ and ${}^m\text{C}^{3i18}$ residues are attracted to the aromatic residues in repeat interfaces I/II and III/IV, respectively. The side chain of ${}^m\text{C}^{1i18}$ orients in the I/II repeat interface where it interacts with L^{1o10} , L^{2i12} , and Y^{2i16} . The ammonium group of ${}^m\text{C}^{2i18}$ occurs inside the pore, while orientation of ${}^m\text{C}^{3i18}$ in the III/IV repeat interface is stabilized by π -cation interactions with F^{3i22} and F^{4i12} and hydrophobic interactions with I^{3o10} . The side chain of ${}^m\text{C}^{4i18}$ is equally stable in the pore orientation and in the IV/I interface orientation where it experiences π -cation interactions with F^{1i16} .

The side chains of ${}^m\text{C}^{i19}$ s are exposed to the central cavity of the pore (Figure 4.2 C, D) in two orientations: upward to the focus of P-helices and downward to F^{2i22} , F^{3i22} , and F^{4i22} (Figure 4.2D). The latter orientation is more stable due to π -cation interactions. In both orientations, the ammonium group is close to the pore axis. These results are consistent with the SCAM data that the residual current is small in ${}^m\text{C}^{i19}$ channels (Zhen et al., 2005).

Despite that the C^α - C^β vectors in positions *i22* point to the pore axis, the measured currents in the ${}^m\text{C}^{i22}$ channels are almost the same as in the control channel. The side chain of ${}^m\text{C}^{i22}$ can adopt two favourable orientations: in the pore interacting with neighbouring F^{i22} or in the repeat interface interacting with surrounding F or Y residues in positions *i12*, *i16*, or *i18* (Figure 4.4). Another possibility for the weak MTSET inhibition is that large hydrophobic residues in positions *i19*, *i22*, and *i26* prevent the ionization of C^{i22} and thus would prevent the reaction with MTSET.

In the ${}^m\text{C}^{i23}$ channels, the currents are inhibited by 43.6 - 87.7%. In all four repeats, the energetically preferable conformations of the ${}^m\text{C}^{i23}$ side chains are oriented into the pore. For example, the pore orientation of ${}^m\text{C}^{i23}$ is stabilized by interactions with L^{1i26} , F^{2i22} , F^{4i30} , F^{4i22} , and I^{4i26} .

MTS-modified cysteines in positions that do not face the pore

Despite that the C^α - C^β vectors in positions *i16*, *i20*, *i21*, *i24*, *i25*, and *i29* point away from the pore axis, the currents of the corresponding ${}^m\text{C}$ channels are different from the control (Zhen et al., 2005). Our models provide rationale for these observations as described below.

Residues ${}^m\text{C}^{i16}$ block current by 33.2 - 41.9%. The corresponding side chains can adopt two orientations with the ammonium group either approaching the pore or facing away from the pore and interacting with residues at the C-end of S6 or N-end of S5 (Figure 4.5A). In the low-energy conformations, the side chain of ${}^m\text{C}^{i16}$ wraps anti-clockwise around the inner helix so that its ammonium groups reaches the inner-pore edge and interacts with residues in positions *i12* of the *mutated* S6 and positions *i18*, *i19*, and *i22* of the *posterior* S6. In the other low-energy conformation, the side chains of ${}^m\text{C}^{i16}$ are oriented away from the pore and interact with residues in positions *i12* and *i13* of the

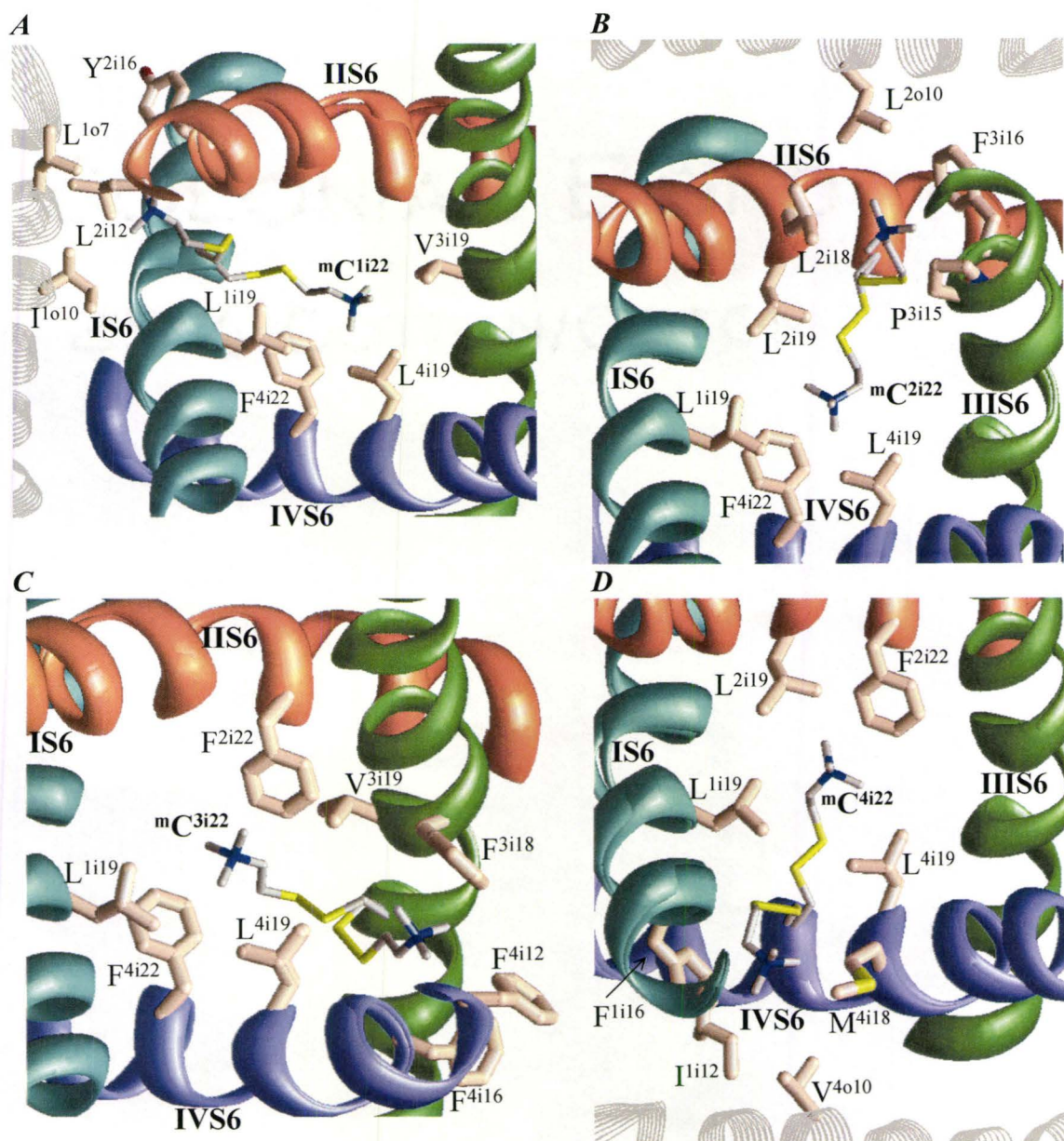


Figure 4.4. The top view of MTS-modified cysteines in position *1i22* (A), *2i22* (B), *3i22* (C), and *4i22* (D). The side chains of ^mCⁱ22s can adopt two orientations, either occupying the pore or the repeat interface. The side chain of ^mCⁱ22 is stabilized in the repeat interface by hydrophobic or cation- π interactions with residues in positions *i12*, *i16*, or *i18*. P-loops are not shown for clarity. The S6s in repeats I, II, III, and IV are respectively colored cyan, orange, green, and violet; S5s are shown as gray strands.

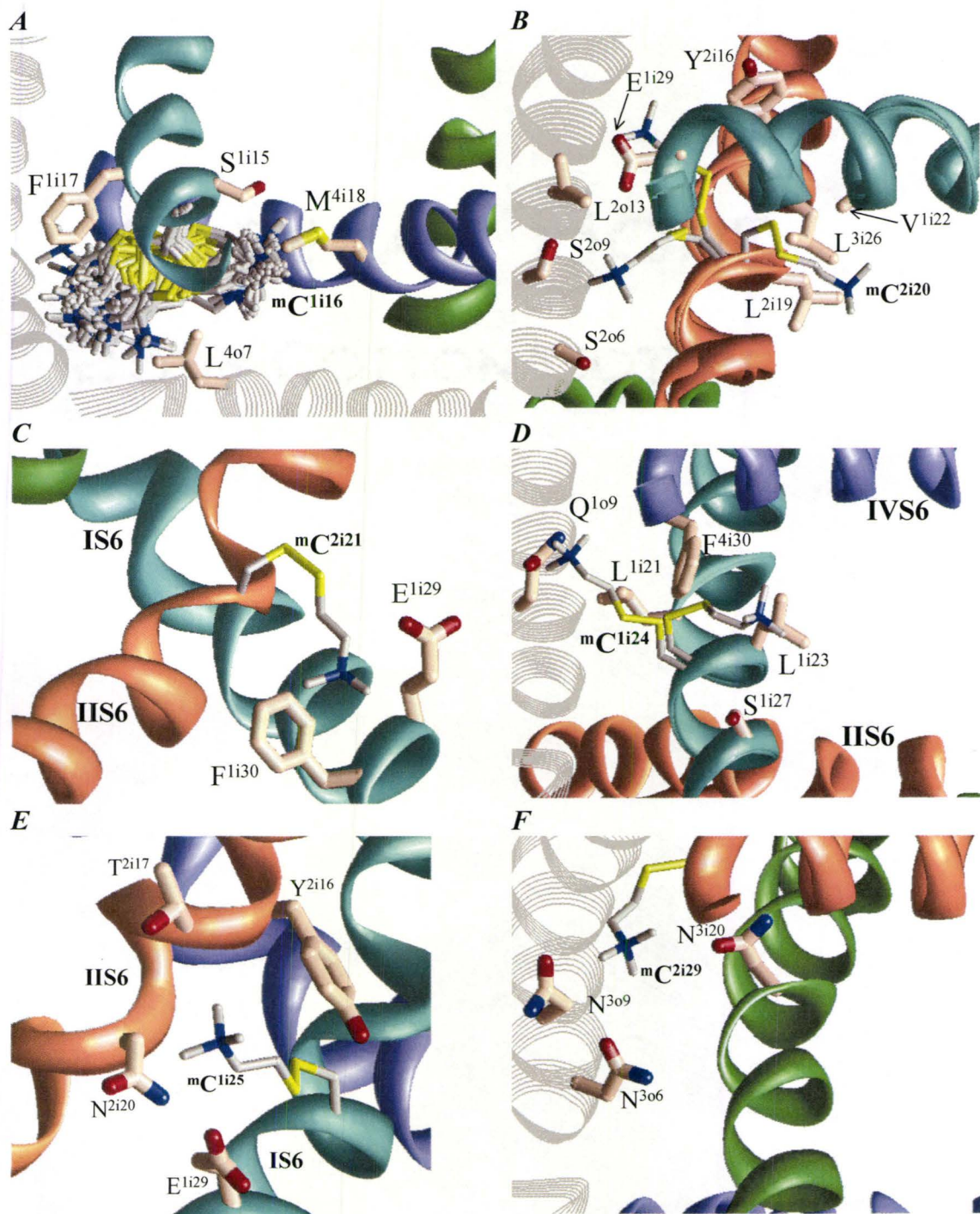


Figure 4.5. Preferred orientations of MTS-modified cysteine in non-pore facing residues in the open $\text{Ca}_v2.1$ channel. **A**, The top view of the 1000 most energetically favourable orientations of $\text{mC}^{\text{I}116}$. The ammonium group of $\text{mC}^{\text{I}116}$ binds towards the pore or the outer helices. For clarity, the backbone of position $\text{I}111 - \text{I}111$ is not shown. **B**, The

cytoplasmic view of the superposition of three favourable binding modes of ${}^m\text{C}^{2i20}$. **C**, The side view of ${}^m\text{C}^{2i21}$, which is stabilized by F^{1i30} in the domain interface, thus does not block current. **D**, The cytoplasmic view of ${}^m\text{C}^{1i24}$, which adopts two modes, one inside the pore stabilized by S^{1i27} and L^{1i23} , while the other mode faces away to interact with L^{1i21} , Q^{1o9} , and F^{4i30} . **E**, The side view of ${}^m\text{C}^{1i25}$ stabilized by Y^{2i16} , E^{1i29} , N^{2i20} , and T^{2i17} in the domain interface, thus does not block current. **F**, The cytoplasmic view of ${}^m\text{C}^{2i29}$ interacting with N^{3o9} , N^{3o6} , and N^{3i20} . The S6s in repeats I, II, III, and IV are respectively colored cyan, orange, green, and violet; S5s are shown as gray strands. For clarity, the P-loops are not shown.

mutated S6 and positions *o7*, *i25*, and *i29* of the *posterior* repeat. Thus, in neither of the two orientations ${}^m\text{C}^{i16}$ s completely occlude the inner pore. This explains the rather high residual current in the ${}^m\text{C}^{i16}$ channels (Zhen et al., 2005).

Residues ${}^m\text{C}^{i20}$ substitute native asparagines that are highly conserved in Ca^{2+} and Na^{2+} channels. The function of these asparagines is unclear. Mutants C^{i20} and C^{4i20} are non-functional. In the ${}^m\text{C}^{2i20}$ and ${}^m\text{C}^{3i20}$ channels, the currents are reduced by 56.2% and 42.0%, respectively. The side chains of ${}^m\text{C}^{2i20}$ and ${}^m\text{C}^{3i20}$ can adopt three orientations. In one of them the ammonium group occurs in the pore, but in the energetically most preferable orientations the ammonium groups of ${}^m\text{C}^{2i20}$ and ${}^m\text{C}^{3i20}$ face the S5 helix of the *mutated* repeat (Figure 4.5B).

The C^α - C^β vectors of ${}^m\text{C}^{i21}$ s direct to the S5 helices. The C^{4i21} mutant is not functional. The ${}^m\text{C}^{i21}$ and ${}^m\text{C}^{2i21}$ residues do not block the current, whereas ${}^m\text{C}^{3i21}$ inhibit the current by $\sim 40\%$. The side chains of ${}^m\text{C}^{i21}$ and ${}^m\text{C}^{2i21}$ fit between the *mutated* S5 and the *posterior-repeat* S6 (Figure 4.5C). Cation- π interactions with F^{4i30} and electrostatic interactions with Q^{i09} stabilize the ammonium group of ${}^m\text{C}^{i21}$ in the IV/I repeat interface. Similar interactions with F^{i30} and E^{i29} stabilize the ammonium group of ${}^m\text{C}^{2i21}$ also in the I/II repeat interface. The side chain of ${}^m\text{C}^{3i21}$ orients into the pore, where its ammonium group is stabilized by cation- π interactions with F^{3i18} and F^{3i22} .

Despite the C^α - C^β vectors of ${}^m\text{C}^{i24}$ s direct to the cytoplasm (Figure 4.1B), MTSET inhibits the current of C^{i24} s channels by 73.6 - 100%. In the most preferable conformations of ${}^m\text{C}^{i24}$, the ammonium groups occur in the pore, but an orientation facing the N-end of S5 is also possible (Figure 4.5D). Cation- π interactions with F^{i30} , F^{3i30} , and F^{4i30} attract the ammonium groups of ${}^m\text{C}^{2i24}$, ${}^m\text{C}^{4i24}$, and ${}^m\text{C}^{i24}$, respectively, towards the pore. The pore-oriented ${}^m\text{C}^{i24}$ is stabilized by the side chains of *mutated* *i27*, *mutated* *i23*, and *anterior* *i30*. The ammonium group of ${}^m\text{C}^{3i24}$ is not involved in cation- π interactions, and occurs farther from the pore, because instead of F^{i30} as in repeats I, III, and IV, there is a Leu in repeat II.

The residual current in channel ${}^m\text{C}^{2i25}$ is small, while in channels ${}^m\text{C}^{i25}$, ${}^m\text{C}^{3i25}$, and ${}^m\text{C}^{4i25}$ it is large. The C^α - C^β vectors in position *i25* direct away from the pore axis (Figure 4.1). Interactions with aromatic side chains in positions *i16* stabilize orientations of ${}^m\text{C}^{i25}$, ${}^m\text{C}^{3i25}$, and ${}^m\text{C}^{4i25}$ away from the pore axis (Figure 4.5E), while large side chains of L^{i26} , L^{3i26} or V^{4i26} prevent orientations inside the pore. In contrast, π -cation interactions with F^{2i22} stabilize orientation of ${}^m\text{C}^{2i25}$ to the pore, and this orientation is not opposed by the small side chain of A^{2i26} .

Intriguingly, the C^{2i29} mutant is the only channel for which the application of MTSET increases rather than decreases current (Zhen et al., 2005). In our model, the ammonium group of ${}^m\text{C}^{2i29}$ is oriented in the repeat interface and binds between the side chains of N^{3o9} , N^{3o6} , and N^{3i20} (Figure 4.5F). Such clustering of the MTS-modified cysteine with three asparagines is not found in other models explored in the current study.

Position *i29* is far below position *i14*, where the gating-hinge glycines are located in K^+ channels. Superposition of X-ray structures of K^+ channels shows that position *i29* is shifted significantly between the open and closed conformations. We suggest that the strong electrostatic attractions of the ${}^mC^{2i29}$ ammonium group to the side chain carbonyls of the N^{309} , N^{306} , and N^{3i20} stabilize the open-gate conformation of the pore domain. This can explain the unique feature of the ${}^mC^{2i29}$ channel observed in experiments (Zhen et al., 2005).

Modified cysteines in the outer helices of $Ca_v2.1$

Despite that the outer helices do not line the inner pore, substantial decrease of the current versus the control level is observed in ${}^mC^{2o10}$ and ${}^mC^{4o10}$ channels. The current in the channel ${}^mC^{3o10}$ is close to the control, while experimental data for the C^{1o10} channel are unavailable. Side chains of ${}^mC^{2o10}$ and ${}^mC^{4o10}$ occur either between the inner and outer helices in the *mutated* repeat or between the *mutated* and *anterior* inner helices (Figure 4.6). Energetically preferable conformations of the ${}^mC^{2o10}$ and ${}^mC^{4o10}$ side chains occur between the inner helices and extend toward the inner pore. The side chain of F^{3i18} precludes the protrusion of the ${}^mC^{3o10}$ side chain into the inner pore and stabilizes orientation in the repeat interface due to π -cation interactions (Figure 4.6B).

Channels ${}^mC^{3o15}$, ${}^mC^{4o12}$, and ${}^mC^{4o17}$ show rather large residual currents. The side chain of ${}^mC^{4o17}$ approaches the inner pore, while side chains of ${}^mC^{3o15}$ and ${}^mC^{4o12}$ face away the pore suggesting that these mutations could indirectly affect the current.

Currents correlate with the distance of the MTS nitrogen from the pore axis

The above sections provide multiple examples that the flexible side chains of MTS-modified cysteines adopt essentially different orientations relative to the inner pore. These orientations depend on the sequential positions of the mutated residues in the inner and outer helices of individual repeats. Particular conformations and orientations are stabilized by electrostatic and cation- π interactions of the ammonium group of the MTS-modified cysteine with neighbouring residues. Figure 4.7A shows the experimental inhibition currents plotted against the distance between the pore axis and the ammonium nitrogen as calculated for the energetically most preferable conformations of corresponding mC residues. A clear correlation is observed with only two significant outliers, ${}^mC^{4o10}$ and ${}^mC^{1i24}$. Figure 4.7B illustrates the $Ca_v1.2$ pore and the ammonium nitrogens of mC residues (shown as spheres) in the energetically most preferable conformations. The spheres are coloured yellow or blue depending on the current inhibition level in respective channels. It is clear that substantial inhibition is observed when the ammonium groups are inside the pore, weak inhibition is observed when the ammonium groups are outside the pore, and intermediate inhibition is observed when the

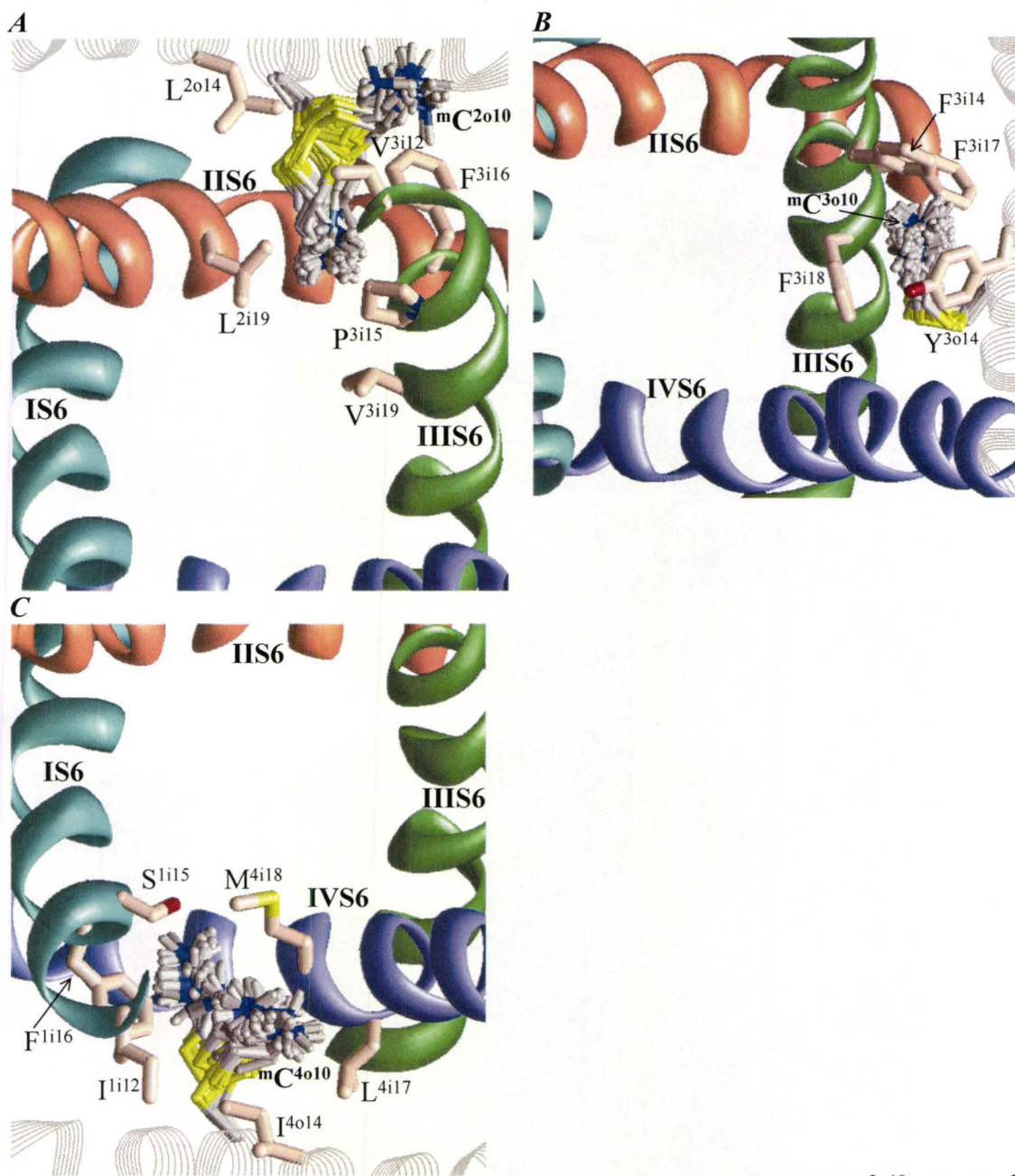


Figure 4.6. The top view of the lowest-energy orientations of (A) mC^{2o10} , (B) mC^{3o10} , and (C) mC^{4o10} . mC^{2o10} and mC^{4o10} can extend their ammonium group toward the inner pore, thus inhibit current. mC^{3o10} is stabilized inside the repeat interface by cation- π interaction with F³ⁱ¹⁸ and Y^{3o14}. P-loops are not shown for clarity. The S6s in repeats I, II, III, and IV are respectively colored cyan, orange, green, and violet; S5s are shown as gray strands.

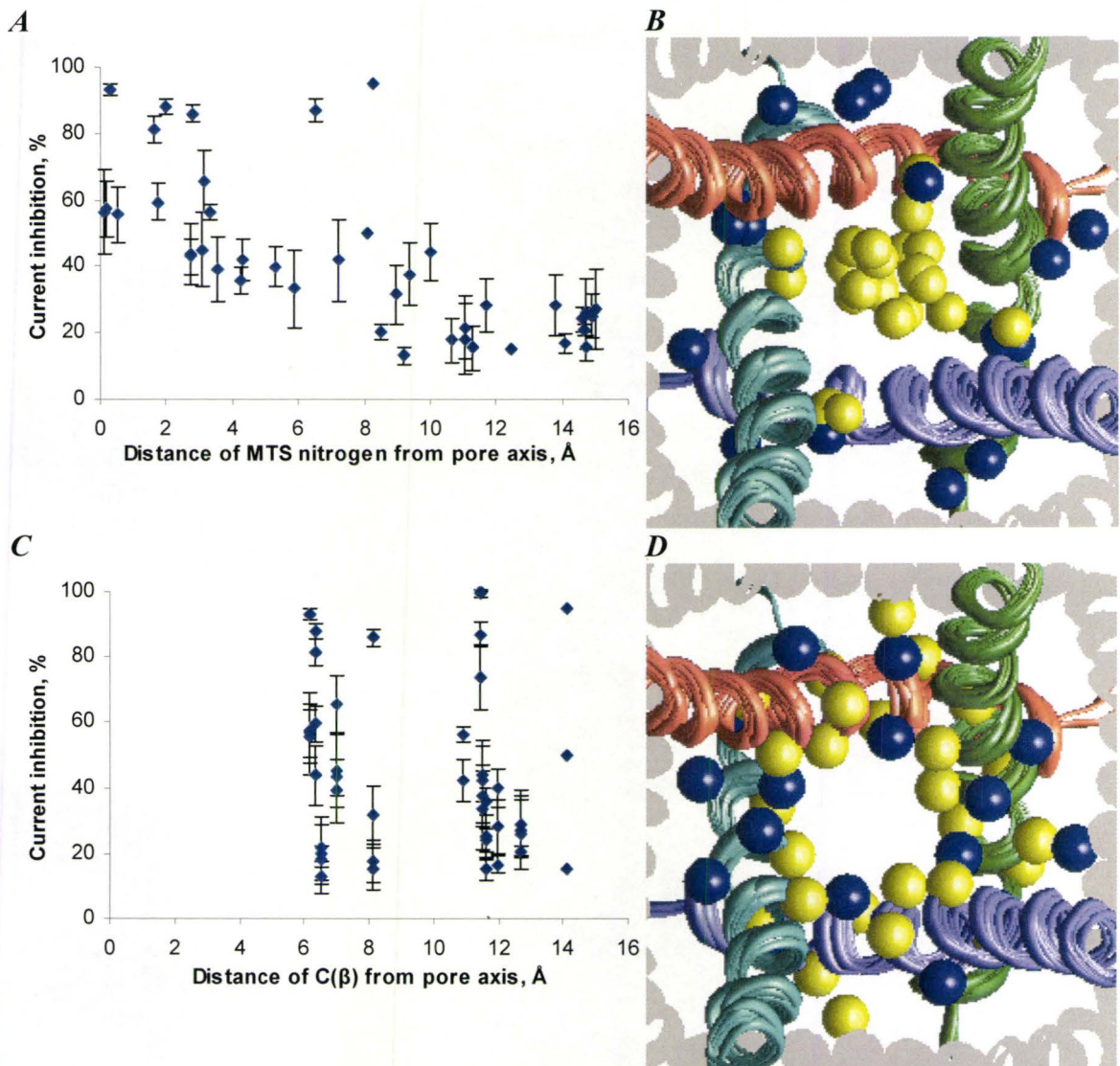


Figure 4.7. Distance of MTS nitrogen (A, B) and C^β (C, D) from the pore axis. Shown are data points for positions *i15* - *i25* and *o10*, excluding positions that produced non-functional channels when mutated to Cys. **A** and **C**, The current inhibition with standard deviation taken from Zhen et al. (2005) plotted against the distance of the ^mC ammonium nitrogen and C^β from the pore axis, respectively. No standard deviations are available for positions *2o10*, *3o10*, and *4o10*. The location of the ^mC ammonium nitrogen was taken from the energetically most favourable orientation of ^mC. **B** and **D**, The top view of the open Ca_v2.1 channel model with the ^mC ammonium nitrogen and C^β atoms shown as spheres, respectively. P-loops are not shown for clarity. Classified from Zhen et al. (2005), yellow spheres represent positions that were significantly inhibited by MTSET (30-100%) compared to the control channel (19% inhibition). Blue spheres represent positions that exhibited similar MTSET inhibition (<30%) as the control channel (Zhen et al. 2005). A correlation between current inhibitions and the distance of the ^mC ammonium nitrogen is visible (**A** and **B**), but poor correlation is seen with C^β atom (**C** and **D**).

ammonium groups are on the border of the pore. The significance of the observed correlation is discussed later. On the other hand, Figure 4.7 *C* and *D* demonstrates that the location of the C^β atom has no correlation with the current inhibition.

DISCUSSION

Voltage-gated Na⁺ and Ca²⁺ channels evolved from K⁺ channels and are believed to share similar membrane topology (Anderson and Greenberg, 2001). In the absence of X-ray structures of Na⁺ and Ca²⁺ channels, their homology models based on available X-ray structures of K⁺ channels are used to interpret numerous experimental data obtained in mutational, electrophysiological, and ligand-binding experiments. The first and most crucial step in homology modeling is the sequence alignment of K⁺ channels with Na⁺ and Ca²⁺ channels. Since the sequence similarity between the Ca²⁺ and Na⁺ channels is rather high, alignment between these channels is unambiguous (Zhorov and Tikhonov, 2004). In contrast, due to poor sequence similarity between K⁺ channels on one hand and Ca²⁺ and Na⁺ channels on the other hand, there is no consensus alignment for transmembrane segments in the pore-forming domains of these channels. In particular, proposed alignments for the inner helices (Huber et al., 2000; Zhorov et al., 2001; Lipkind and Fozzard, 2003; Shafrir et al., 2008; Stary et al., 2008) differ in positions of asparagines (Table 4.2) that are highly conserved in every domain of eukaryotic Ca²⁺ and Na²⁺ channels and are present in the homotetrameric bacterial NaChBac channel (Ren et al., 2001). In the alignment by Lipkind and Fozzard (2003), these residues do not appear in matching positions of the four repeats. Kv1.2-based models of the L-type Ca²⁺ channel (Stary et al., 2008) and NaChBac channel (Shafrir et al., 2008) have been built with the alignment in which an insertion is introduced immediately before the conserved asparagines (Table 4.2).

Intensive mutational, electrophysiological, and pharmacological studies identified residues that, when mutated, affect action of ligands that bind in the pore domain of voltage-gated Ca²⁺ (Hockerman et al., 1997) and Na⁺ channels (Catterall et al., 2005). Homology models of these channels have been built based on the X-ray structures of K⁺ channels and were used to visualize binding sites and propose binding mechanisms of various drugs including benzothiazepines (Tikhonov and Zhorov, 2008), dihydropyridines (Zhorov et al., 2001; Lipkind and Fozzard, 2003; Cosconati et al., 2007; Tikhonov and Zhorov, 2009), phenylalkylamines (Lipkind and Fozzard, 2003; Cheng et al., 2009), local anaesthetics (Lipkind and Fozzard, 2005; Tikhonov and Zhorov, 2007; Bruhova et al., 2008), and batrachotoxin (Tikhonov and Zhorov, 2005b). Despite different underlying alignments used in these models and different details of ligand-channel interactions predicted in the models, the above studies agree that the X-ray structures of K⁺ channels are reasonable templates for the homology modeling of Na⁺ and Ca²⁺ channels. This opinion was undermined by the interpretation of meticulous SCAM experiments with Cav2.1 suggesting that Ca²⁺ and K⁺ channels have different patterns of pore-lining

residues (Zhen et al., 2005). This interpretation also questions the symmetric arrangement of repeats of Ca^{2+} channels around the pore axis.

Earlier we proposed models for complexes of Na^+ and Ca^{2+} channels with different ligands (Tikhonov and Zhorov, 2005b; Tikhonov et al., 2006; Tikhonov and Zhorov, 2007; Bruhova et al., 2008; Tikhonov and Zhorov, 2008). All these models are based on the same sequence alignment, which is shown in Table 4.1. This alignment was also questioned by the proposed interpretation of the SCAM study (Zhen et al., 2005). In this study we do not doubt the experimental observations described in the meticulous SCAM study (Zhen et al., 2005), but show that interpretations of these observations requires analysis of additional factors, which were apparently not considered in the original study. These factors are conformational flexibility of long side chains of MTS-modified cysteines and their interaction with neighbouring residues of the channels. In the current study, we used the $\text{K}_v1.2$ -based model of $\text{Ca}_v2.1$ based on alignment shown in Table 4.1. We reasoned that if our models explain the SCAM results, this supports the alignment and the spatial disposition of the transmembrane helices in the pore-forming domains between the K^+ and Ca^{2+} channels.

Interpretation of SCAM experiments is not straightforward. Several factors should be taken into consideration (Karlin and Akabas, 1998). MTS reagents, such MTSET, react with water-accessible ionized cysteine residues to form a covalent bond. If the cysteine is exposed to the lipid bilayer or is buried inside the protein, the ionization of the thiol group is suppressed. Upon application of a MTS reagent the current of the channel is measured. It is assumed that the current change is due to reaction between the MTS reagent and the engineered cysteine. The current may be unaffected because of two reasons. First, the reaction does not proceed due to hydrophobic environment, steric constraints, lack of protonated Cys residues, or other causes. Second, the MTS-modified cysteine does not affect ion permeation through the channel.

A brief application of the MTS reagent may results in incomplete chemical modification of cysteines (Liu et al., 1997), but prolonged exposure increases the probability of disulfide formation even with partially buried cysteines. The prolonged exposure in experiments with $\text{Ca}_v2.1$ (Zhen et al., 2005) may explain the fact that cysteines in different sides of the helical-wheel representations of S6s and S5s were modified despite some positions do not face the permeation pathway. To resolve these apparent paradoxes, we modeled in this study the $\text{Ca}_v2.1$ mutants with MTS-modified cysteines in all the positions for which current reductions are reported (Zhen et al., 2005).

Besides the kinetic effects, other factors need to be considered to interpret the SCAM data. The MTS-modified cysteine has a long flexible side chain: in an all-trans conformation the distance between C^α and ammonium nitrogen is 8.4 Å. Prediction of energetically optimal conformations of MTS-modified cysteines resembles docking of ligands in proteins, but the MTS-modified cysteines can be considered as “ligands” tethered to the channel protein. Docking of the tethered ligands makes calculations less

Table 4.2. Proposed inner helix alignments between K⁺, Na⁺, and Ca²⁺ channels

| Channel | Segment | # | 1 | 11 | 21 |
|--|---------|----|------|------------------------|-------------|
| Alignment proposed by Zhorov et al. (2001) | | | | | |
| KcsA | M2 | i | 86 | LWGRLVAVVV MVAGITSFGL | VTAALATWFFV |
| K _v 1.2 | S6 | i | 385 | IGGKIVGSLC AIAGVLTIAL | PVPVIVSNFN |
| Ca _v 1.2 | IS6 | 1i | 409 | ELPWVYFVSL VIFGSFFVLN | LVLGVLSGEF |
| | IIS6 | 2i | 757 | MLVCIYFIIL FISPNIILLN | LFLAIAVDNL |
| | IIIS6 | 3i | 1170 | VEISIFFIIY IIIIAFFMMN | IFVGFVIVTF |
| Na _v 1.4 | IVS6 | 4i | 1480 | SFAVFYFISF YMLCAFLIIN | LFVAVIMDNF |
| | IS6 | 1i | 415 | KTYMIFVVI IFLGSFYLIN | LILAVVAMAY |
| | IIS6 | 2i | 770 | AMCLTVFLMV MVIGNLVVLN | LFLALLLSSF |
| | IIIS6 | 3i | 1262 | LYMYLYFVIF IIFGSFFTLN | LFIGVIIDNF |
| | IVS6 | 4i | 1565 | SIGICFFCSY IIISFLIVVN | MYIAIILENF |
| Alignment proposed by Lipkind and Fozzard (2000) | | | | | |
| KcsA | M2 | i | 86 | LWGRLVAVVV MVAGITSFGL | VTAALATWFFV |
| Na _v 1.4 | IS6 | 1i | 416 | TYMIFVVI IFLGSFYLINL | ILAVVAMAYA |
| | IIS6 | 2i | 770 | AMCLTVFLMV MVIGNLVVLN | LFLALLLSSF |
| | IIIS6 | 3i | 1262 | LYMYLYFVIF IIFGSFFTLN | LFIGVIIDNF |
| | IVS6 | 4i | 1565 | SIGICFFCSY IIISFLIVVN | MYIAIILENF |
| Alignment proposed by Lipkind and Fozzard (2001) | | | | | |
| KcsA | M2 | i | 86 | LWGRLVAVVV MVAGITSFGL | VTAALATWFFV |
| Ca _v 1.2 | IS6 | 1i | 409 | ELPWVYFVSL VIFGSFFVLN | LVLGVLSGEF |
| | IIS6 | 2i | 757 | MLVCIYFIIL FISPNIILLN | LFLAIAVDNL |
| | IIIS6 | 3i | 1169 | RVEISIFFII YIIIIAFFMM | NIFVGFVIVT |
| | IVS6 | 4i | 1480 | SFAVFYFISF YMLCAFLIIN | LFVAVIMDNF |
| Alignment proposed by Lipkind et al. (2003) | | | | | |
| KcsA | M2 | i | 86 | LWGRLVAVVV MVAGITSFGL | VTAALATWFFV |
| Ca _v 1.2 | IIIS6 | 3i | 1170 | VEISIFFIIY IIIIAFFMMN | IFVGFVIVTF |
| | IVS6 | 4i | 1481 | FAVFYFISFY MLCAFLIINL | FVAVIMDNFD |
| Alignment proposed by Huber et al. (2000) | | | | | |
| KcsA | M2 | i | 86 | LWGRLVAVVV MVAGITSFGL | VTAALATWFFV |
| Ca _v 1.2 | IS6 | 1i | 410 | LPWVYFVSLV IFGSFFVLNL | VLGVLSGEFS |
| | IIS6 | 2i | 758 | LVCYFIILF ISPNYILLNL | FLAIAVDNLA |
| | IIIS6 | 3i | 1171 | EISIFFIIYI IIIIAFFMMNI | FVGFVIVTFQ |
| | IVS6 | 4i | 1481 | FAVFYFISFY MLCAFLIINL | FVAVIMDNFD |
| Alignment proposed by Stary et al. (2008) | | | | | |
| K _v 1.2 | S6 | i | 385 | IGGKIVGSLC AIAGVLTIA- | LPVPVIVSNF |
| Ca _v 1.2 | IS6 | 1i | 409 | ELPWVYFVSL VIFGSFFVLN | LVLGVLSGEF |
| | IIS6 | 2i | 757 | MLVCIYFIIL FISPNIILLN | LFLAIAVDNL |
| | IIIS6 | 3i | 1170 | VEISIFFIIY IIIIAFFMMN | IFVGFVIVTF |
| | IVS6 | 4i | 1480 | SFAVFYFISF YMLCAFLIIN | LFVAVIMDNF |

^a Highlighted in green is the prokaryotic gating hinge (Gly) that is conserved among K⁺ channels. The Asn residues conserved in all four repeats of Na⁺ and Ca²⁺ channels are highlighted grey.

time-consuming and results more reliable. Due to the long flexible chain, an ^mC side chain at a pore-lining position can turn out of the pore and bury inside the protein between S5 and S6. On the other hand, the ammonium group of an ^mC side chain at a non-pore-lining position can reach the pore through the repeat-interface or by wrapping around the *mutated* inner helix. Thus, the exposure of the ammonium group to the pore may not correlate with the angle between $\text{C}^\alpha\text{-C}^\beta$ bond and the line drawn from the C^α atom to the pore axis. The energetically optimal location of the ammonium group in the ^mC side chain depends on its interactions with neighbouring residues, among which electrostatic attractions (including stabilization of the ammonium group at the nucleophilic focus of P-helices) and cation- π interactions play the major role.

Our calculations predict a correlation between the distance of ^mC nitrogen from the pore axis and the current inhibition in respective channels (Figure 4.7). This correlation is important. First, it shows that interpretation of the SCAM data is possible in quantitative rather than discrete terms. Second, it supports the underlying sequence alignment between the Ca^{2+} and K^+ channels (Table 4.1). Third, it implies four-fold symmetry of transmembrane helices in the pore-forming domain of Ca^{2+} channels and a similar disposition of transmembrane helices in the pore-forming domains of K^+ and Ca^{2+} channels. Forth, it shows that significant block is observed only when the ammonium group occurs in the inner pore.

Experiments with fluorinated aromatic residues (Santarelli et al., 2007b; Ahern et al., 2008; Xiu et al., 2009) proved the long-proposed role of cation- π interactions in ligand-receptor recognition. Despite the AMBER force field does not have a specific energy term to account for cation- π interactions, such interactions are seen in the low-energy structures as the ammonium group attraction to partial negative charges of aromatic residues (Tikhonov and Zhorov, 2007; Bruhova et al., 2008). Using the same force field in the current study, we found many structures in which the ammonium group of MTS-modified cysteine is attracted to aromatic residues via cation- π interactions. These interactions were particularly important for stabilization of the ammonium group of the $^m\text{C}^{3o10}$, $^m\text{C}^{1i18}$, $^m\text{C}^{3i18}$, and $^m\text{C}^{4i18}$ side chains inside the repeat interface as well as $^m\text{C}^{i19}$ in the pore. Thus, cation- π interactions may stabilize not only ligand-protein complexes, but specific orientations of MTS-modified cysteines.

According to our models, the repeat interface would provide accessibility to MTSET to reach the engineered cysteines in non-pore facing positions on inner and outer helices. Through these interfaces the ammonium group of MTS-modified Cys can extend into the inner pore and decrease current. Interesting examples are $^m\text{C}^{2o10}$ and $^m\text{C}^{4o10}$ whose ammonium groups can approach the inner pore only via the repeat interface. This prediction is consistent with our previous studies in which we demonstrate that the repeat interface dubbed the “sidewalk” provides the extracellular access route of local anaesthetics into Na^+ channels (Bruhova et al., 2008) as well as benzothiazepines (Tikhonov and Zhorov, 2008) and dihydropyridines (Tikhonov and Zhorov, 2009) in Ca^{2+} channels. The X-ray structure of KcsA with hydrophobic cations shows that hydrophobic

moieties of the ligands can extend from the pore to the subunit interface in K^+ channels (Lenaeus and Gross, 2008).

CONCLUSION

In this study, we used molecular modeling to reinterpret the results of the meticulous SCAM study of $Ca_v2.1$ (Zhen et al., 2005). We found that the level of the current block does not necessarily correlate with the orientation of the C^α - C^β bond on the engineered cysteine to the inner pore, but correlates with the distance between the energetically optimal position of the mC ammonium group and the pore axis. Our study supports the sequence alignments between K^+ and Ca^{2+} channels earlier proposed for the inner (Zhorov et al., 2001) and outer (Huber et al., 2000) helices and suggests that the $K_v1.2$ X-ray structure is a suitable template to model the Ca^{2+} channels in the open-state conformation.

CHAPTER FIVE

ACCESS AND BINDING OF LOCAL ANESTHETICS IN THE CLOSED SODIUM CHANNEL

CHAPTER FIVE PREFACE

The work presented in this chapter was previously published in:

Bruhova I, Tikhonov DB and Zhorov BS (2008) Access and binding of local anesthetics in the closed sodium channel. *Molecular pharmacology* **74**:1033-45.

and

Tikhonov DB, Bruhova I and Zhorov BS (2006) Atomic determinants of state-dependent block of sodium channels by charged local anesthetics and benzocaine. *FEBS Letters* **580**:6027-32.

Permission has been granted from the publishers to reproduce the material here.

I have performed all of the molecular simulations described in this chapter.

ABSTRACT

Local anaesthetics (LAs) are known to bind Na^+ channels in the closed, open, and inactivated states and reach their binding sites via extracellular and intracellular access pathways. Despite intensive studies, no atomic-scale theory is available to explain the diverse experimental data on the LA actions. Here we attempt to contribute to this theory by simulating access and binding of LAs in the KcsA-based homology model of the closed Na^+ channel. We used Monte Carlo minimizations to model the channel with representative local anaesthetics QX-314, cocaine, and tetracaine. We found the nucleophilic central cavity to be a common binding region for the ammonium group of LAs, whose aromatic group can extend either along the pore axis (vertical binding mode) or to the III/IV domain interface (horizontal binding mode). The vertical mode was earlier predicted for the open channel, but only the horizontal mode is consistent with mutational data on the closed-channel block. To explore hypothetical access pathways of the permanently charged QX-314, we pulled the ligand via the selectivity filter, the closed activation gate, and the III/IV domain interface. Only the last pathway, which leads to the horizontal binding mode, does not impose steric obstacles. The LA ammonium group mobility within the central cavity is more restricted in the vertical mode than in the horizontal mode. Therefore, occupation of the selectivity-filter DEKA locus by a Na^+ ion destabilizes the vertical mode thus favouring the horizontal mode. LA binding in the closed channel requires the resident Na^+ ion to leave the nucleophilic central cavity through the selectivity filter, whereas the LA egress should be coupled with reoccupation of the cavity by Na^+ . This hypothesis on the coupled movement of Na^+ and LA in the closed channel explains seemingly contradictory data on how the outer-pore mutations as well as tetrodotoxin and μ -conotoxin binding affect the ingress and egress of LAs.

INTRODUCTION

Blockade of Na^+ channels by LAs is a well-known and medically important phenomenon. The mechanisms of action and structure-function relationships of LAs have been intensively studied more than 30 years (Catterall, 2000a; Ruetsch et al., 2001; Nau and Wang, 2004; Fozzard et al., 2005). Inside the Na^+ channel pore, LAs bind state-dependently. Various LAs including etidocaine (Ragsdale et al., 1994), cocaine (Wright et al., 1998), and cocaethylene (Xu et al., 1994) block the closed Na^+ channel. Three terms are used to describe this phenomenon: the closed-channel block, tonic block, or resting-channel block. In this paper we use the first term. Under high-frequency stimulation, the blocking effect increases. This phenomenon is called frequency-dependent or use-dependent block. Experiments on the state-dependent action of LAs demonstrated that generally LAs have a stronger potency in the open or inactivated channels compared to the closed channels (Hille, 1977; Chahine et al., 1992; Ragsdale et al., 1994; Xu et al., 1994; Wright et al., 1997). Two major hypotheses have been proposed to explain these effects. According to the “modulated receptor” hypothesis (Hille, 1977), LAs can bind to the closed, open and inactivated channel states, but with different

affinity. According to the “guarded receptor” hypothesis (Starmer et al., 1984), LAs have a permanent affinity to their receptor, while the block depends on the frequency and duration of the channel gating, which imposes an energy barrier for the ingress and egress of the ligand.

Intensive mutational studies (Ragsdale et al., 1994; Wright et al., 1998; Li et al., 1999; Yarov-Yarovoy et al., 2001; Yarov-Yarovoy et al., 2002) demonstrated that the binding site for LAs is located in the inner pore, between the activation gate and the selectivity filter and involves residues in domains I, III, and IV. Residues in domain IV, particularly F⁴ⁱ¹⁵ and Y⁴ⁱ²² were found critical for the use-dependent block by LAs (Ragsdale et al., 1994). Interestingly, mutations of these residues had qualitatively different effects on the closed-channel and use-dependent block. Closed-channel block by tetracaine requires a hydrophobic residue in position 4i15, while Y⁴ⁱ²² is important for the use-dependent block (Li et al., 1999). In agreement to these results, use-dependent block by cocaine is sensitive to mutations F⁴ⁱ¹⁵C and Y⁴ⁱ²²C (O'Leary and Chahine, 2002). In case of the closed-channel block by cocaine, mutation Y⁴ⁱ²²K had no effect, whereas mutations F⁴ⁱ¹⁵K and N⁴ⁱ²⁰K decreased the cocaine potency by 2- and 3-folds, respectively (Wright et al., 1998). In contrast, the cocaine potency in the inactivated channel decreased in the same mutants, 6-, 21.3-, and 27.4-fold, respectively, indicating that cocaine blocks the channel state-dependently (Wright et al., 1998). The mechanisms responsible for qualitatively different effect of mutations on the closed-channel block and use-dependent block are unresolved.

The access of LAs to and from the open pore is conceptually clear. Upon channel activation, LAs enter through the open intracellular gate and move along the ion-conducting hydrophilic pathway to their binding site in the inner pore. Understanding of the hydrophilic pathway was advanced by the X-ray structures of K⁺ channels that have been crystallized in the closed (Doyle et al., 1998) and open states (Jiang et al., 2002b; Jiang et al., 2002a; Jiang et al., 2003a; Jiang et al., 2003b; Long et al., 2005a; Long et al., 2005b). In the open conformation, the inner helices bend and form a wide vestibule, which is readily accessible for drugs from the cytoplasm.

In the closed state, the straight inner helices converge at the cytoplasmic side and obstruct ion permeation (Doyle et al., 1998). The bulky LA molecules are unlikely to pass through the closed gate. It was suggested that LAs reach the inner pore of the closed channel via a hydrophobic pathway (Hille, 1977). Since lipid-soluble compounds can cross the membrane, they are active when applied both the extra- and intracellularly (Nettleton and Wang, 1990). Quaternary analogs of LAs such as QX-222 and QX-314 cannot cross the membrane and therefore are used as probes for exploring the access pathways into the channels. When applied intracellularly, the quaternary LAs can only block the open Na⁺ channels (Hille, 1977). Unlike neuronal (Na_v1.2) and skeletal-muscle (Na_v1.4) channels, cardiac (Na_v1.5) Na⁺ channels are blocked by quaternary LAs applied extracellularly (Alpert et al., 1989; Qu et al., 1995). The mutation F⁴ⁱ¹⁵A of Na_v1.5 effects

both intra- and extracellular block by QX-314 suggesting that extracellular and intracellular LAs target the same site in the inner pore (Qu et al., 1995).

Several studies suggest that extracellularly applied LAs can reach their binding site through the outer pore. TTX binding to the outer pore of Na_v1.5 reduced the external QX-314 access and recovery after the use-dependent block (Qu et al., 1995). Mutations of Na_v1.4 also showed the involvement of the DEKA locus in the external access and binding of QX-314 (Sunami et al., 1997). Residue Y^{1p51}, which is critical for isoform-specific TTX action, affects the external access of QX-222 (Sunami et al., 2000). Mutation S^{4p49}L, one position upstream the DEKA locus, enhanced the external QX-314 access and dissociation (Sasaki et al., 2004). Cys substitutions of T^{3p48}, F^{3p49}, and S^{4p49} are accessible by the externally applied Cd²⁺ (Yamagishi et al., 1997) and sulfhydryl reagents (Yamagishi et al., 1997; Struyk and Cannon, 2002). All these data support a hypothesis that the outer pore of Na⁺ channels may be permeable to LAs and compounds of similar size.

Another set of data suggests the involvement of the inner helices in the hydrophobic pathway of LAs. The mutation of T⁴ⁱ⁸ in Na_v1.5 to V, which is a native residue in Na_v1.2, reduced block by external QX-314 (Qu et al., 1995). Mutation of I⁴ⁱ¹¹A created an external pathway for LAs in the brain (Ragsdale et al., 1994) and muscle Na⁺ channels (Wang et al., 1998; Sunami et al., 2001). This mutation does not affect ion permeation or binding of toxins to the outer pore (Sunami et al., 2001). A μ-CTX mutant R13N binds to the outer pore of Na⁺ channels, but does not fully block the current. External QX-222 increased block of the I⁴ⁱ¹¹A Na_v1.4 mutant in the presence of the μ-CTX mutant R13N suggesting that the outer pore is not the access route for the LA (Sunami et al., 2001). Furthermore, the mutation I⁴ⁱ¹¹C in Na_v1.5 enhanced binding and facilitated escape of cocaethylene from the closed channel (O'Leary et al., 2003).

The coexistence of two pathways for charged LAs, one through the outer pore and another through the domain interface, was previously discussed (Lee et al., 2001). Based on the models of Na_v1.4 and Na_v1.5, we earlier hypothesized that the hydrophobic pathway goes through the “sidewalk” along the IIIP helix between the inner helices IIIS6 and IVS6 (Tikhonov and Zhorov, 2005a; Tikhonov et al., 2006). In this study, we elaborate this hypothesis by docking various ligands and exploring computationally various hypothetical access pathways.

In the absence of X-ray structures of voltage-gated Na⁺ channels, their homology models have been proposed to explain the effects of LAs (Lipkind and Fozzard, 2005; Tikhonov et al., 2006; Tikhonov and Zhorov, 2007). Unlike previous studies that were focused on explaining the use-dependent block, the goal of this study is to explore access pathways and binding of LAs in the closed Na⁺ channel. We address the following questions. What are the binding modes of QX-314, cocaine, and tetracaine in the closed channel? What are the energetically possible ingress and egress routes for LAs in the closed channel? What is the impact of Na⁺ ions in the pore on the access and binding of

LAs in the closed channel? Our study predicts that the LA molecules adopt different orientations in the closed and open channels. The energetically most favourable pathway for the LA molecule to and from the closed channel is the interface between domains III and IV, whereas the selectivity filter and the closed activation gate impose large energy barriers for LAs. Finally, we propose that the occupancy of the pore with a Na^+ ion affects both access and binding of LAs. These results provide a novel structural interpretation for a large body of experimental data.

METHODS

Our model of the closed rNa_v1.5 included the outer helices, P-loops, and the inner helices whose backbones were built according to the X-ray structure of KcsA (Doyle et al., 1998). Extracellular linkers between the P-loops and transmembrane helices were not modeled. The ascending limbs of P-loops including the selectivity filter were taken from our earlier model (Tikhonov and Zhorov, 2005a). The sequences of P-loops and inner helices of K^+ and Na^+ channels were aligned as proposed earlier (Zhorov and Tikhonov, 2004), see Table 5.1. The outer helices, which align unambiguously between Na^+ and Ca^{2+} channels, were aligned with KcsA as proposed by Huber et al. (2000). Ionizable residues were treated as neutral except for the DEKA-locus ionizable residues, which were charged. The EEDD locus of the outer pore was proposed to bind four Na^+ ions between domains (Tikhonov and Zhorov, 2007). To make the locus more flexible, we did not use here the interdomain Na^+ bridges but neutralized the four acidic residues by four protons. Since the EEDD locus is more than 15 Å away from the binding site of LAs in the inner pore, this approximation would bias the LAs access through the selectivity filter, but is unlikely to affect the ligand binding in the inner pore. Cocaine and tetracaine models were protonated based on the data that protonated cocaine blocks Na^+ channels (Nettleton and Wang, 1990). The DEKA locus was loaded either by an explicit water molecule or a Na^+ ion, which were initially constrained, respectively to the D and K or D and E side chains. In the subsequent MCM trajectories the constraints were removed, but neither the water molecule nor the Na^+ ion moved away from the DEKA locus.

The general molecular modelling protocols used in this chapter have been previously described in Chapter 1. Hydration energy was calculated by the implicit-solvent method (Lazaridis and Karplus, 1999a). Hydration of the lipid-facing residues in the outer helices is unrealistic, but because these residues are not involved in the binding of LAs and because the channel folding does not change in our model, the hydration of S5s has a minimal impact on our results.

The ligands contained both heavy atoms and hydrogens. The protein was modeled in the united-atom approximation, but an all-atom model was also used to assess cation- π interactions of the ligand with aromatic residues. A cutoff of 8 Å was used for nonbonded interactions, but those involving ions and ionized groups were calculated without a cutoff. The homology model of the ligand-free closed channel was MC-minimized until 2,000

Table 5.1. Sequences of ion channels ^{a,b} and effect of mutations in Na⁺ channels ^{c-l}

| Channel | Segment ^b | # | 1 | 11 | 21 | | |
|----------------------------------|----------------------|----|-----------|--------------------|--------------------|-------------------|--------------|
| KcsA | M1 | o | 14 | ALHWRAAGAA | TVLLVIVLLA | GSYLAVLAER | |
| Na _v 1.5 | IS5 | 1o | 242 | IQSVKKLADV | MVLTVFCLSV | FALIGLQLFM | |
| | IIS5 | 2o | 825 | GNSVGALGNL | TLVLAIIVFI | FAVVGMLQFQ | |
| | IIIS5 | 3o | 1321 | VGAIPSIMNV | LLVCLIFWLI | FSIMGVNLFA | |
| | IVS5 | 4o | 1644 | MMSLPALFNI | GLLLFLVMFI | YSIFGMANFA | |
| | | | 33 | 41 | 51 | | |
| KcsA | P | p | 59 | LITYPRAL | WWSVETATTV | GYGDLYPV | |
| Na _v 1.4 | IP | 1p | 383 | YDTFSWAF | LALFRLMTQD | <u>YWENL</u> FQL | ^c |
| | IIP | 2p | 738 | MNDFHFSF | LIVFRILCGE | WIETMWDC | ^c |
| | IIIP | 3p | 1220 | YDNVGLGY | LSSLQVATFK | GWMDIMYA | |
| Na _v 1.5 | IVP | 4p | 1512 | FETFGNSI | ICLFEITTS <u>A</u> | GWDGLLNP | ^c |
| | IP | 1p | 356 | FDSFAWAF | LALFRLMTQD | <u>CWERLY</u> QQ | ^d |
| | IIP | 2p | 884 | MMDFHAF | LIIFRILCGE | WIETMWDC | |
| | IIIP | 3p | 1404 | FDNVGAGY | LALLQVATFK | GWMDIMYA | |
| | IVP | 4p | 1696 | FQTFANSM | LCLFQITTS <u>A</u> | GWDGLLSP | ^e |
| Pore-facing position | | | | | | ** *** | |
| Sidewalk-facing position in IIIP | | | | | | * *** | |
| | | | 1 | 11 | 21 | | |
| KcsA | M2 | i | 86 | LWGRLVAVVV | MVAGITSFGL | VTAALATWFEV | |
| Na _v 1.2 | IS6 | 1i | 399 | KTYMIFVVLV | IFLGSFY <u>LIN</u> | LILAVVAMAY | ^f |
| | IIS6 | 2i | 957 | TMCLTVFMMV | <u>MVIGNLVVLN</u> | LFLALLLSSF | ^g |
| | IIIS6 | 3i | 1447 | LYMYLYFVIF | IIFGSF <u>FTLN</u> | LFIGVIIDNF | ^h |
| | IVS6 | 4i | 1750 | SVGIFFFVSY | <u>IIISFLV</u> VVN | <u>MYIAVILENF</u> | ⁱ |
| Na _v 1.4 | IS6 | 1i | 415 | KTYMIFVVI | IFLGSFY <u>LIN</u> | LILAVVAMAY | |
| | IIS6 | 2i | 770 | AMCLTVFLMV | MVIGNLVVLN | LFLALLLSSF | |
| | IIIS6 | 3i | 1262 | LYMYLYFVIF | IIFGSF <u>FTLN</u> | LFIGVIIDNF | ^j |
| | IVS6 | 4i | 1565 | SIGICFF <u>CSY</u> | <u>IIISFLIVVN</u> | <u>MYIAIILENF</u> | ^k |
| Na _v 1.5 | IS6 | 1i | 388 | KIYMIFFMLV | IFLGSFYLVN | LILAVVAMAY | |
| | IIS6 | 2i | 916 | SLCLLVFLLV | MVIGNLVVLN | LFLALLLSSF | |
| | IIIS6 | 3i | 1446 | LYMYIYFVVF | IIFGSF <u>FTLN</u> | LFIGVIIDNF | |
| | IVS6 | 4i | 1748 | AVGILFF <u>TTY</u> | <u>IIISFLIVVN</u> | <u>MYIAIILENF</u> | ^l |
| Pore-facing position | | | | | | * * ** * | |
| Sidewalk-facing positions IIS6 | | | | | | * * | |
| Sidewalk-facing positions IVS6 | | | | | | * ** * | |

^a Bold-typed are residues whose mutations are described under footnotes referred to in the rightmost column. Residues whose mutations affect closed-channel block are shaded. Residues whose mutations affect access of LAs are underlined.

^b The standard segment name includes the domain number and symbols S5, S6, or P, for respective transmembrane segment or membrane-reentering P-loop. An alternative segment name, which is used in residue labels, includes the domain number and

symbols o, p, and i for the outer helices, inner helices, and P-loops, respectively (see Chapter 1). The absolute numbers (#) of the first residue in a segment are shown for the following sequences: Na_v1.2 (SCN2A_RAT), Na_v1.4 (SCN4A_RAT), and Na_v1.5 (SCN5A_RAT). Relative numbers of residues are shown above the aligned sequences. For the transmembrane segments, the relative numbers are counted from the beginnings of the respective KcsA helices as seen in the X-ray structure (Doyle et al., 1998). Relative numbers of residues in P-loop are counted from the DEKA-locus, whose residues are assigned number 50 to avoid negative numbers for residues in P-helices.

- ^c Mutations at the DEKA locus (D^{1p50}A, E^{2p50}A, and A^{4p50}D) allowed external block by QX-222 and QX-314 and accelerated the recovery from block by internal QX-314 (Sunami et al., 1997). Mutation Y^{1p51}C enabled the external block by QX-222 (Sunami et al., 2000).
- ^d Mutation C^{1p51}Y reduced the external QX-314 block (Sunami et al., 2000).
- ^e Mutation S^{4p49}L accelerated recovery of hNa_v1.5 from internally applied QX-314 and enhanced tonic block by mexiletine and QX-314 (Sasaki et al., 2004).
- ^f Mutation Y¹ⁱ¹⁷A increased the affinity of etidocaine to the closed channel (Yarov-Yarovoy et al., 2002).
- ^g Mutations M²ⁱ¹¹A, N²ⁱ¹⁵A, and V²ⁱ¹⁸A increased closed-channel block by etidocaine (Yarov-Yarovoy et al., 2002).
- ^h Mutations L³ⁱ¹⁹A, N³ⁱ²⁰A, and I³ⁱ²³A decreased affinity of inactivated channels to LAs, but did not decrease the closed-channel block (Yarov-Yarovoy et al., 2001). Mutations L³ⁱ¹⁹A and N³ⁱ²⁰A increased the closed-channel block by lamotrigine and etidocaine. Mutation I³ⁱ²³A increased the affinity for lamotrigine but not etidocaine to the closed channel.
- ⁱ Mutation I⁴ⁱ¹¹A accelerated the channel recovery after use-dependent block and allowed external QX-314 block (Ragsdale et al., 1994). Alanine mutations of F⁴ⁱ¹⁵, N⁴ⁱ²⁰, and Y⁴ⁱ²² significantly decreased use-dependent block by etidocaine (Ragsdale et al., 1994). In the Na_v1.3 channel, closed-channel block requires a hydrophobic residue at position 4i15, while use-dependent block by tetracaine requires an aromatic residue 4i15 and Y⁴ⁱ²² (Li et al., 1999).
- ^j Mutation of L³ⁱ¹⁹ had no effect on closed-channel block by bupivacaine (Nau et al., 2003).
- ^k Mutation C⁴ⁱ⁸T allowed the external QX-222 block (Sunami et al., 2000). Mutant I⁴ⁱ¹¹A allows block by the external QX-314 (Wang et al., 1998) and QX-222 (Sunami et al., 2001). Benzocaine and etidocaine are less potent in the F⁴ⁱ¹⁵A mutant (Wang et al., 1998). Lysine substitutions showed that Y⁴ⁱ²² is important for the use-dependent block, but not the closed-channel block by cocaine, while F⁴ⁱ¹⁵ and N⁴ⁱ²⁰ are important for both the use-dependent and closed-channel block (Wright et al., 1998).
- ^l T⁴ⁱ⁸V reduced external QX-314 block; F⁴ⁱ¹⁵A inhibited the binding of both external and internal QX-314 (Qu et al., 1995). I⁴ⁱ¹¹C accelerated recovery and facilitated closed-state untrapping of cocaethanol (O'Leary et al., 2003). Mutation Y⁴ⁱ²²C significantly reduced use-dependent block by cocaine (O'Leary and Chahine, 2002).

consecutive energy minimizations did not decrease the energy of the apparent global minimum found. For docking of LAs, the multi-MCM protocol (Bruhova and Zhorov, 2007; Tikhonov and Zhorov, 2007) was employed as follows. First, 60,000 starting points with random positions, orientations, and conformations of the ligand were seeded within a 14 Å-edge cube whose center was placed in the cavity center. The size of the cube was chosen to ensure sampling in the central pore and in the domain interfaces. Each starting point was optimized in an MCM trajectory of 10 steps to remove steric overlaps with the channel. Three hundreds lowest-energy structures found at this stage were further MC-minimized in longer trajectories to refine the protein-ligand complexes. These trajectories were terminated after 1,000 consecutive steps did not decrease the energy. All the complexes within 10 kcal/mol from the apparent global minimum were analyzed.

Access pathways for LAs were explored by pulling QX-314 along a specific direction with the step of 0.5 Å (Tikhonov and Zhorov, 1998). At each position, the energy was MC-minimized. For QX-314 pulled through the selectivity filter or the closed activation gate, the pulling direction coincides with the pore axis. For the ligand pulled between domains III and IV, the pulling direction is parallel to helix IIIIP. The ligand was pulled by the *para*-carbon of the benzene ring. The ligand flip-flop was prevented as described (Bruhova and Zhorov, 2007). For each pathway, three independent trajectories were calculated and the ligand-channel energies at each position were averaged.

RESULTS

LA Binding

Three structurally different LAs were chosen in our study: QX-314, which is a permanently charged derivative of lidocaine, cocaine with bulky fused rings, and tetracaine with an elongated hydrophobic tail attached to its benzene ring (Figure 5.1). The LAs were docked in the closed Na_v1.5 model whose DEKA locus was loaded by either a water molecule (H₂O-DEKA model) or a Na⁺ ion (Na⁺-DEKA model).

LAs in the H₂O-DEKA model

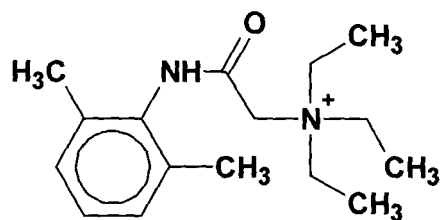
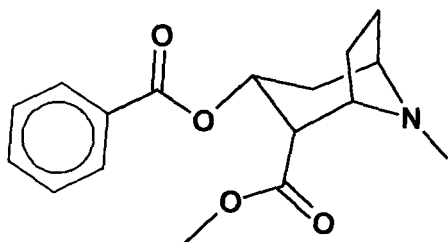
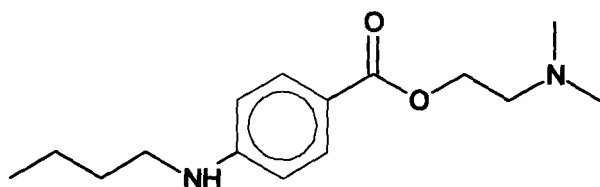
Figures 5.2A,B show multiple randomly generated starting points. The multi-MCM of the starting points yielded ensembles of 50 most favourable complexes for each of the three compounds studied. In each complex, the ligand occurred in the inner pore. In most cases, the ammonium group was found in the central cavity, near the focus of P-helices (Figures 5.2C, 5.3A). The DEKA-locus side chains strongly contribute to the binding of all three LAs because the electrostatic attraction of the ammonium group to D^{1p50} and E^{2p50} overweighs the repulsion from K^{3p50}. Furthermore, carbonyl groups of residues in positions *p47* through *p50* of all four repeats also stabilize the ligand via electrostatic interactions.

The ligand orientation greatly varied between the complexes. All three LAs have an elongated shape. Let us define the long axis of a ligand as a line drawn between the ammonium nitrogen and the *para*-carbon of the benzene ring. Three energetically favourable binding modes of LAs inside the channel can be categorized as vertical, horizontal, and angular. In the first two modes, the ligand long axis is either parallel or perpendicular to the pore axis (Figure 5.2 *D,F*). In the angular mode, the ligand long axis is at $45\pm 10^\circ$ to the pore axis (Figure 5.2 *E*). QX-314 (Figure 5.2) and cocaine (Figure 5.3) can adopt all the three binding modes. Tetracaine (Figure 5.4) adopts only the horizontal mode because its long hydrophobic tail does not fit in the closed pore.

Energetics of the binding modes is given in Table 5.2. The vertical mode is stabilized by rings of residues in positions *i22* and *i15*. In the vertical mode, the hydrophobic bundle of residues *i22* from all four repeats anchors the LA benzene ring (Figures 5.2*D* and 5.3*C*). In particular, F²ⁱ²² and Y⁴ⁱ²² π -stack to opposite faces of the drug's benzene ring. In some cases the ligand's carbonyl or the secondary amine group H-bonds with the OH group of Y⁴ⁱ²². Residue F³ⁱ²² at the bottom of the binding pocket interacts with the benzene ring in the edge-to-face manner (Burley and Petsko, 1985; Singh and Thornton, 1985). I¹ⁱ²² also contributes to the bottom of the binding pocket, while F⁴ⁱ¹⁵ binds to the ligand side.

In the horizontal binding mode the aromatic ring protrudes in the III/IV domain interface. Despite this orientation was not biased in our calculations, practically no low-energy complexes were found in which the aromatic ring of LAs were protruding in the other (I/II, II/III, or IV/I) domain interfaces. Only in the case of tetracaine, a few complexes were found where the aromatic ring protruded in the other interfaces, but their ligand-channel energy was weak. The horizontal binding mode is stabilized mainly by π -stacking interactions with F⁴ⁱ¹⁵ (Table 5.2). Due to the horizontal ligand orientation, residues in the cytoplasmic halves of S6s practically do not contribute to the ligand binding. The long tail of tetracaine reaches W^{3o18} that contributes -0.7 kcal/mol to ligand-channel energy. In the angular binding mode, which is intermediate between the vertical and horizontal modes, the benzene ring of the ligands binds between F⁴ⁱ¹⁵ and Y⁴ⁱ²².

Generally, the horizontal binding mode has more preferable electrostatic energy than the vertical one due to a stronger attraction of the ligand's ammonium group to the nucleophilic C-ends of the P-helices (Table 5.2). This is compensated by a larger dehydration cost of the horizontal mode vs. the vertical one. Interactions with the S6s are more important for the vertical mode. Contributions of the key binding determinants in IVS6 to the vertical and horizontal modes are different: in the vertical mode, Y⁴ⁱ²² contributes more than F⁴ⁱ¹⁵, but only F⁴ⁱ¹⁵ contributes significantly to the horizontal mode. The above characteristics of the binding modes are similar for the three LA docked in this study suggesting that other LAs may bind similarly in the closed Na⁺ channel.

**QX-314****Cocaine****Tetracaine****Figure 5.1. Chemical structures of LAs that are used in calculations.**

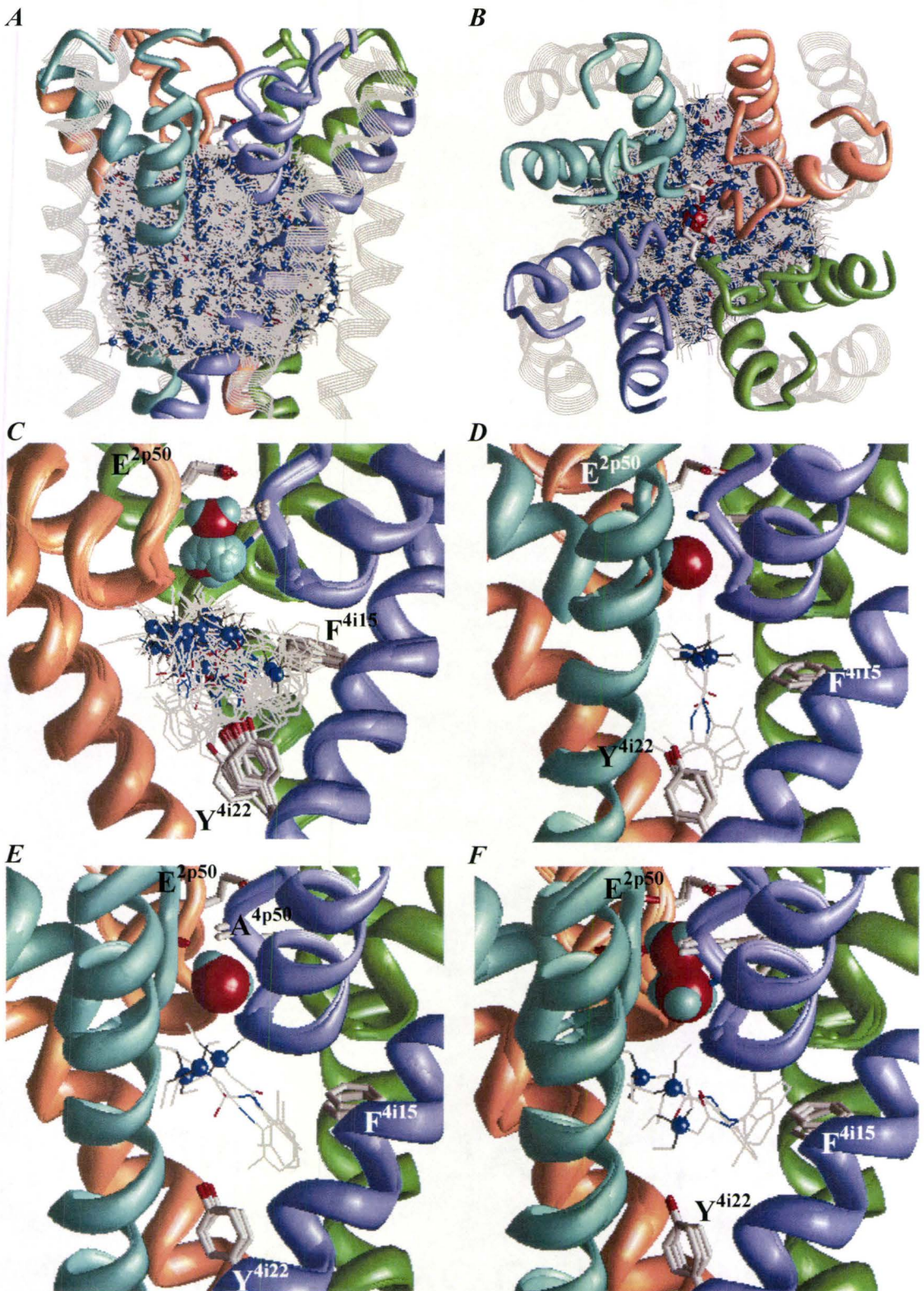


Figure 5.2. Searching for energetically favourable binding modes of QX-314 in the closed Na_v1.5 with a water molecule in the selectivity filter. The inner helices and P-loops of domains I, II, III, and IV are coloured cyan, orange, green, and violet, respectively. The outer helices are shown as grey strands. The water molecule is space-filled. The side chains of residues in the DEKA locus as well as conserved F⁴ⁱ¹⁵ and Y⁴ⁱ²² are shown as sticks. The ligand is wire-frame with the ammonium nitrogen shown as a blue sphere. **A** and **B**, Side and top views at the superposition of starting points. For clarity, only 6,000 of the 60,000 starting points are shown. **C**, Fifty lowest-energy binding modes. **D**, **E**, and **F**, Superposition of the lowest energy vertical, angular, and horizontal binding modes, respectively. For clarity the outer helices are not shown in **C-F**.

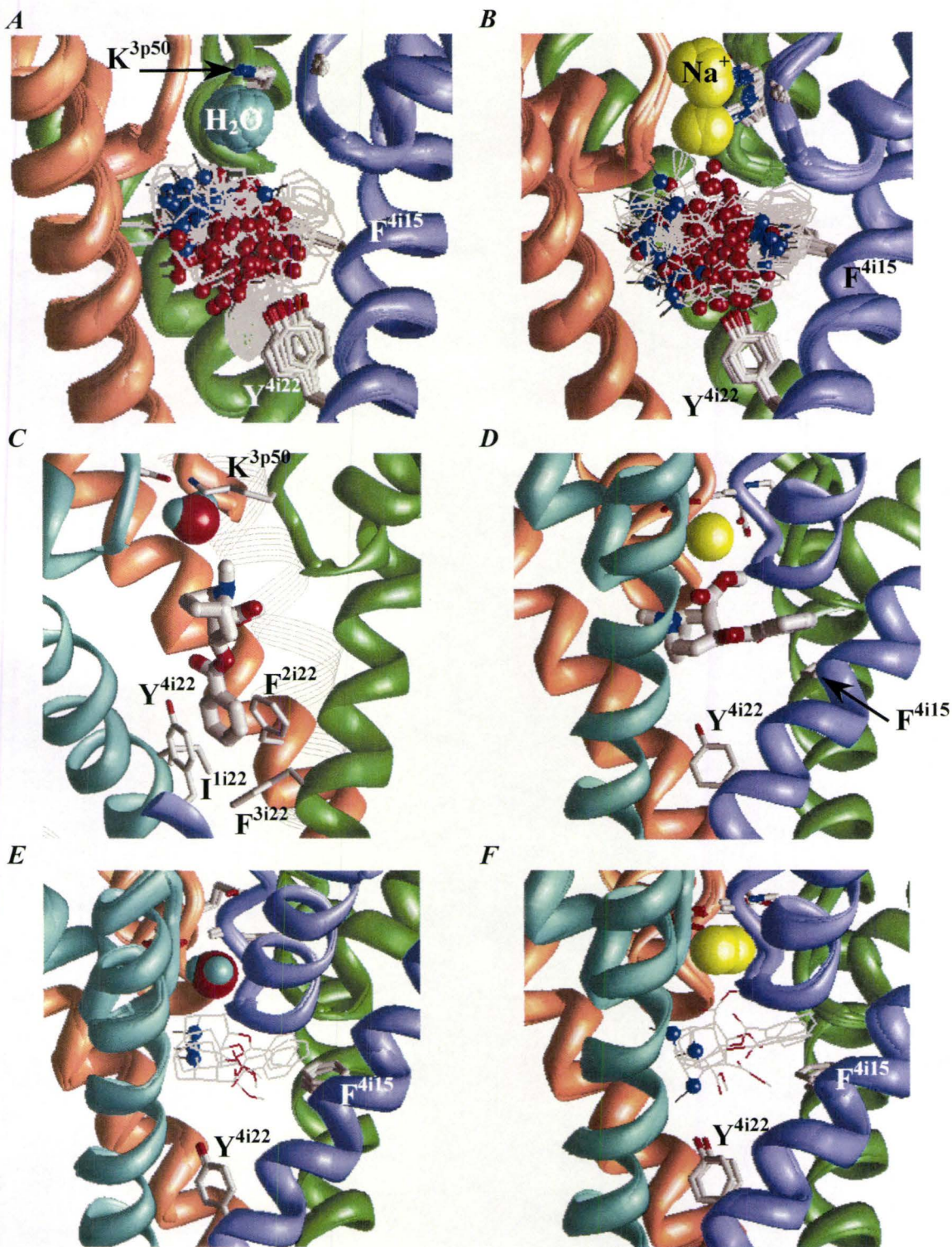


Figure 5.3. Searching for energetically favourable binding modes of cocaine in the closed Na_v1.5 with a water molecule (A, C, E) or Na⁺ ion (B, D, F) in the DEKA locus. For clarity the outer helices are not shown. A and B, Fifty lowest-energy binding

modes in the H₂O-DEKA and Na⁺-DEKA models, respectively. **C**, A vertical binding mode of cocaine. The ligand's aromatic group interacts with three aromatic residues in positions *i22*. **D**, The energetically most favourable binding mode of cocaine in the Na⁺-DEKA model. The oxygen atoms of cocaine approach the Na⁺ ion, while the aromatic ring of the drug extends to the sidewalk between helices IIIS6 and IVS6. **E** and **F**, The superposition of the energetically best horizontal binding modes.

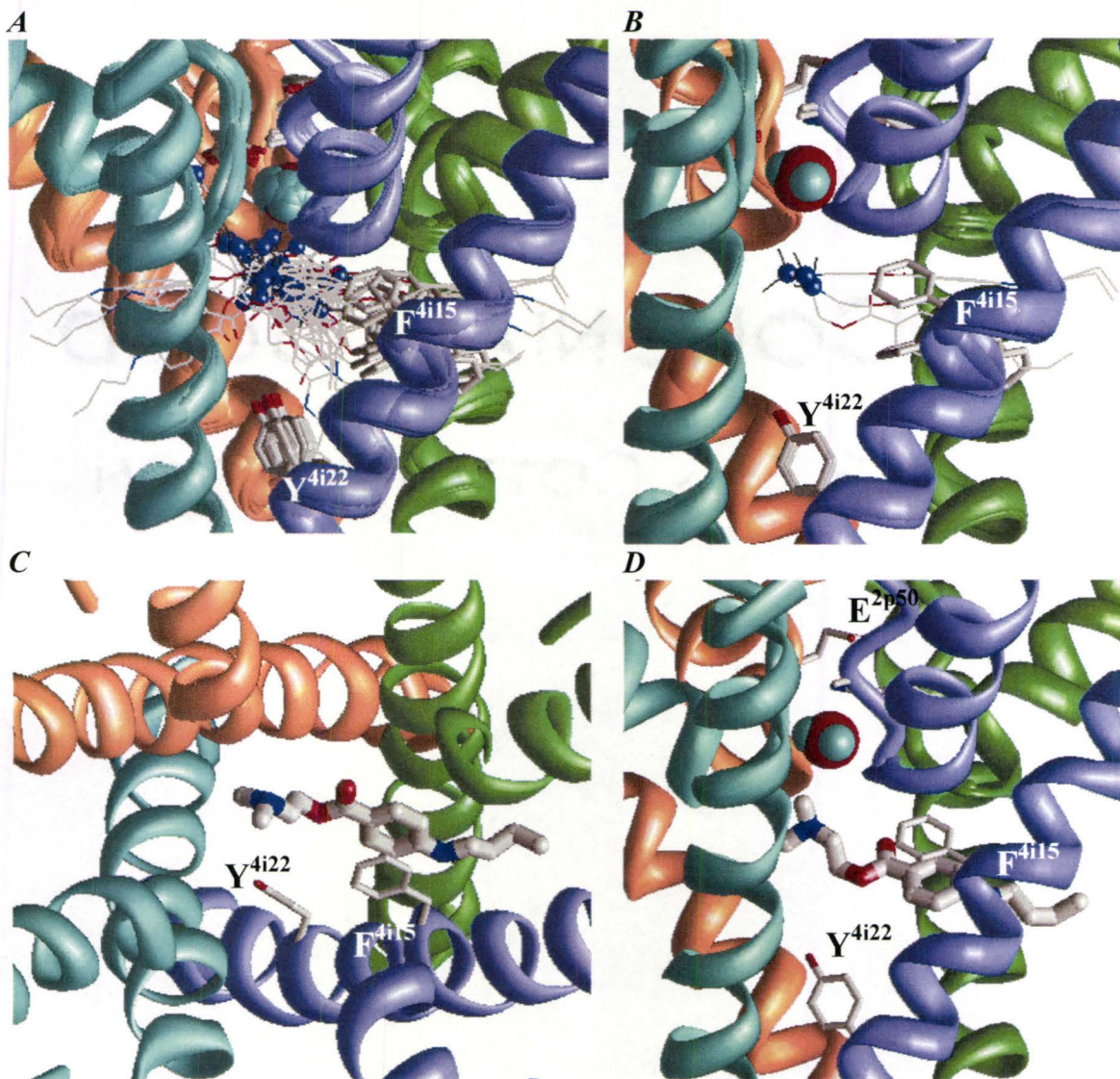


Figure 5.4. Searching for energetically favourable binding modes of tetracaine in the closed Na_v1.5 channel with a water molecule in the DEKA locus. *A*, Fifty lowest-energy complexes. In most of the complexes, the drug's aromatic ring protrudes in the III/IV domain interface. *B*, The superposition of three lowest-energy complexes representing the horizontal binding mode. *C* and *D*, The side and top views of the lowest-energy complex representing the horizontal binding mode. Note π -stacking of the drug's aromatic ring with F⁴¹⁵.

Table 5.2. Energetically favourable binding modes of LAs in the closed Na_v1.5 with the DEKA locus loaded by either H₂O or Na⁺.

| Ligand-channel energy and its components ^a | Cocaine ^b | | | QX-314 ^b | | | Tetracaine |
|---|-----------------------|------------------|-----------------|-----------------------|------------------|-----------------|-------------------------|
| | Vertical ^c | | Horizontal | Vertical ^c | | Horizontal | Horizontal ^d |
| | H ₂ O | H ₂ O | Na ⁺ | H ₂ O | H ₂ O | Na ⁺ | H ₂ O |
| Total | -40.6 | -38.2 | -36.2 | -39.3 | -39.0 | -31.3 | -35.2 |
| van der Waals | -24.4 | -26.1 | -31.5 | -23.3 | -21.9 | -22.7 | -27.1 |
| Desolvation | 13.2 | 23.3 | 28.1 | 8.7 | 14.1 | 14.2 | 14.4 |
| Electrostatics | -29.4 | -35.5 | -32.8 | -24.8 | -30.8 | -22.7 | -22.4 |
| Segments ^e | | | | | | | |
| P-loops | -19.9 | -23.3 | -30.7 | -18.8 | -24.6 | -25.0 | -20.7 |
| All S6s | -19.8 | -14.9 | -10.8 | -19.7 | -13.6 | -14.1 | -12.3 |
| Key determinants of action ^f | | | | | | | |
| Phe ⁴ⁱ¹⁵ | -0.2 | -3.9 | -2.9 | -1.0 | -2.2 | -2.4 | -2.1 |
| Tyr ⁴ⁱ²² | -3.2 | -0.6 | -0.4 | -3.5 | -0.4 | -0.6 | 0.0 |

^a Ligand-receptor energy, its components, and contributions (kcal/mol) from individual segment and specific residues.

^b The lowest-energy structure for each binding mode is shown. The entropy contributions were not taken into account, which is a standard approximation in homology modeling. These contributions would partially compensate the large enthalpy of ligand-channel interactions.

^c The Na⁺-DEKA model energy is not shown because it is much weaker than in the H₂O-DEKA model.

^d The Na⁺-DEKA model with tetracaine was not explored.

^e The energy values include both the side chain and backbone contribution to ligand binding.

^f The energy values include only the side chain contributions to ligand binding.

LAs in the Na⁺-DEKA model

Earlier we predicted that the binding mode of lidocaine in the open Na⁺ channel depends dramatically on whether a Na⁺ ion or a water molecule populates the DEKA locus (Tikhonov et al., 2006; Tikhonov and Zhorov, 2007). In this study, we placed a Na⁺ ion in outer pore of the closed Na_v1.5 in a position equivalent to the K⁺ ion position 4 in the outer pore of K⁺ channels (Tikhonov and Zhorov, 2007). In this position, the Na⁺ ion counterbalances the excessive negative charge in the DEKA locus, which becomes less attractive for the pore-bound cations than in the H₂O-DEKA model.

Cocaine and QX-314 were docked by the multi-MCM method. In the majority of the 50 lowest-energy structures collected for each ligand, the ammonium group is displaced from the selectivity filter in the cytoplasmic direction due to electrostatic repulsion from the Na⁺ ion in the DEKA locus. In the vertical binding mode, the repulsion energy between the ammonium group and the Na⁺ ion is as strong as 13.0 kcal/mol. Because of the limited space in the central cavity, the drugs had a tendency to adopt the horizontal binding mode with the aromatic ring protruding in the III/IV domain interface (Figure 5.3 B). In this mode, the ligand ammonium group and the Na⁺ ion are more distant from each other than in the vertical mode. As a consequence, the repulsion between the Na⁺ ion and the ligand in the horizontal binding mode varies from 1.5 to 8 kcal/mol, which is much weaker than in the vertical mode (Table 5.2). In the lowest-energy complex, the cocaine ester group is attracted by the Na⁺ ion, while the benzene ring π -stacks with F⁴¹⁵ (Figure 5.3 D). In some complexes, the Na⁺ ion relocated from the starting position to the extracellular face of the DEKA locus (Figure 5.3 D), the level equivalent to position 2 in K⁺ channels (Tikhonov and Zhorov, 2007). This relocation decreased the Na⁺-ligand repulsion.

Thus, in the Na⁺-DEKA and H₂O-DEKA models the LAs adopt the horizontal and vertical binding modes, respectively and the LA binding energy significantly depends on the occupancy of the DEKA locus.

The above docking experiments of our study have been performed with the united-atom model of the channel, which is insensitive to cation- π interactions because atomic charges at aromatic carbons are close to zero. To assess a possibility of cation- π interactions, we created and MC-minimized an all-atom model of the closed channel and docked QX-314 in the vertical and horizontal modes with constraints imposing either π -stacking or cation- π interactions between QX-314 and F⁴¹⁵. After MC-minimizing the complexes, constraints were removed and the second round of MC-minimizations provided structures shown in Figure 5.5. The structures with cation- π interactions were found less preferable than those with stacking interactions (Table 5.3).

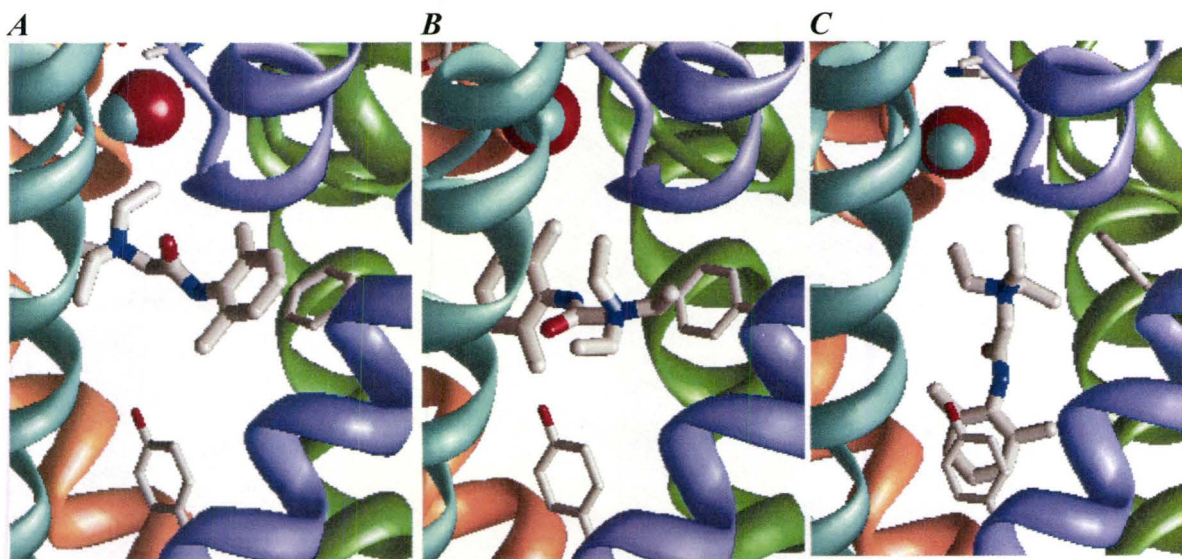


Figure 5.5. All-atom model of the closed Na_v1.5 with a water molecule in the DEKA locus and QX-314 in the inner pore. For clarity the outer helices are not shown. *A*, QX-314 in a horizontal binding mode with its benzene ring π -stacking with F⁴ⁱ¹⁵. *B*, QX-314 in a horizontal binding mode with its ammonium group interacting with F⁴ⁱ¹⁵. This mode is 5.8 kcal/mol less preferable than the mode shown at *A* because of weaker electrostatic attraction to the DEKA locus (see Table 5.3). *C*, QX-314 in a vertical binding mode with its benzene ring π -stacking with Y⁴ⁱ²² and ammonium group approaching F⁴ⁱ¹⁵. This binding mode resembles the open-channel block (Tikhonov and Zhorov, 2007). However, the closed activation gate pushes QX-314 closer to the selectivity filter and therefore the ammonium group does not form a strong cation- π complex. Indeed, the partitioned interaction energy between the ligand cationic group and the benzene ring of F⁴ⁱ¹⁵ is 3.8 kcal/mol less favourable than in complex TEA : benzene, which was MC-minimized with the same force field (data not shown). Note that binding modes *A* and *C* are similar to those found with the united-atom approximation.

Table 5.3. Interaction energy (kcal/mol) of QX-314 with the all-atom Na_v1.5 model

| Energy | Complex shown in Figure | | |
|----------------------------|-------------------------|--------------|--------------|
| | 5.5A | 5.5B | 5.5C |
| Total | -35.4 | -29.6 | -33.8 |
| van der Waals | -24.6 | -21.2 | -23.5 |
| Desolvation | 15.2 | 10.5 | 7.9 |
| Electrostatics | -25.9 | -18.8 | -18.2 |
| Segments | | | |
| P-loops | -25.3 | -13.5 | -15.7 |
| All S6s | -11.2 | -15.5 | -18.3 |
| Key determinants of action | | | |
| Phe ⁴ⁱ¹⁵ | -3.5 | -3.1 | -2.9 |
| Tyr ⁴ⁱ²² | -0.2 | -1.5 | -3.6 |

Access pathways of QX-314

The extracellular access of LAs to the closed Na^+ channels is discussed in several studies (Ragsdale et al., 1994; Qu et al., 1995; Sunami et al., 1997; Sunami et al., 2001), but it remains unclear whether LAs pass between the III/IV domain interface or through the selectivity filter. To address this, we pulled QX-314 through these two hypothetical pathways (Figures 5.6, 5.7). As a control, the ligand was also pulled through the closed activation gate (Figure 5.6A). The vertical binding mode was chosen as a starting position for pulling QX-314 through the selectivity filter and the closed gate, while the horizontal mode was used as the starting point for pulling the ligand via the III/IV interface. None of the computed profiles have ligand-receptor energy better than in the starting point (Figures 5.6C, 5.8). This agrees with the notion that the inner pore is the energetically preferable binding site for LAs.

Pulling QX-314 through the closed gate (Figure 5.6A) imposes a van der Waals energy barrier of 60 kcal/mol (Figure 5.6C) indicating that the closed gate is impassable. Two peaks of the energy profile at positions -10 and -17 Å are determined by repulsion between the ligand's ammonium group and residues in positions *i22* and *i26*, which face the pore axis. Thus, as expected, the closed activated gate does not allow QX-314 to reach the central cavity from the cytoplasm.

Pulling QX-314 through the selectivity filter not loaded with a water molecule or a Na^+ ion (Figure 5.6B) results in the energy barrier of 33 kcal/mol, which is caused by steric clashes and unfavourable desolvation (Figure 5.6C). Residues in positions *p49* and *p50* form the tightest rings. In particular, K^{3p50} , G^{2p49} , and S^{4p49} contribute to the large energy barrier. Residues in positions *p51*, *p52*, and *p53* do not impose energy barriers but attract the ligand.

Pulling QX-314 through the III/IV domain interface (Figure 5.7) did not cause high-energy barriers (Figure 5.8). Residues of the IIIP-helix interact with the ligand all along the pathway. The ligand-channel energy weakens as the ligand leaves the central cavity and loses electrostatic attractions from the DEKA locus and nucleophilic C-ends of P-helices. Residues T^{4i8} and I^{4i11} contribute only weakly to the drug-channel energy at the drug-binding site (position 0), but their contributions increase along the pathway. The most significant interaction of QX-314 with I^{4i11} corresponds to the rightmost part of the profile, indicating that I^{4i11} affects the drug access much stronger than the drug binding in the inner pore. Residue T^{4i8} , which is far from the pore axis, faces the III/IV interface. The experimentally observed effect of mutations in this position on the external drug access can be explained by direct interaction with the ligand entering the domain interface. It should be noted that both T^{4i8} and I^{4i11} interact with the drug at the rightmost part of the pathway (Figure 5.8) and concertedly attract the ligand at this part where the ligand-channel attraction energy is rather small, while the desolvation cost increases. Therefore changes in the size and hydrophobicity in positions *4i8* and *4i11* can significantly affect access of ligands through the domain interface. Thus, the computed

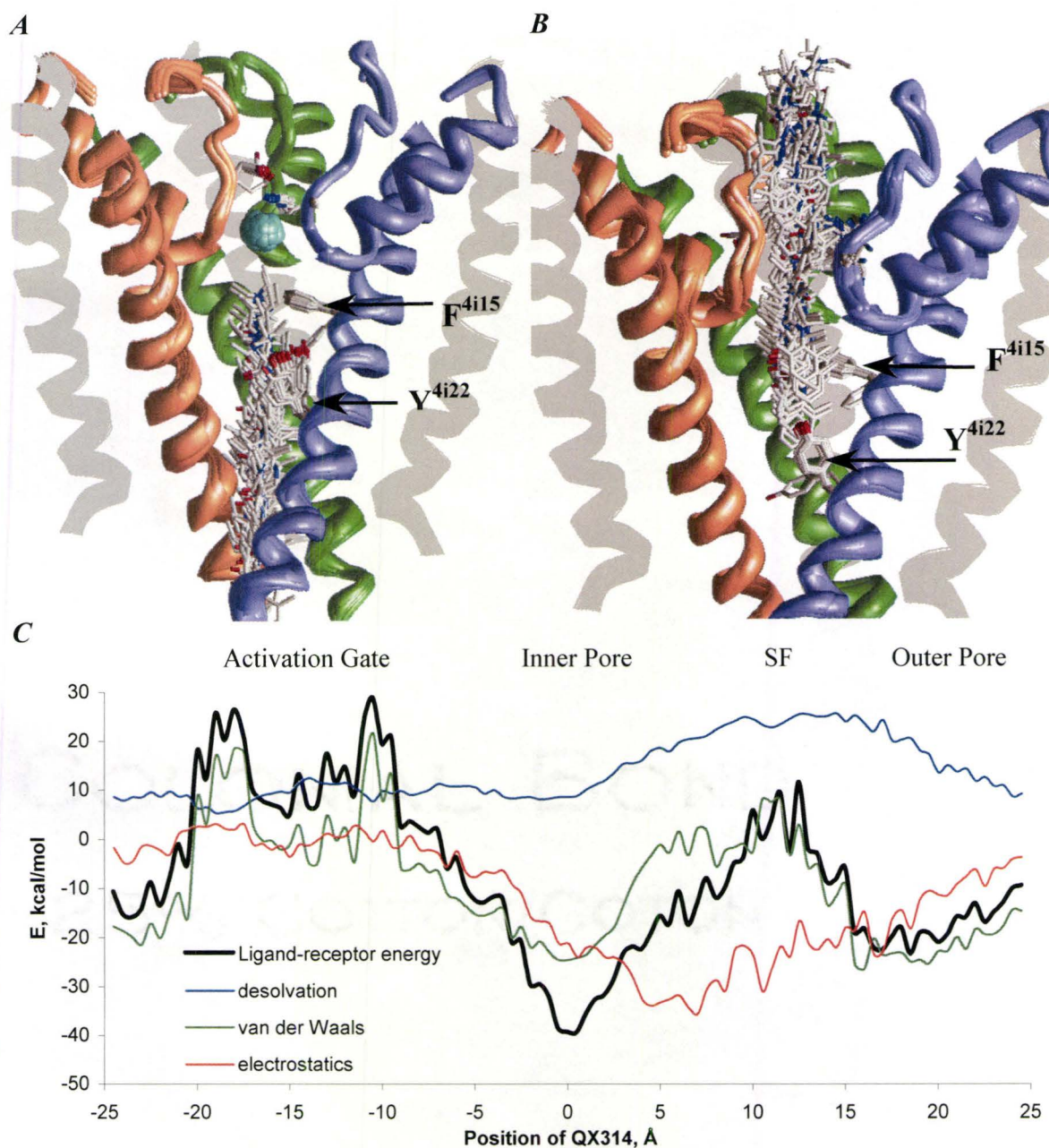


Figure 5.6. Exploring hypothetical access pathways of QX-314. *A* and *B*, Superposition of the MC-minimized structures obtained for QX-314 pulled out of the pore through the selectivity filter (*A*) and the closed activation gate (*B*). QX-314, DEKA residues, F⁴ⁱ¹⁵ and Y⁴ⁱ²² are shown as sticks. For clarity, domain I is not shown. *C*, The MC-minimized energy profiles showing the total drug-channel energy and its components. From the starting position 0, which corresponds to the lowest-energy vertical binding mode of QX-314 (Figure 5.2D), the ligand was pulled at 0.5 Å steps either through the selectivity filter (positions 0 to 25) or through the activation gate (positions 0 to -25).

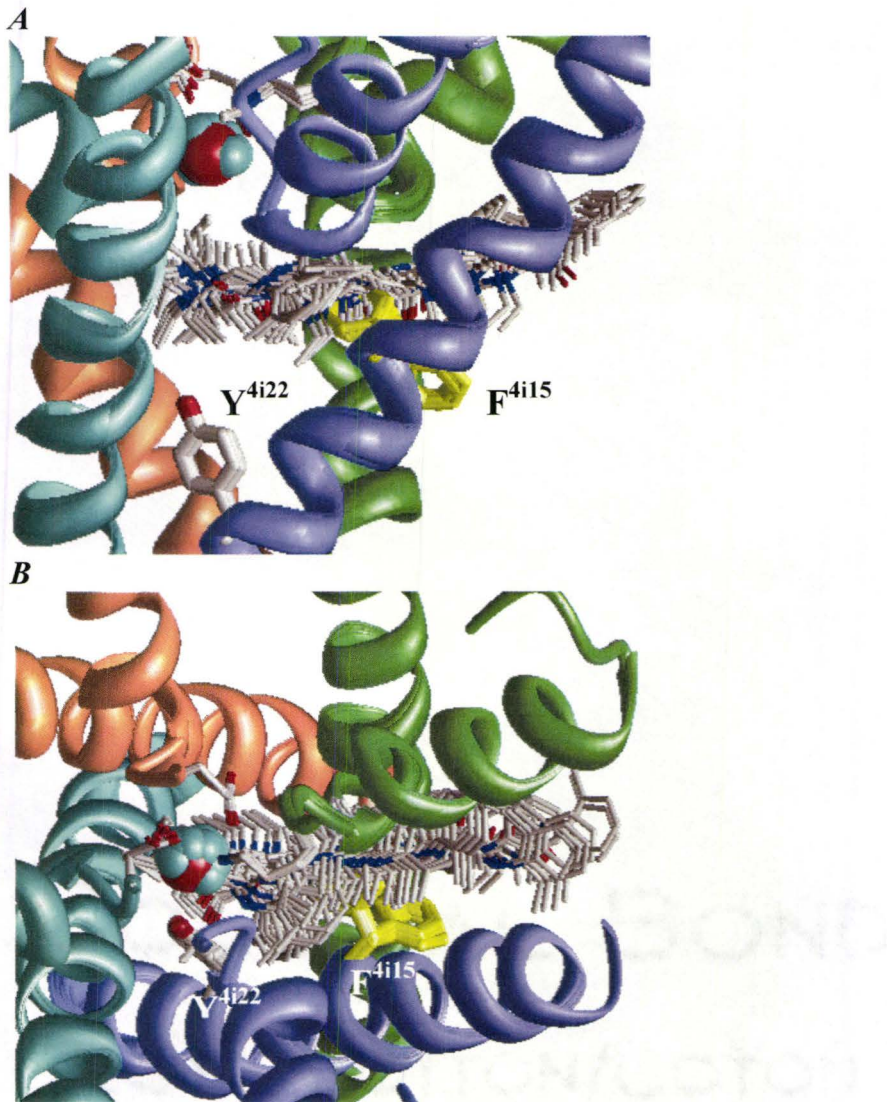


Figure 5.7. Pulling QX-314 through the sidewalk, between segments IIP, IIS6, and IVS6. *A* and *B*, The side and top views of the superposition of QX-314 pulled from the starting position 0, which corresponds to the horizontal binding found from random sampling (Figure 5.2 *F*).

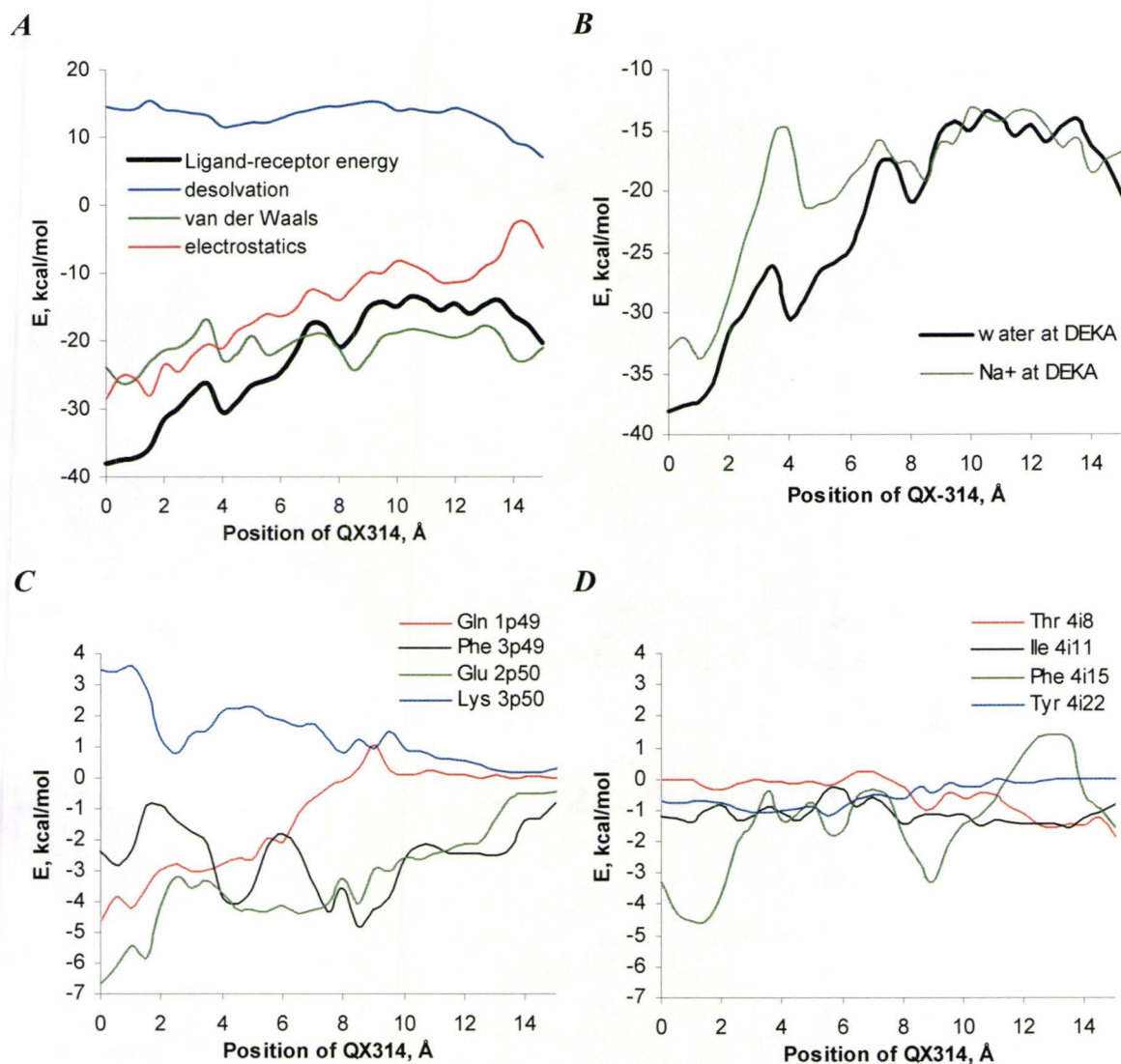


Figure 5.8. The MC-minimized energy profile of QX-314 pulled through the sidewalk. *A*, The energy profile with total drug-channel energy and its components. Position 0 corresponds to the lowest-energy drug-channel complex, which was found in the multi-MCM search and which represents the horizontal binding mode (Figure 5.2 *F*). The ligand was pulled at 0.5 Å steps. *B*, The energy profile of QX-314 pulled through the III-IV interface of the H₂O-DEKA and Na⁺-DEKA models. *C* and *D*, Most significant energy contributors to the energy profile.

energy profile through the III/IV domain interface agrees with the hydrophobic access pathway concept.

Comparison of the energy profiles calculated in the H₂O-DEKA and Na⁺-DEKA models show that the Na⁺ ion significantly destabilizes QX-314 in position 0 and along the access pathway (Figure 5.8 *B*). In position 0, the difference between the drug-channel energies of the two models is 5 kcal/mol. The difference in positions 3 to 6 is much larger because in this narrow part of the pathway the Na⁺ ion and the ligand's ammonium nitrogen approach each other as close as 6 Å. Besides this electrostatic repulsion, the Na⁺ ion does not significantly affect the ligand trajectory and contributions of individual residues to the ligand-channel energy.

Residue F⁴ⁱ¹⁵ plays a key role in the access pathway of QX-314 (Figures 5.7 and 5.8*D*). At position 0, F⁴ⁱ¹⁵ faces the pore and π -stacks with the benzene ring of QX-314. As QX-314 is pulled between domains III and IV, F⁴ⁱ¹⁵ reorients to let QX-314 pass. The reorientation causes an energy barrier at position 3.5 Å from the start. The barrier is much higher in the Na⁺-DEKA model than in the H₂O-DEKA model.

DISCUSSION

Understanding molecular determinants of state-dependent action of LAs, which are widely used clinically and in experiments, are of obvious importance. Residues F⁴ⁱ¹⁵ and Y⁴ⁱ²² have long been known as critical determinants of the use-dependent block. LAs in the vertical but not in horizontal mode can simultaneously bind to both F⁴ⁱ¹⁵ and Y⁴ⁱ²², which are separated by two helical turns of IVS6. Several structural models of Na⁺ channels visualized the vertical binding mode and analyzed contacts of LAs with LA-sensing residues (Lipkind and Fozzard, 2000; Fozzard et al., 2005; Lipkind and Fozzard, 2005; Tikhonov et al., 2006; McNulty et al., 2007; Tikhonov and Zhorov, 2007).

It is well known that effects of mutations on the block of the open/inactivated and closed channels are different (Hille, 1977; Chahine et al., 1992; Ragsdale et al., 1994; Xu et al., 1994; Wright et al., 1997; Nau et al., 2003), but molecular determinants of this difference were unclear. Here we systematically simulated binding of structurally different LAs in the closed-channel model. The chosen LAs contain an ammonium group and a benzene ring but essentially vary in size and chemical structure. Since the central cavity in the closed channel is rather small, it was unclear how these ligands interact with ligand-sensing residues. Furthermore, since occupation of the DEKA locus in the closed state is unknown, we populated the locus by either a water molecule or a Na⁺ ion. Unbiased docking using a powerful multi-MCM search resulted in ensembles of complexes in which QX-314 and cocaine adopted vertical, horizontal, or intermediate (angular) binding modes. In contrast, only the horizontal binding mode was found for tetracaine, because the vertical mode of this elongated drug does not fit in the confined

central cavity of the closed channel. The horizontal binding mode of tetracaine was also recently proposed by another group (Scheib et al., 2006).

Ragsdale and coauthors (Li et al., 1999) systematically studied state-dependent action of tetracaine on $\text{Na}_v1.3$ and its mutants and demonstrated that frequency-dependent block requires an aromatic residue (F, Y, or W) in position *4i15*, while the closed-channel block requires a hydrophobic residue in this position. Furthermore, the frequency-dependent block required Y^{4i22} , while the resting-channel block was possible with S, A, C, I, or F in this position. These data support our conclusion that tetracaine blocks the closed channel in the horizontal mode. Indeed, F^{4i15} contributes -2.1 kcal/mol, while Y^{4i22} did not have a noticeable contribution (Table 5.2).

Docking of QX-314 and cocaine did not predict a single binding mode. However, experimental data suggests that the horizontal binding mode in the closed channel is preferable for these drugs and possibly other LAs. Indeed, mutation Y^{4i22}K had no effect on the closed-channel block of $\text{rNa}_v1.4$ by cocaine, while mutations F^{4i15}K lowered the LA affinity twofold (Wright et al., 1998). The $\text{hNa}_v1.5$ mutation I^{4i11}C weakly affects the use-dependent block by cocaine, while Y^{4i22}C had the strongest effects (O'Leary and Chahine, 2002). Thus, residues in the C-terminal half of IVS6 affect predominantly the use-dependent block, while residues at the N-terminal half affect mainly the closed-channel block. Mutation N^{4i20}K also decreased cocaine binding threefold (Wright et al., 1998), but this residue does not face the pore in our model and probably affects the ligand binding allosterically. Indeed, mutations of N^{4i20} affect slow inactivation (Chen et al., 2006). Thus, experimental data support the notion that LAs bind to the closed channel in the horizontal mode, but they block the open channel in the vertical mode.

A recent study (Ahern et al., 2008) provides additional support for our model. The authors used a series of fluorinated derivatives of aromatic amino acids (Santarelli et al., 2007a; Santarelli et al., 2007b) to systematically reduce the negative electrostatic potential at aromatic carbons of F^{4i15} and Y^{4i22} . The disruption of π -cation interaction of F^{4i15} abolished the use-dependent block by lidocaine without affecting the closed-channel block. Fluorination of Y^{4i22} had no effect. This result strongly suggests that π -cation interactions takes place only at F^{4i15} and only in the use-dependent block. In our models of the use-dependent block (Tikhonov et al., 2006; Tikhonov and Zhorov, 2007) the amino-groups of LAs are located near the F^{4i15} and can form the π -cation contact. Contrary to this, in the horizontal binding mode (that we suggest to correspond to the closed channel block) F^{4i15} interacts with the LAs' aromatic rings rather than with the ammonium groups. Thus, despite the united-atom approximation, which is used in our model, is unable to reveal the π -cation interactions, our models agree with experimental data (Ahern et al., 2008).

The vertical binding mode, which likely corresponds to the use-dependent block, and the horizontal binding mode, which is proposed here for the closed-channel block have similar structural components. In both binding modes, the amino-group of LAs is

located below the selectivity filter in the region, which is attractive for cationic particles due to the cooperative effect of the P-helices macrodipoles. However, in the horizontal mode the aromatic moiety of the drugs faces the domain interface and the channel lumen is not completely occluded especially by ligands with a small ammonium group (lidocaine). This raises a question about the mechanism of channel block. A recent study (McNulty et al., 2007) suggested that for asymmetrically bound LAs the block is caused by a combination of electrostatic and hydrophobic effects. This mechanism is plausible and fully agrees with our models. Moreover, effects of charge and hydrophobicity on the action of sodium channel ligands were the subjects of our recent studies (Tikhonov and Zhorov, 2005b; Wang et al., 2006; Wang et al., 2007b; Wang et al., 2007a). Sodium channel activators like batrachotoxin and veratridine bind in the sodium channel to the site, which significantly overlaps with the LA binding site. These drugs do not completely occlude the channel. The charged groups of these drugs do not face the pore. Rather, the drugs expose hydrophilic groups to the remaining lumen. As a result, the channel is conducting despite the presence of relatively large molecules in the pore. Introduction of positively charged residues in position 2115 does not abolish channel conductance but inverses batrachotoxin action from activation to block.

Relations between slow inactivation and binding of cationic LAs

In the closed Na^+ -DEKA models, there is a significant electrostatic repulsion between the ammonium group of the ligand and the Na^+ ion. The repulsion weakens the LA-channel interaction energy. These results suggest that LAs should have higher affinity to channels that lack Na^+ in the DEKA locus and that the binding of LAs should prevent Na^+ to occupy the DEKA locus.

Our models provide an explanation to the notion that cationic LAs bind preferably to slow-inactivated (as known as C-type inactivated) channels (Fozzard et al., 2005). The presence of a Na^+ ion in the DEKA locus would destabilize the binding of a cationic ligand. Slow-inactivated channels do not permeate ions and therefore may lack Na^+ in the DEKA locus. X-ray structures suggest that the extracellular gate closure in K^+ channels may be associated with the ion deficiency in the selectivity filter (Zhou et al., 2001b; Zhou and MacKinnon, 2003). The binding of cationic ligands in the inner pore of K^+ channels enhances slow inactivation (Grissmer and Cahalan, 1989; Choi et al., 1991). The cause of this phenomenon may be the depletion of a K^+ ion from the selectivity filter by a cationic ligand (Lenaeus et al., 2005). Berneche and Roux (2005) suggested that the rearrangements of the selectivity filter in KcsA caused by ion deficiency might be associated with slow inactivation. By analogy with K^+ channels, we propose that the H_2O -DEKA and Na^+ -DEKA models correspond, respectively, to the slow inactivated and conducting states of the Na^+ channel. Docking LAs in the H_2O -DEKA and Na^+ -DEKA models explains the state-dependent action of cationic ligands by repulsion between the ligand's ammonium group and an ion in the DEKA locus. Cationic LAs bind stronger to the slow-inactivated (H_2O -DEKA) channels and stabilize the slow-inactivated state by

antagonizing occupation of the DEKA ring by an ion. Certainly, slow inactivation is a complex process that probably involves yet unknown structural rearrangements of the channel protein. Our simple model of the slow-inactivated state just suggests that the DEKA locus occupancy by either a cation or a water molecule may be of critical importance for the state-dependent ligand binding.

LA access through the III/IV domain interface

Previous studies proposed two possible access pathways of LAs to the inner pore of the closed Na^+ channel: through the selectivity filter and through the domain interface (see Introduction). Residues, which when mutated affect the LA access, face either the pore axis or the domain interface (Table 5.1). Except for residues at the P-loop turn, which can face both pathways, all other positions face either the first or the second pathway. Both pathways were proposed to coexist (Lee et al., 2001). However, positive values of van der Waals energy at positions 10 to 13 of the pathway through the selectivity filter (Figure 5.6C) indicate steric clashes of the LA molecule with the P-loop residues, which face the pore axis. In contrast, van der Waals energy component is negative all along the access pathway through the sidewalk (Figure 5.8A). The existence of this pathway readily explains mutational data about the involvement of residues in positions *4i8*, *4i11*, *4i15*, and *4p49* in the extracellular access (Table 5.1). All these residues face the sidewalk and interact with QX-314 according to the energy profiles (Figure 5.8 C, D). In particular, the $\text{Na}_v1.5$ mutation T^{4i8}V , which increases the sidewalk hydrophobicity, renders the channel less sensitive to the extracellular block by LAs (Qu et al., 1995). Mutation I^{4i11}A in the muscle and brain Na^+ channels makes them sensitive to extracellularly applied quaternary LAs (Ragsdale et al., 1994; Wang et al., 1998; Sunami et al., 2001). Furthermore, mutation I^{4i11}C facilitates escape of the trapped cocaethylene from $\text{Na}_v1.5$ (O'Leary et al., 2003). Our models explain the effects of these mutations: the bulky I^{4i11} in the wild type $\text{Na}_v1.4$ prevents LAs to enter the pore, while smaller A^{4i11} enables LAs to pass. A naturally occurring $\text{hNa}_v1.5$ mutation S^{4p49}L accelerates recovery from the block by internally applied QX-314, enhances the closed-channel block by mexiletine and QX-314, and attenuates the use-dependent block by mexiletine (Sasaki et al., 2004). The S^{4p49}L mutation was suggested to effect the LA access through the selectivity filter (Sasaki et al., 2004), but in our model S^{4p49} faces the sidewalk and contributes to LA binding.

Our present model predicts that LAs also access the closed Na^+ channel via III/IV domain interface. However, since mutations of the outer-pore residues and toxin binding in the outer pore are also known to influence the LA access into the closed channel, the challenge is to explain these experimental observations in view of our model. We propose here that the above influence is mediated by Na^+ ions that can occupy two nucleophilic sites, one in the DEKA locus and another in the cavity center. The antagonism between the Na^+ ion in the DEKA locus and LA binding in the open channel was described before (Tikhonov and Zhorov, 2007). Our present calculations show that occupation of the

DEKA locus by a Na^+ ion also affects LA binding in the closed channel (Table 5.2) and hinders the LAs access to the pore via the III/IV domain interface (Figure 5.8 B). In view of these data, mutations in the ascending limbs, which are likely to affect Na^+ binding in the DEKA locus, should affect access of LAs through the domain interface. For example, mutations D^{1p50}A and E^{2p50}A at the DEKA locus make the $\text{Na}_v1.4$ channel sensitive to the external QX-222 (Sunami et al., 1997). The authors of this study proposed a straightforward interpretation of the experiments, according to which substitutions of large residues in the outer pore with small residues can provide a path for the external QX-222. We do not rule out this interpretation, but in view of our calculations, the above mutations would destabilize Na^+ in the DEKA locus and hence facilitate the LAs access through the domain interface.

In the X-ray structure of $\text{K}_v1.2$ the voltage-sensor domain does not block the sidewalk, but to enter it a ligand should interact with lipids and/or an auxiliary subunit of the channel. In the absence of experimental data, we cannot consider structural details of these interactions. A weakly hydrated tetraalkylammonium cation like QX-314 has more chances to pass by hydrophobic residues of the sidewalk than strongly hydrated inorganic or ammonium cations. For example, energy calculations suggest that trialkylammonium-methanethiosulfonate reagents, which are used in the substituted cysteine-accessibility method, can reach those levels in the pore of ion channels, which are closed for hydrated inorganic ions (Tikhonov et al., 2004; Tikhonov and Zhorov, 2007).

The fact that TTX reduces the rates of extracellular QX-314 block and recovery from the use-dependent block support a hypothesis that LA access their binding site through the selectivity-filter (Qu et al., 1995). Here we propose an alternative explanation for these observations. It involves a Na^+ ion in the central cavity (Figure 5.9) at position, which is equivalent to the K^+ binding site seen in X-ray structures of K^+ channels. Since a Na^+ ion and LAs appear to be competitors for the nucleophilic cavity center, the Na^+ ion should leave this site to allow LA binding (Figure 5.9A). However, the closed channel, which is blocked by TTX, does not provide the escape route for the Na^+ ion. Residing the cavity, the Na^+ ion prevents QX-314 access in the TTX-blocked closed channel (Figure 5.9B). The TTX-induced reduction of the channel recovery from the use-dependent block can be also explained. In the absence of TTX, the escape of LAs through the sidewalk releases the nucleophilic site in the cavity center and this site will be occupied by the incoming Na^+ ion. In the TTX-blocked closed channel, Na^+ cannot access the cavity and replace the LA molecule. It would be an energetically non-preferable situation if a LA molecule leaves the nucleophilic cavity center and this region is not reoccupied by a Na^+ ion.

In contrast to TTX, the μ -CTX mutant R13N binds to the outer pore of Na^+ channels without completely blocking the Na^+ current (Sunami et al., 2001). In the $\text{Na}_v1.4$ mutant I^{4i1}A , externally applied QX-222 reaches the inner pore of the toxin-bound channel and further blocks the current. In view of our model, the incomplete block of the closed channel by the peptide toxin does not prevent exchange of Na^+ and LAs in the

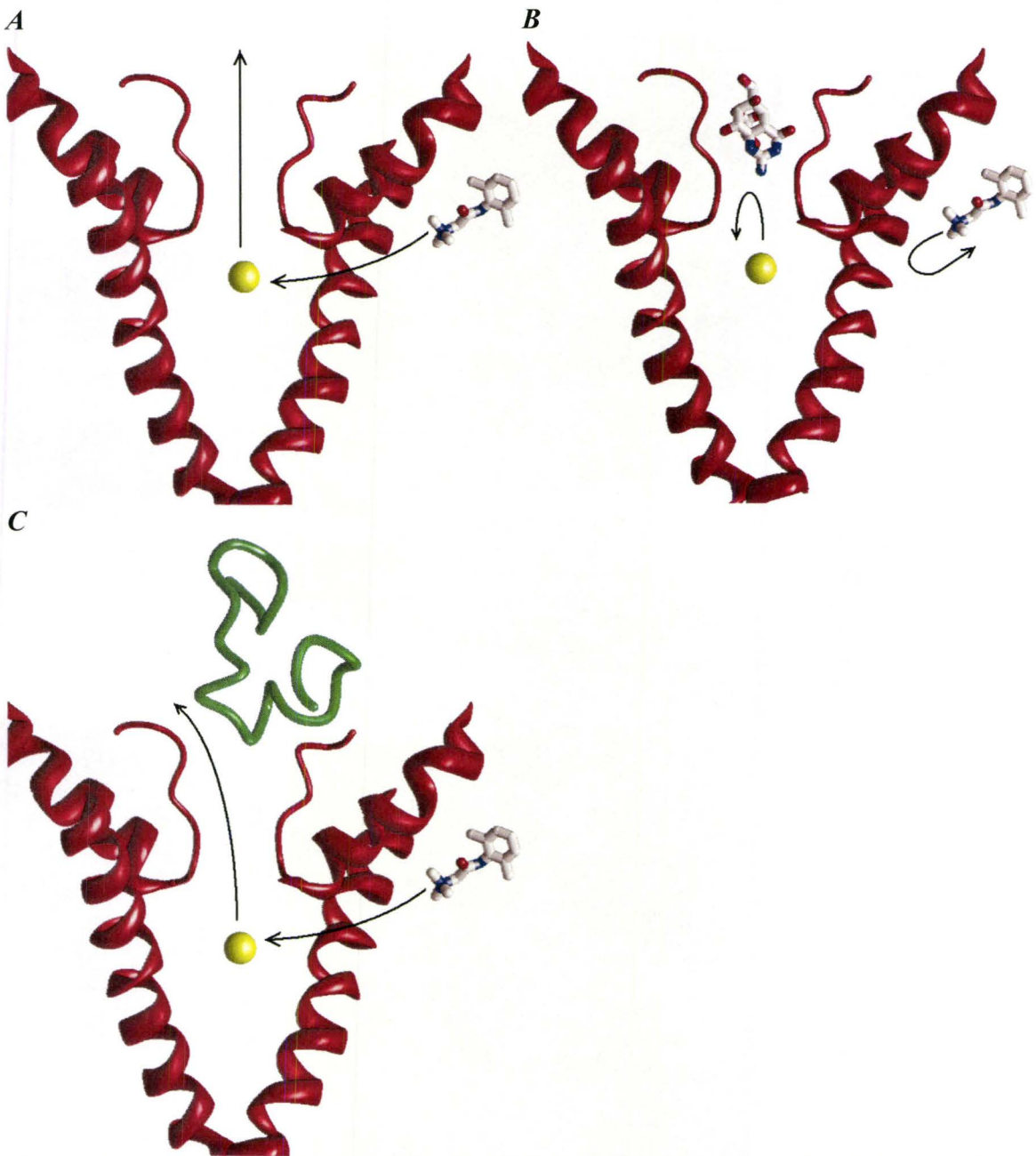


Figure 5.9. A scheme of coupled movement of Na^+ and a LA molecule in the closed Na^+ channel. *A*, An LA molecule accessing the inner pore via the sidewalk repels the resident Na^+ ion, which can move away via the unblocked outer pore and release the nucleophilic central cavity for binding of the LA ammonium group. *B*, When the outer pore is blocked by TTX, the Na^+ ion in the central cavity lacks a hydrophilic escape route, remains in the central cavity, and prevents the LAs access. *C*, the μ -CTX mutant (green ribbon), binds in the outer pore, but does not completely block the Na^+ current. The Na^+ ion can escape through the incompletely blocked outer pore and free the nucleophilic central cavity for the LAs binding. See *Discussion* for more details.

central cavity (Figure 5.9C). Thus, comparison of the effects of TTX and the μ -CTX mutant on the LA ingress and egress in the closed channel suggests that movement of inorganic and organic cations is coupled in the Na^+ channel.

The residues whose mutations affect access of LAs in the closed channel are clustered in two groups: one group is localized at the sidewalk and another in the outer pore including the selectivity filter. The hypothesis of the coupled movement of organic and inorganic ions explains why mutations in both clusters affect the drug access through the sidewalk. However, it is difficult to explain how mutations of S6 residues could affect the drug access via the selectivity filter. Indeed, because the access-controlling S6 residues are not buried inside the protein, they are unlikely to allosterically affect the access via the outer pore. Furthermore, the energy profile at Figure 5.8C suggests sterical hindrances for a LA molecule at the selectivity-filter level, but even in the absence of the hindrances the coupled-movement hypothesis suggest that the access to the closed channel through the selectivity filter is unlikely. Indeed, an LA molecule approaching the central cavity through the selectivity filter would encounter an electrostatic repulsion from the Na^+ ion residing in the cavity center. The Na^+ ion cannot escape through the closed activation gate, or through the hydrophobic sidewalks, or through the outer pore, which is blocked by the approaching LA molecule. Therefore, displacement of the resident Na^+ ion by the LA molecule coming through the selectivity filter is hardly possible.

P-loop channels have nucleophilic sites in the outer pore, the selectivity filter, and the central cavity. Numerous experimental data show that the interaction between cations at nucleophilic sites leads to the coupled movement in the multi-ion pores. For example, K^+ ions are thought to move through the selectivity filter of K^+ channels by sequentially occupying sites 1/3 and 2/4 (Zhou and MacKinnon, 2003). A recent experimental and theoretical study of the tetrabutylammonium-blocked KcsA shows that the position of the organic cation in the cavity depends on the selectivity-filter occupancy by K^+ ions (Faraldo-Gomez et al., 2007). Here we applied the concept of the coupled movement to explain seemingly contradictory experimental data on access and binding of LAs in Na^+ channels.

Modeling limitations

In this work we used a rather simple method of energy calculations. The atom-atom energy terms included van der Waals interactions, implicit solvent, and Coulomb's electrostatics, but lacked an explicit term for cation- π interactions. We also neglected the entropy component of free energy. Despite the limited precision of coarse-grained methods, they are widely used for homology modeling of proteins, which, like sodium channels, have a limited sequence similarity with X-ray templates. Employment of high-precision time-consuming methods in such cases seems impractical because an assumption that the model and the template have a similar backbone geometry influences

results to a greater extent than approximations of energy calculations. To compensate these limitations, we generated a large number of starting points, which cover virtually all ligand-binding scenarios (Figure 5.2*A,B*). Subsequent MC-minimizations yielded ensembles of energetically possible binding scenarios, which include different structures (Figures 5.2-5.4). Analysis of these ensembles allowed us to find particular binding modes, which agree with experimental data. For example, the vertical binding mode of QX-314 in the H₂O-DEKA model of the closed channel corresponds to the lowest-energy structure (Table 5.2), but the horizontal binding mode, which has a slightly higher energy, is consistent with a large number of experimental data. Taking into account a limited precision of energy calculations in the homology model, we concluded that it is the horizontal binding mode, which correspond to the closed-channel block.

CHAPTER SIX

SUMMARY

Eukaryotic voltage-gated channels are pharmaceutically important targets for treating severe pain, cardiac arrhythmia, epilepsy, and other disorders. Hence, the three-dimensional structures of these channels are needed to further understand the mechanism of channel modulation by ligands and develop more potent and selective drugs. During my graduate studies, I have used molecular modelling to tackle several unanswered questions regarding the structure of eukaryotic voltage-gated ion channels and the action of their blockers. Are prokaryotic and eukaryotic K^+ channels structurally similar? Is the pore architecture of K^+ channels similar to Ca^{2+} channels? Why do nucleophilic ligands block the hydrophobic pore of K^+ channels? Do LAs bind differently in the closed and open Na^+ channel? What is the extracellular route of LAs into the closed Na^+ channel?

Prokaryotic and eukaryotic K^+ channels are structurally similar

The X-ray structures of prokaryotic K^+ channels in the closed and open state suggest a gating-hinge role for a Gly in position *114*, which is conserved among most members of the K^+ channel superfamily (Jiang et al., 2002a). Unlike prokaryotic K^+ channels, eukaryotic K_v1 - K_v4 families contain a Pro-X-Pro motif in the inner helix. Webster et al. (2004) performed Cd^{2+} -binding experiments with cysteine mutations at the PVP motif of the *Shaker*, a member of the K_v1 family. They propose that eukaryotic K^+ channels have a different gating mechanism and have a much narrower open pore than prokaryotic K^+ channels due to the PVP motif. Their Cd^{2+} -binding experiments provided valuable distant constraints, which we incorporated into our homology models of the mutant *Shaker* channels using the available K^+ channel X-ray structures (Chapter 2). The KvAP-based model easily satisfied the experimental distant constraints of Webster et al. (2004). Thus, our study suggest the following: 1) a novel alignment of outer helices between the KvAP and the *Shaker* channel; 2) the open pore diameter of the *Shaker* channel is at least 10 Å wide to accommodate correolide, a *Shaker* channel blocker; 3) the pore-domain of the KvAP X-ray structure is in its native form; 4) the pore-forming domain of KvAP and the *Shaker* channel is structurally similar, thus KvAP is a suitable structure for modelling eukaryotic K^+ channels; 5) a structural conservation between prokaryotic and eukaryotic voltage-gated potassium channels in the pore-region.

Upon publication of our work, the open voltage-gated $K_v1.2$ *Shaker* channel was published as the first eukaryotic K^+ channel X-ray structure (Long et al., 2005a). This structure finally resolved the dispute and demonstrated that prokaryotic and eukaryotic K^+ channels are indeed structurally similar. $K_v1.2$ resembles KvAP, however is slightly narrower, approximately 9 Å in diameter. Later, another X-ray structure of KvAP was published explaining that without lipids the KvAP voltage sensor is disturbed but the pore-forming domain stays in its native state (Lee et al., 2005).

The features of the our open *Shaker* channel model (Bruhova and Zhorov, 2005) were confirmed by the X-ray structure of $K_v1.2$ (Figure 6.1). Our alignment between the outer helices of KvAP and *Shaker* is correct as can be seen with superimposed X-ray

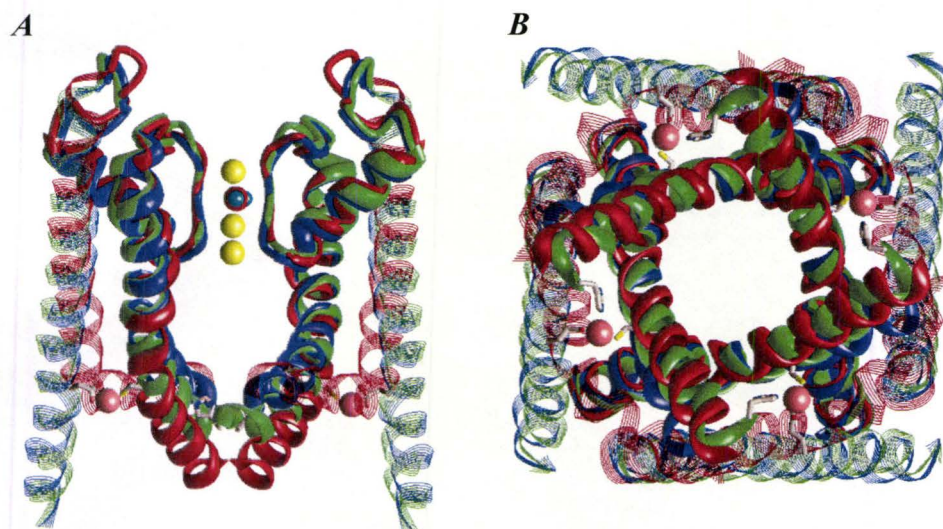


Figure 6.1. The comparison of our KvAP-based model of the locked-open *Shaker* channel to two open X-ray structures. The superposition of the side (A) and cytoplasmic (B) views of the KvAP X-ray structure, the KvAP-based model of the locked-open *Shaker* channel, and the Kv1.2 X-ray structure is shown in blue, green, and red, respectively. MCM with constraints from Cd²⁺-binding experiments (Webster et al., 2004) predicted the pore geometry of the *Shaker* channel with a RMSD of 2.5 Å. The following colouring scheme is used: inner helices and pore helices - ribbons; outer helices - strands; the selectivity-filter region and extracellular segments - rods; K⁺ ions - yellow spheres; water molecules - space filled.

Table 6.1. The C^αRMSD (Å) of the Kv1.2 X-ray, the KvAP X-ray, and the KvAP-based model of the locked-open *Shaker* channel.

| Compared structures | Alpha carbons in the inner helix | | | | |
|---|----------------------------------|---------|---------|---------|--------|
| | 1 - 13 | 14 - 20 | 21 - 24 | 25 - 34 | 1 - 34 |
| X-ray Kv1.2 vs. X-ray KvAP | 0.98 | 1.98 | 5.22 | 7.18 | 4.42 |
| X-ray Kv1.2 vs. KvAP-based locked-open <i>Shaker</i> model | 1.10 | 1.24 | 2.97 | 3.87 | 2.49 |
| X-ray KvAP vs. KvAP-based model of the locked-open <i>Shaker</i> | 0.99 | 1.07 | 2.56 | 4.47 | 2.69 |

structures, while other alignments (Jiang et al., 2003a; Shrivastava et al., 2004) do not survive this test. Imposing the Cd^{2+} -constraints to the KvAP-based model of the *Shaker* channel caused the model deforms towards the Kv1.2 X-ray structure. The root mean square deviation of the inner-helices C $^{\alpha}$ atoms (C $^{\alpha}$ RMSD) between the KvAP-based locked-open *Shaker* model (Bruhova and Zhorov, 2005) and Kv1.2 X-ray structure (Long et al., 2005a) is 2.5 Å (Table 6.1). This demonstrates that this molecular modelling approach using valuable experimental constraints can be used to predict the structures of proteins.

Metal ions are indispensable components to the binding of ligands in K $^{+}$ channels

The inner pore of most K $^{+}$ channels is lined with hydrophobic residues, however this region harbours receptors for a variety of ligands with multiple nucleophilic atoms, such as correolide and chromanol. Our study (Chapter 3) suggests that these nucleophilic ligands form a ternary complex with the K $^{+}$ ion at the selectivity filter and the channel. The participation of conducting ions in the binding of ligands to the pore region was earlier proposed in molecular modelling studies of Ca $^{2+}$ and Na $^{+}$ channels (Zhorov and Ananthanarayanan, 1996; Zhorov et al., 2001; Tikhonov and Zhorov, 2005b; Tikhonov et al., 2006; Wang et al., 2006). Experiments addressing the mechanism of action of batrachotoxin in the Na $_{v}$ 1.4 channel (Wang et al., 2006) confirmed important predictions of the ternary-complex model. However, the direct experimental validation of the ternary-complex concept is still difficult. The major problems are the uncertain location of the metal ions, relatively low stability of their complexes with the channels, conformational flexibility of drugs, and unknown location of their binding sites. Correolide seems to be an appropriate ligand to investigate the possibility of its ternary association with the receptor and K $^{+}$ ion because of four reasons. First, the drug has a semirigid conformation that would not change significantly upon the binding to the channel and/or to the ion. Second, the size of correolide is compatible with the size of the open pore (Zhorov and Tikhonov, 2004; Bruhova and Zhorov, 2005), thus decreasing the uncertainty of the binding-site location. Third, correolide has an ellipsoidal shape with an epoxy group at one pole and ester group at another pole. These groups can accept but not donate H-bonds and interact with metal ions. The nucleophilic character of correolide and the predominantly hydrophobic character of the inner helices in Kv1.3 suggest that a K $^{+}$ ion in position 4 or 5 may provide an electrophilic site for drug binding. Fourth, approximate locations of K $^{+}$ ions in potassium channels are known from experiments. Importantly, in this study multiple positions and orientations of correolide in the channel were intensively sampled to avoid any bias on the ternary association of the drug with the channel and K $^{+}$. The results suggest that the ternary complexes can explain peculiarities of correolide structure, results of mutational analysis of correolide binding, as well as coupling of correolide and K $^{+}$ binding sites (Zhorov and Tikhonov, 2004).

Ca²⁺ channels and K⁺ channels are structurally similar

X-ray structures of Ca²⁺ and Na⁺ channels are unavailable. In these circumstances, homology models of Ca²⁺ channels based on K⁺ channels X-ray structures can provide atomic-details of structure. Homology models depend on the alignment between K⁺ and Ca²⁺ channels, however due to poor sequence similarity, there is no consensus and several different alignments have been proposed (Huber et al., 2000; Zhorov et al., 2001; Lipkind and Fozzard, 2003; Stary et al., 2008). Zhen et al. (2005) used SCAM to identify pore-lining residues in Ca_v2.1 and concluded that their results are inconsistent with any published sequence alignments between Ca²⁺ and K⁺ channels. This conclusion casts doubts on homology models of Ca²⁺ channels and the structural similarity between K⁺ and Ca²⁺ channels.

We have reinterpreted SCAM observations (Zhen et al., 2005) by modelling MTSET-substituted cysteine mutants of Ca_v2.1 based on K_v1.2 using previously published alignments for the outer (Huber et al., 2000) and inner (Zhorov et al., 2001) helices. Our model revealed that certain pore-facing residues are surrounded by large hydrophobic residues. A Cys in a hydrophobic environment would not ionize and thus would not react with MTSET. We observed that MTSET adopts a variety of orientations due to its long flexible chain. MTSET behaves like a tethered ligand and binds at an energetically most favourable orientation within the channel. Depending on the surrounding residues, the ammonium group of MTSET can either bury inside the protein between domains or extend into the pore. Our model of the K_v1.2-based Ca_v2.1 is consistent with the SCAM observations, validates the above-mentioned alignment between Ca²⁺ and K⁺ channels and suggests that the K_v1.2 X-ray structure is a suitable template to model Ca²⁺ channels.

We have used the same alignment to homology model both Ca²⁺ and Na⁺ channels based on X-ray structures of K⁺ channels. These models explain the action of benzothiazepines (Tikhonov and Zhorov, 2008), dihydropyridines (Zhorov et al., 2001; Tikhonov and Zhorov, 2009), batrachotoxin (Wang et al., 2006), local anaesthetics (Tikhonov et al., 2006; Tikhonov and Zhorov, 2007; Bruhova et al., 2008), and tetrodotoxin and saxitoxin (Tikhonov and Zhorov, 2005a). The fact that our alignment is consistent with both SCAM data and many ligand-binding studies, strongly suggest that this alignment is correct.

Local anaesthetics in the closed Na⁺ channel

LAs are known to block Na⁺ channels in the closed, open, and inactivated states. A conserved phenylalanine in segment IVS6 is important for both the open and closed-channel block, while conserved tyrosine in the same domain is important for the open, but not the closed-channel block by cocaine (Wright et al., 1998) and tetracaine (Li et al., 1999). To rationalize these observations, we docked cocaine, tetracaine, and the

permanently charged QX-314 in the closed $\text{Na}_v1.5$ model. We found that the ammonium group of the LAs binds near the focus of the P-loop helices, while the aromatic group extends either along the pore axis (vertical binding mode) or into the III/IV domain interface (horizontal binding mode). In the horizontal mode, all three drugs expand into the IIS6/IVS6 interface and, in agreement with mutational data, their benzene rings interact with the conserved Phe but does not interact with Tyr. The horizontal mode is readily occupied upon the ligand entering into the resting channel via the III/IV interface. This mode is also the most stable one in the presence of Na^+ in the selectivity filter. The vertical binding mode is energetically preferable in the open channel (Tikhonov and Zhorov, 2007) and the ligand could remain in this mode upon the channel closure. Indeed, cocaine and QX-314 can adopt the vertical mode in the closed channel due to π -stacking with Tyr in IVS6, but tetracaine is too long to adopt this mode. In agreement to experimental data, our study suggests that the LAs bind in a horizontal binding mode in the closed Na^+ channel.

Extracellular access pathway of LAs into the closed Na^+ channel is located between repeats III and IV

If LAs block the inner pore of the closed channel, how do they get there? Experiments with permanently charged LAs determined that LAs block the open pore from the intracellular side, but, intriguingly, LAs block the closed channel from the extracellular side (Lee et al., 2001). Intracellular LAs enter the open channel evidently through the widely open activation gates, as seen in the X-ray structure of open K^+ channels. However, the extracellular access pathway of LAs into the closed Na^+ channel was not obvious. Mutations at the selectivity filter and TTX-binding studies (Sunami et al., 1997; Sunami et al., 2000) suggested that the external pathway for LAs is through the selectivity filter. On the other hand, mutations in repeat IV and ligand-binding studies with μ -conotoxin (Ragsdale et al., 1994; Qu et al., 1995; Sunami et al., 2001) suggests that LAs pass between repeats III and IV to reach the inner pore.

We have simulated the extracellular access of QX-314 by pulling the ligand through the selectivity filter and between repeats III and IV (Chapter 5). When pulled through the selectivity filter, QX-314 has to overcome large energy barriers mainly due to steric clashes of the ligand with P-loop residues. On the contrary, QX-314 passes through the III-IV sidewalk without experiencing energy barriers. The final orientation of the LA obtained at the inner-pore end of the III-IV pathway is very similar to the horizontal binding mode of LAs found by random docking. In agreement with experimental data, the ligand passing through the III-IV sidewalk directly interacts with IVS6 residues identified to be involved in extracellular LA access.

Our models suggest that the external path for LAs into the closed Na^+ channel is between IIS6, IVS6, and IIIP. However, why do mutations at the selectivity filter and TTX-binding studies affect the extracellular path of LAs? We propose that these

observations can be explained in a model in which a Na^+ ion can occupy two nucleophilic sites, one in the DEKA locus and another at the focus of the P-loop macrodipoles in the inner pore. We believe that a LA molecule competes with a Na^+ ion for the nucleophilic site in the inner pore. As the LA molecule passes through the III-IV interface into the inner pore, the Na^+ ion escapes through the selectivity filter of the wild-type Na^+ channel. However, if the selectivity filter is mutated or blocked by TTX, the Na^+ ion does not have an escape route, thus stays in the inner pore and prevents LAs to bind.

The extracellular access of drugs is not an exclusive feature of Na^+ channels. Mutations of various residues that face the III/IV domain interface affect the binding of drugs to L-type Ca^{2+} channels (Hockerman et al., 1997). Permanently charged benzothiazepines (Hering et al., 1993; Seydl et al., 1993) and dihydropyridines (Kass et al., 1991; Kwan et al., 1995) block the L-type Ca^{2+} channel from the extracellular side. Dihydropyridines were proposed to access Ca^{2+} channels via the III/IV domain interface (Yamaguchi et al., 2003). The recent X-ray structures of KcsA with hydrophobic cations show long hydrophobic moieties bound in the interface between S6, S5, and P-helices, which is suggested to provide an alternative access pathway for drugs to the inner pore (Lenaeus and Gross, 2008).

In conclusion, in this work we have built and explored homology models of voltage-gated K^+ , Na^+ , and Ca^{2+} channels and their complexes with various ligands. In particular, we demonstrated that 1) K^+ channel X-ray structures are suitable templates for modelling the pore-domain region of voltage-gated Na^+ and Ca^{2+} channels, 2) metal cations in the selectivity filter region of ion channels stabilize nucleophilic drugs, but destabilize cationic drugs, and 3) the repeat interface may provide an access pathway for drug entry from the extracellular side into the pore of the closed channel. Results of this work may be useful for future drug design.

REFERENCES

- Ahern CA, Eastwood AL, Dougherty DA and Horn R (2008) Electrostatic contributions of aromatic residues in the local anesthetic receptor of voltage-gated sodium channels. *Circulation research* **102**(1):86-94.
- Alam A and Jiang Y (2009a) High-resolution structure of the open NaK channel. *Nature structural & molecular biology* **16**(1):30-34.
- Alam A and Jiang Y (2009b) Structural analysis of ion selectivity in the NaK channel. *Nature structural & molecular biology* **16**(1):35-41.
- Alpert LA, Fozzard HA, Hanck DA and Makielski JC (1989) Is there a second external lidocaine binding site on mammalian cardiac cells? *The American journal of physiology* **257**(1 Pt 2):H79-84.
- Ananthanarayanan VS (1991) Peptide hormones, neurotransmitters, and drugs as Ca²⁺ ionophores: implications for signal transduction. *Biochem Cell Biol* **69**:93-95.
- Andersen O (1984) Chelation of cadmium. *Environmental health perspectives* **54**:249-266.
- Anderson PA and Greenberg RM (2001) Phylogeny of ion channels: clues to structure and function. *Comparative biochemistry and physiology* **129**(1):17-28.
- Backx PH, Yue DT, Lawrence JH, Marban E and Tomaselli GF (1992) Molecular localization of an ion-binding site within the pore of mammalian sodium channels. *Science (New York, NY)* **257**(5067):248-251.
- Bao J, Miao S, Kayser F, Kotliar AJ, Baker RK, Doss GA, Felix JP, Bugianesi RM, Slaughter RS, Kaczorowski GJ, Garcia ML, Ha SN, Castonguay L, Koo GC, Shah K, Springer MS, Staruch MJ, Parsons WH and Rupprecht KM (2005) Potent Kv1.3 inhibitors from correolide-modification of the C18 position. *Bioorganic & medicinal chemistry letters* **15**(2):447-451.
- Bebout DC, Stokes SW and Butcher RJ (1999) Comparison of Heteronuclear Coupling Constants for Isostructural Nitrogen Coordination Compounds of (111/113)Cd and (199)Hg. *Inorg Chem* **38**(6):1126-1133.
- Berneche S and Roux B (2005) A gate in the selectivity filter of potassium channels. *Structure* **13**(4):591-600.
- Berweger CD, Thiel W and van Gunsteren WF (2000) Molecular-dynamics simulation of the beta domain of metallothionein with a semi-empirical treatment of the metal core. *Proteins* **41**(3):299-315.
- Bodi I, Yamaguchi H, Hara M, He M, Schwartz A and Varadi G (1997) Molecular studies on the voltage dependence of dihydropyridine action on L-type Ca²⁺ channels. Critical involvement of tyrosine residues in motif IIIS6 and IVS6. *J Biol Chem* **272**(40):24952-24960.
- Bradley P, Misura KM and Baker D (2005) Toward high-resolution de novo structure prediction for small proteins. *Science (New York, NY)* **309**(5742):1868-1871.
- Bruhova I, Tikhonov DB and Zhorov BS (2008) Access and binding of local anesthetics in the closed sodium channel. *Molecular pharmacology* **74**(4):1033-1045.

- Bruhova I and Zhorov BS (2005) KvAP-based model of the pore region of shaker potassium channel is consistent with cadmium- and ligand-binding experiments. *Biophysical journal* **89**(2):1020-1029.
- Bruhova I and Zhorov BS (2007) Monte Carlo-energy minimization of correolide in the Kv1.3 channel: possible role of potassium ion in ligand-receptor interactions. *BMC Struct Biol* **7**:5.
- Burley SK and Petsko GA (1985) Aromatic-aromatic interaction: a mechanism of protein structure stabilization. *Science (New York, NY)* **229**(4708):23-28.
- Cannon SC (1997) From mutation to myotonia in sodium channel disorders. *Neuromuscul Disord* **7**(4):241-249.
- Catterall WA (2000a) From ionic currents to molecular mechanisms: the structure and function of voltage-gated sodium channels. *Neuron* **26**(1):13-25.
- Catterall WA (2000b) Structure and regulation of voltage-gated Ca²⁺ channels. *Annual review of cell and developmental biology* **16**:521-555.
- Catterall WA, Goldin AL and Waxman SG (2005) International Union of Pharmacology. XLVII. Nomenclature and structure-function relationships of voltage-gated sodium channels. *Pharmacological reviews* **57**(4):397-409.
- Chahine M, Chen LQ, Barchi RL, Kallen RG and Horn R (1992) Lidocaine block of human heart sodium channels expressed in *Xenopus* oocytes. *J Mol Cell Cardiol* **24**(11):1231-1236.
- Chanda B, Asamoah OK, Blunck R, Roux B and Bezanilla F (2005) Gating charge displacement in voltage-gated ion channels involves limited transmembrane movement. *Nature* **436**(7052):852-856.
- Chandy KG, Cahalan MD, Pennington M, Norton RS, Wulff H and Gutman GA (2001) Potassium channels in T lymphocytes: toxins to therapeutic immunosuppressants. *Toxicon* **39**:1269-1276.
- Chandy KG and Gutman GA (1993) Nomenclature for mammalian potassium channel genes. *Trends Pharmacol Sci* **14**(12):434.
- Chen Y, Yu FH, Surmeier DJ, Scheuer T and Catterall WA (2006) Neuromodulation of Na⁺ channel slow inactivation via cAMP-dependent protein kinase and protein kinase C. *Neuron* **49**(3):409-420.
- Cheng RCK, Tikhonov DB and Zhorov BS (2009) Modeling L-type calcium channel with phenylalkylamines. *Biophys J* **96**(3):183a.
- Choi KL, Aldrich RW and Yellen G (1991) Tetraethylammonium blockade distinguishes two inactivation mechanisms in voltage-activated K⁺ channels. *Proceedings of the National Academy of Sciences of the United States of America* **88**(12):5092-5095.
- Choudhary G, Yotsu-Yamashita M, Shang L, Yasumoto T and Dudley SC, Jr. (2003) Interactions of the C-11 hydroxyl of tetrodotoxin with the sodium channel outer vestibule. *Biophys J* **84**(1):287-294.
- Cordero-Morales JF, Jogini V, Lewis A, Vasquez V, Cortes DM, Roux B and Perozo E (2007) Molecular driving forces determining potassium channel slow inactivation. *Nature structural & molecular biology* **14**(11):1062-1069.
- Cordes FS, Bright JN and Sansom MS (2002) Proline-induced distortions of transmembrane helices. *Journal of molecular biology* **323**:951-960.

- Cosconati S, Marinelli L, Lavecchia A and Novellino E (2007) Characterizing the 1,4-dihydropyridines binding interactions in the L-type Ca²⁺ channel: model construction and docking calculations. *J Med Chem* **50**(7):1504-1513.
- del Camino D, Holmgren M, Liu Y and Yellen G (2000) Blocker protection in the pore of a voltage-gated K⁺ channel and its structural implications. *Nature* **403**(6767):321-325.
- Dewar MJS, Zoebisch EG, Healy EF and Stewart JJP (1985) The Development and Use of Quantum-Mechanical Molecular-Models .76. Am1 - a New General-Purpose Quantum-Mechanical Molecular-Model. *Journal of the American Chemical Society* **107**(13):3902-3909.
- Doering CJ and Zamponi GW (2003) Molecular pharmacology of high voltage-activated calcium channels. *Journal of bioenergetics and biomembranes* **35**(6):491-505.
- Douplnik CA, Lim NF, Kofuji P, Davidson N and Lester HA (1995) Intrinsic gating properties of a cloned G protein-activated inward rectifier K⁺ channel. *The Journal of general physiology* **106**(1):1-23.
- Doyle DA, Morais Cabral J, Pfuetzner RA, Kuo A, Gulbis JM, Cohen SL, Chait BT and MacKinnon R (1998) The structure of the potassium channel: molecular basis of K⁺ conduction and selectivity. *Science (New York, NY)* **280**(5360):69-77.
- Durell SR, Shrivastava IH and Guy HR (2004) Models of the structure and voltage-gating mechanism of the shaker K⁺ channel. *Biophys J* **87**(4):2116-2130.
- Ertel EA, Campbell KP, Harpold MM, Hofmann F, Mori Y, Perez-Reyes E, Schwartz A, Snutch TP, Tanabe T, Birnbaumer L, Tsien RW and Catterall WA (2000) Nomenclature of voltage-gated calcium channels. *Neuron* **25**(3):533-535.
- Faraldo-Gomez JD, Kutluay E, Jogini V, Zhao Y, Hegginbotham L and Roux B (2007) Mechanism of intracellular block of the KcsA K⁺ channel by tetrabutylammonium: insights from X-ray crystallography, electrophysiology and replica-exchange molecular dynamics simulations. *Journal of molecular biology* **365**(3):649-662.
- Felix JP, Bugianesi RM, Schmalhofer WA, Borris R, Goetz MA, Hensens OD, Bao JM, Kayser F, Parsons WH, Rupprecht K, Garcia ML, Kaczorowski GJ and Slaughter RS (1999) Identification and biochemical characterization of a novel nortriterpene inhibitor of the human lymphocyte voltage-gated potassium channel, Kv1.3. *Biochemistry* **38**(16):4922-4930.
- Flynn GE and Zagotta WN (2003) A cysteine scan of the inner vestibule of cyclic nucleotide-gated channels reveals architecture and rearrangement of the pore. *The Journal of general physiology* **121**:563-582.
- Fozzard HA, Lee PJ and Lipkind GM (2005) Mechanism of local anesthetic drug action on voltage-gated sodium channels. *Current pharmaceutical design* **11**(21):2671-2686.
- Gerlach U, Brendel J, Lang HJ, Paulus EF, Weidmann K, Bruggemann A, Busch AE, Suessbrich H, Bleich M and Greger R (2001) Synthesis and activity of novel and selective I(Ks)-channel blockers. *Journal of medicinal chemistry* **44**(23):3831-3837.

- Goetz MA, Hensens OD, Zink DL, Borris RP, Morales F, Tamayo-Castillo G, Slaughter RS, Felix J and Ball RG (1998) Potent Nor-triterpenoid blockers of the voltage-gated potassium channel Kv(1.3) from *Spachea correae*. *Tetrahedron Letters* **39**(19):2895-2898.
- Goldin AL, Barchi RL, Caldwell JH, Hofmann F, Howe JR, Hunter JC, Kallen RG, Mandel G, Meisler MH, Netter YB, Noda M, Tamkun MM, Waxman SG, Wood JN and Catterall WA (2000) Nomenclature of voltage-gated sodium channels. *Neuron* **28**(2):365-368.
- Grissmer S and Cahalan M (1989) TEA prevents inactivation while blocking open K⁺ channels in human T lymphocytes. *Biophys J* **55**(1):203-206.
- Gutman GA, Chandy KG, Grissmer S, Lazdunski M, McKinnon D, Pardo LA, Robertson GA, Rudy B, Sanguinetti MC, Stuhmer W and Wang X (2005) International Union of Pharmacology. LIII. Nomenclature and molecular relationships of voltage-gated potassium channels. *Pharmacological reviews* **57**(4):473-508.
- Guy HR and Seetharamulu P (1986) Molecular model of the action potential sodium channel. *Proceedings of the National Academy of Sciences of the United States of America* **83**(2):508-512.
- Hanner M, Green B, Gao YD, Schmalhofer WA, Matyskiela M, Durand DJ, Felix JP, Linde AR, Bordallo C, Kaczorowski GJ, Kohler M and Garcia ML (2001) Binding of correolide to the K(v)1.3 potassium channel: characterization of the binding domain by site-directed mutagenesis. *Biochemistry* **40**(39):11687-11697.
- Hanner M, Schmalhofer WA, Green B, Bordallo C, Liu J, Slaughter RS, Kaczorowski GJ and Garcia ML (1999) Binding of correolide to K(v)1 family potassium channels. Mapping the domains of high affinity interaction. *Journal of Biological Chemistry* **274**(36):25237-25244.
- Heginbotham L, Lu Z, Abramson T and MacKinnon R (1994) Mutations in the K⁺ channel signature sequence. *Biophysical Journal* **66**(4):1061-1067.
- Heinemann SH, Terlau H, Stuhmer W, Imoto K and Numa S (1992) Calcium channel characteristics conferred on the sodium channel by single mutations. *Nature* **356**(6368):441-443.
- Heinz U, Bauer R, Wommer S, Meyer-Klaucke W, Papamichaels C, Bateson J and Adolph HW (2003) Coordination geometries of metal ions in d- or l-captopril-inhibited metallo-beta-lactamases. *J Biol Chem* **278**(23):20659-20666.
- Hering S, Savchenko A, Strubing C, Lakitsch M and Striessnig J (1993) Extracellular localization of the benzothiazepine binding domain of L-type Ca²⁺ channels. *Molecular pharmacology* **43**(5):820-826.
- Hille B (1977) Local anesthetics: hydrophilic and hydrophobic pathways for the drug-receptor reaction. *The Journal of general physiology* **69**(4):497-515.
- Hille B (2001) *Ion channels of excitable membranes*. Sinauer Associates Inc, Sunderland, Massachusetts USA.
- Hockerman GH, Peterson BZ, Johnson BD and Catterall WA (1997) Molecular determinants of drug binding and action on L-type calcium channels. *Annual review of pharmacology and toxicology* **37**:361-396.

- Holmgren M, Shin KS and Yellen G (1998) The activation gate of a voltage-gated K⁺ channel can be trapped in the open state by an intersubunit metal bridge. *Neuron* **21**(3):617-621.
- Huber I, Wappl E, Herzog A, Mitterdorfer J, Glossmann H, Langer T and Striessnig J (2000) Conserved Ca²⁺-antagonist-binding properties and putative folding structure of a recombinant high-affinity dihydropyridine-binding domain. *The Biochemical journal* **347 Pt 3**:829-836.
- Isom LL, De Jongh KS and Catterall WA (1994) Auxiliary subunits of voltage-gated ion channels. *Neuron* **12**(6):1183-1194.
- Jiang Y, Lee A, Chen J, Cadene M, Chait BT and MacKinnon R (2002a) Crystal structure and mechanism of a calcium-gated potassium channel. *Nature* **417**(6888):515-522.
- Jiang Y, Lee A, Chen J, Cadene M, Chait BT and MacKinnon R (2002b) The open pore conformation of potassium channels. *Nature* **417**(6888):523-526.
- Jiang Y, Lee A, Chen J, Ruta V, Cadene M, Chait BT and MacKinnon R (2003a) X-ray structure of a voltage-dependent K⁺ channel. *Nature* **423**(6935):33-41.
- Jiang Y, Ruta V, Chen J, Lee A and MacKinnon R (2003b) The principle of gating charge movement in a voltage-dependent K⁺ channel. *Nature* **423**(6935):42-48.
- Kaczorowski GJ and Garcia ML (1999) Pharmacology of voltage-gated and calcium-activated potassium channels. *Current Opinion in Chemical Biology* **3**(4):448-458.
- Karlin A and Akabas MH (1998) Substituted-cysteine accessibility method. *Methods Enzymol* **293**:123-145.
- Kass RS, Arena JP and Chin S (1991) Block of L-type calcium channels by charged dihydropyridines. Sensitivity to side of application and calcium. *J Gen Physiol* **98**(1):63-75.
- Keating MT and Sanguinetti MC (2001) Molecular and cellular mechanisms of cardiac arrhythmias. *Cell* **104**(4):569-580.
- Kirsch GE, Alam M and Hartmann HA (1994) Differential effects of sulfhydryl reagents on saxitoxin and tetrodotoxin block of voltage-dependent Na channels. *Biophys J* **67**(6):2305-2315.
- Koo GC, Blake JT, Shah K, Staruch MJ, Dumont F, Wunderler D, Sanchez M, McManus OB, Sirotina-Meisher A, Fischer P, Boltz RC, Goetz MA, Baker R, Bao J, Kayser F, Rupprecht KM, Parsons WH, Tong XC, Ita IE, Pivnichny J, Vincent S, Cunningham P, Hora D, Jr., Feeney W and Kaczorowski G (1999) Correolide and derivatives are novel immunosuppressants blocking the lymphocyte Kv1.3 potassium channels. *Cellular Immunology* **197**(2):99-107.
- Kwan YW, Bangalore R, Lakitsh M, Glossmann H and Kass RS (1995) Inhibition of cardiac L-type calcium channels by quaternary amlodipine: implications for pharmacokinetics and access to dihydropyridine binding site. *J Mol Cell Cardiol* **27**(1):253-262.
- Labro AJ, Raes AL, Bellens I, Ottschytch N and Snyders DJ (2003) Gating of shaker-type channels requires the flexibility of S6 caused by prolines. *J Biol Chem* **278**(50):50724-50731.

- Laine M, Lin MC, Bannister JP, Silverman WR, Mock AF, Roux B and Papazian DM (2003) Atomic proximity between S4 segment and pore domain in Shaker potassium channels. *Neuron* **39**(3):467-481.
- Lazaridis T and Karplus M (1999a) Discrimination of the native from misfolded protein models with an energy function including implicit solvation. *J Mol Biol* **288**(3):477-487.
- Lazaridis T and Karplus M (1999b) Effective energy function for proteins in solution. *Proteins* **35**(2):133-152.
- Lee PJ, Sunami A and Fozzard HA (2001) Cardiac-specific external paths for lidocaine, defined by isoform-specific residues, accelerate recovery from use-dependent block. *Circulation research* **89**(11):1014-1021.
- Lee SY, Lee A, Chen J and MacKinnon R (2005) Structure of the KvAP voltage-dependent K⁺ channel and its dependence on the lipid membrane. *Proceedings of the National Academy of Sciences of the United States of America* **102**(43):15441-15446.
- Lenaeus MJ and Gross A (2008) Structural basis of quaternary ammonium binding to potassium channels. *Bioophys J* **S-2008**:943-Plat.
- Lenaeus MJ, Vamvouka M, Focia PJ and Gross A (2005) Structural basis of TEA blockade in a model potassium channel. *Nature structural & molecular biology* **12**(5):454-459.
- Lerche C, Bruhova I, Lerche H, Steinmeyer K, Wei AD, Strutz-Seeböhm N, Lang F, Busch AE, Zhorov BS and Seeböhm G (2007) Chromanol 293B binding in KCNQ1 (Kv7.1) channels involves electrostatic interactions with a potassium ion in the selectivity filter. *Molecular pharmacology* **71**(6):1503-1511.
- Li HL, Galue A, Meadows L and Ragsdale DS (1999) A molecular basis for the different local anesthetic affinities of resting versus open and inactivated states of the sodium channel. *Mol Pharmacol* **55**(1):134-141.
- Li RA, Tsushima RG, Kallen RG and Backx PH (1997) Pore residues critical for mu-CTX binding to rat skeletal muscle Na⁺ channels revealed by cysteine mutagenesis. *Biophys J* **73**(4):1874-1884.
- Li Z and Scheraga HA (1987) Monte Carlo-minimization approach to the multiple-minima problem in protein folding. *Proc Natl Acad Sci U S A* **84**(19):6611-6615.
- Lipkind GM and Fozzard HA (2000) KcsA crystal structure as framework for a molecular model of the Na⁽⁺⁾ channel pore. *Biochemistry* **39**(28):8161-8170.
- Lipkind GM and Fozzard HA (2001) Modeling of the outer vestibule and selectivity filter of the L-type Ca²⁺ channel. *Biochemistry* **40**(23):6786-6794.
- Lipkind GM and Fozzard HA (2003) Molecular modeling of interactions of dihydropyridines and phenylalkylamines with the inner pore of the L-type Ca²⁺ channel. *Molecular pharmacology* **63**(3):499-511.
- Lipkind GM and Fozzard HA (2005) Molecular modeling of local anesthetic drug binding by voltage-gated sodium channels. *Molecular pharmacology* **68**(6):1611-1622.
- Liu Y, Holmgren M, Jurman ME and Yellen G (1997) Gated access to the pore of a voltage-dependent K⁺ channel. *Neuron* **19**(1):175-184.

- Long SB, Campbell EB and Mackinnon R (2005a) Crystal structure of a mammalian voltage-dependent Shaker family K⁺ channel. *Science (New York, NY)* **309**(5736):897-903.
- Long SB, Campbell EB and Mackinnon R (2005b) Voltage sensor of Kv1.2: structural basis of electromechanical coupling. *Science* **309**(5736):903-908.
- Lu Z, Klem AM and Ramu Y (2001) Ion conduction pore is conserved among potassium channels. *Nature* **413**(6858):809-813.
- Luzhkov VB, Nilsson J, Arhem P and Aqvist J (2003) Computational modelling of the open-state Kv 1.5 ion channel block by bupivacaine. *Biochimica et Biophysica Acta* **1652**(1):35-51.
- Mackinnon R (2004) Structural biology. Voltage sensor meets lipid membrane. *Science (New York, NY)* **306**(5700):1304-1305.
- MacKinnon R, Cohen SL, Kuo A, Lee A and Chait BT (1998) Structural conservation in prokaryotic and eukaryotic potassium channels. *Science (New York, NY)* **280**(5360):106-109.
- MacKinnon R, Heginbotham L and Abramson T (1990) Mapping the receptor site for charybdotoxin, a pore-blocking potassium channel inhibitor. *Neuron* **5**(6):767-771.
- Matko J (2003) K⁺ channels and T-cell synapses: the molecular background for efficient immunomodulation is shaping up. *Trends Pharmacol Sci* **24**:385-389.
- McNulty MM, Edgerton GB, Shah RD, Hanck DA, Fozzard HA and Lipkind GM (2007) Charge at the lidocaine binding site residue Phe-1759 affects permeation in human cardiac voltage-gated sodium channels. *J Physiol* **581**(Pt 2):741-755.
- Nau C and Wang GK (2004) Interactions of local anesthetics with voltage-gated Na⁺ channels. *The Journal of membrane biology* **201**(1):1-8.
- Nau C, Wang SY and Wang GK (2003) Point mutations at L1280 in Nav1.4 channel D3-S6 modulate binding affinity and stereoselectivity of bupivacaine enantiomers. *Molecular pharmacology* **63**(6):1398-1406.
- Nettleton J and Wang GK (1990) pH-dependent binding of local anesthetics in single batrachotoxin-activated Na⁺ channels. Cocaine vs. quaternary compounds. *Biophys J* **58**(1):95-106.
- O'Leary ME and Chahine M (2002) Cocaine binds to a common site on open and inactivated human heart (Na(v)1.5) sodium channels. *J Physiol* **541**(Pt 3):701-716.
- O'Leary ME, Digregorio M and Chahine M (2003) Closing and inactivation potentiate the cocaethylene inhibition of cardiac sodium channels by distinct mechanisms. *Mol Pharmacol* **64**(6):1575-1585.
- Ogielska EM and Aldrich RW (1998) A mutation in S6 of Shaker potassium channels decreases the K⁺ affinity of an ion binding site revealing ion-ion interactions in the pore. *Journal of General Physiology* **112**(2):243-257.
- Oiki S, Madison V and Montal M (1990) Bundles of amphipathic transmembrane alpha-helices as a structural motif for ion-conducting channel proteins: studies on sodium channels and acetylcholine receptors. *Proteins* **8**(3):226-236.
- Olivera BM, Cruz LJ, de Santos V, LeCheminant GW, Griffin D, Zeikus R, McIntosh JM, Galyean R, Varga J, Gray WR and et al. (1987) Neuronal calcium channel

- antagonists. Discrimination between calcium channel subtypes using omega-conotoxin from *Conus magus* venom. *Biochemistry* **26**(8):2086-2090.
- Paul-Soto R, Zeppezauer M, Adolph HW, Galleni M, Frere JM, Carfi A, Dideberg O, Wouters J, Hemmingsen L and Bauer R (1999) Preference of Cd(II) and Zn(II) for the two metal sites in *Bacillus cereus* beta-lactamase II: A perturbed angular correlation of gamma-rays spectroscopic study. *Biochemistry* **38**(50):16500-16506.
- Penzotti JL, Lipkind G, Fozzard HA and Dudley SC, Jr. (2001) Specific neosaxitoxin interactions with the Na⁺ channel outer vestibule determined by mutant cycle analysis. *Biophys J* **80**(2):698-706.
- Peterson BZ, Johnson BD, Hockerman GH, Acheson M, Scheuer T and Catterall WA (1997) Analysis of the dihydropyridine receptor site of L-type calcium channels by alanine-scanning mutagenesis. *J Biol Chem* **272**(30):18752-18758.
- Qu Y, Rogers J, Tanada T, Scheuer T and Catterall WA (1995) Molecular determinants of drug access to the receptor site for antiarrhythmic drugs in the cardiac Na⁺ channel. *Proc Natl Acad Sci U S A* **92**(25):11839-11843.
- Ragsdale DS, McPhee JC, Scheuer T and Catterall WA (1994) Molecular determinants of state-dependent block of Na⁺ channels by local anesthetics. *Science* **265**(5179):1724-1728.
- Ren D, Navarro B, Xu H, Yue L, Shi Q and Clapham DE (2001) A prokaryotic voltage-gated sodium channel. *Science (New York, NY)* **294**(5550):2372-2375.
- Roux B and MacKinnon R (1999) The cavity and pore helices in the KcsA K⁺ channel: electrostatic stabilization of monovalent cations. *Science (New York, NY)* **285**(5424):100-102.
- Ruetsch YA, Boni T and Borgeat A (2001) From cocaine to ropivacaine: the history of local anesthetic drugs. *Current topics in medicinal chemistry* **1**(3):175-182.
- Ruta V, Chen J and MacKinnon R (2005) Calibrated measurement of gating-charge arginine displacement in the KvAP voltage-dependent K⁺ channel. *Cell* **123**(3):463-475.
- Santarelli VP, Eastwood AL, Dougherty DA, Ahern CA and Horn R (2007a) Calcium block of single sodium channels: role of a pore-lining aromatic residue. *Biophys J* **93**(7):2341-2349.
- Santarelli VP, Eastwood AL, Dougherty DA, Horn R and Ahern CA (2007b) A cation-pi interaction discriminates among sodium channels that are either sensitive or resistant to tetrodotoxin block. *J Biol Chem* **282**(11):8044-8051.
- Sasaki K, Makita N, Sunami A, Sakurada H, Shirai N, Yokoi H, Kimura A, Tohse N, Hiraoka M and Kitabatake A (2004) Unexpected mexiletine responses of a mutant cardiac Na⁺ channel implicate the selectivity filter as a structural determinant of antiarrhythmic drug access. *Mol Pharmacol* **66**(2):330-336.
- Satin J, Kyle JW, Chen M, Bell P, Cribbs LL, Fozzard HA and Rogart RB (1992) A mutant of TTX-resistant cardiac sodium channels with TTX-sensitive properties. *Science (New York, NY)* **256**(5060):1202-1205.

- Sato C, Ueno Y, Asai K, Takahashi K, Sato M, Engel A and Fujiyoshi Y (2001) The voltage-sensitive sodium channel is a bell-shaped molecule with several cavities. *Nature* **409**(6823):1047-1051.
- Scheib H, McLay I, Guex N, Clare JJ, Blaney FE, Dale TJ, Tate SN and Robertson GM (2006) Modeling the pore structure of voltage-gated sodium channels in closed, open, and fast-inactivated conformation reveals details of site 1 toxin and local anesthetic binding. *J Mol Model* **12**(6):813-822.
- Seeböhm G, Chen J, Strutz N, Culberson C, Lerche C and Sanguinetti MC (2003) Molecular determinants of KCNQ1 channel block by a benzodiazepine. *Molecular pharmacology* **64**(1):70-77.
- Seeböhm G, Lerche C, Pusch M, Steinmeyer K, Bruggemann A and Busch AE (2001) A kinetic study on the stereospecific inhibition of KCNQ1 and I(Ks) by the chromanol 293B. *British journal of pharmacology* **134**(8):1647-1654.
- Seydl K, Kimball D, Schindler H and Romanin C (1993) The benzazepine/benzothiazepine binding domain of the cardiac L-type Ca²⁺ channel is accessible only from the extracellular side. *Pflugers Arch* **424**(5-6):552-554.
- Shafir Y, Durell SR and Guy HR (2008) Models of the structure and gating mechanisms of the pore domain of the NaChBac ion channel. *Biophys J* **95**(8):3650-3662.
- Shi N, Ye S, Alam A, Chen L and Jiang Y (2006) Atomic structure of a Na⁺- and K⁺-conducting channel. *Nature* **440**(7083):570-574.
- Shrivastava IH, Durell SR and Guy HR (2004) A model of voltage gating developed using the KvAP channel crystal structure. *Biophys J* **87**(4):2255-2270.
- Singh J and Thornton JM (1985) The Interaction between Phenylalanine Rings in Proteins. *FEBS letters* **191**(1):1-6.
- Stalhandske CM, Persson I, Sandstrom M and Kamienska-Piotrowicz E (1997) Structure of the Solvated Zinc(II), Cadmium(II), and Mercury(II) Ions in N,N-Dimethylthioformamide Solution. *Inorg Chem* **36**(14):3174-3182.
- Starmer CF, Grant AO and Strauss HC (1984) Mechanisms of use-dependent block of sodium channels in excitable membranes by local anesthetics. *Biophysical journal* **46**(1):15-27.
- Szanyi A, Shafir Y, Hering S, Wolschann P and Guy HR (2008) Structural model of the Ca_v1.2 pore. *Channels (Austin)* **2**(3).
- Stea A, Tomlinson WJ, Soong TW, Bourinet E, Dubel SJ, Vincent SR and Snutch TP (1994) Localization and functional properties of a rat brain alpha 1A calcium channel reflect similarities to neuronal Q- and P-type channels. *Proceedings of the National Academy of Sciences of the United States of America* **91**(22):10576-10580.
- Stephan MM, Potts JF and Agnew WS (1994) The microI skeletal muscle sodium channel: mutation E403Q eliminates sensitivity to tetrodotoxin but not to mucotoxins GIIIA and GIIIB. *The Journal of membrane biology* **137**(1):1-8.
- Striessnig J, Grabner M, Mitterdorfer J, Hering S, Sinnegger MJ and Glossmann H (1998) Structural basis of drug binding to L Ca²⁺ channels. *Trends Pharmacol Sci* **19**(3):108-115.

- Struyk AF and Cannon SC (2002) Slow inactivation does not block the aqueous accessibility to the outer pore of voltage-gated Na channels. *J Gen Physiol* **120**:509-516.
- Sunami A, Dudley SC, Jr. and Fozzard HA (1997) Sodium channel selectivity filter regulates antiarrhythmic drug binding. *Proc Natl Acad Sci U S A* **94**(25):14126-14131.
- Sunami A, Glaaser IW and Fozzard HA (2000) A critical residue for isoform difference in tetrodotoxin affinity is a molecular determinant of the external access path for local anesthetics in the cardiac sodium channel. *Proc Natl Acad Sci U S A* **97**(5):2326-2331.
- Sunami A, Glaaser IW and Fozzard HA (2001) Structural and gating changes of the sodium channel induced by mutation of a residue in the upper third of IVS6, creating an external access path for local anesthetics. *Mol Pharmacol* **59**(4):684-691.
- Sunami A, Tracey A, Glaaser IW, Lipkind GM, Hanck DA and Fozzard HA (2004) Accessibility of mid-segment domain IV S6 residues of the voltage-gated Na⁺ channel to methanethiosulfonate reagents. *J Physiol* **561**(Pt 2):403-413.
- Swartz KJ (2004) Towards a structural view of gating in potassium channels. *Nature reviews* **5**(12):905-916.
- Tikhonov DB, Bruhova I and Zhorov BS (2006) Atomic determinants of state-dependent block of sodium channels by charged local anesthetics and benzocaine. *FEBS Lett* **580**(26):6027-6032.
- Tikhonov DB, Mellor IR and Usherwood PN (2004) Modeling noncompetitive antagonism of a nicotinic acetylcholine receptor. *Biophys J* **87**(1):159-170.
- Tikhonov DB, Mellor JR, Usherwood PN and Magazanik LG (2002) Modeling of the Pore Domain of the GLUR1 Channel: Homology with K(+) Channel and Binding of Channel Blockers. *Biophys J* **82**(4):1884-1893.
- Tikhonov DB and Zhorov BS (1998) Kinked-helices model of the nicotinic acetylcholine receptor ion channel and its complexes with blockers: simulation by the Monte Carlo minimization method. *Biophys J* **74**(1):242-255.
- Tikhonov DB and Zhorov BS (2004) In silico activation of KcsA K⁺ channel by lateral forces applied to the C-termini of inner helices. *Biophys J* **87**(3):1526-1536.
- Tikhonov DB and Zhorov BS (2005a) Modeling P-loops domain of sodium channel: homology with potassium channels and interaction with ligands. *Biophys J* **88**(1):184-197.
- Tikhonov DB and Zhorov BS (2005b) Sodium channel activators: Model of binding inside the pore and a possible mechanism of action. *Febs Letters* **579**(20):4207-4212.
- Tikhonov DB and Zhorov BS (2007) Sodium channels: ionic model of slow inactivation and state-dependent drug binding. *Biophys J* **93**(5):1557-1570.
- Tikhonov DB and Zhorov BS (2008) Molecular modeling of benzothiazepine binding in the L-type calcium channel. *J Biol Chem* **283**(25):17594-17604.
- Tikhonov DB and Zhorov BS (2009) Structural model for dihydropyridine binding to l-type calcium channels. *J Biol Chem*.

- Tombola F, Pathak MM and Isacoff EY (2006) How does voltage open an ion channel? *Annual review of cell and developmental biology* **22**:23-52.
- Toyoshima C, Nakasako M, Nomura H and Ogawa H (2000) Crystal structure of the calcium pump of sarcoplasmic reticulum at 2.6 Å resolution. *Nature* **405**(6787):647-655.
- Wang GK, Quan C and Wang S (1998) A common local anesthetic receptor for benzocaine and etidocaine in voltage-gated $\mu 1$ Na⁺ channels. *Pflugers Arch* **435**(2):293-302.
- Wang SY, Barile M and Wang GK (2001) Disparate role of Na⁽⁺⁾ channel D2-S6 residues in batrachotoxin and local anesthetic action. *Molecular pharmacology* **59**(5):1100-1107.
- Wang SY, Mitchell J, Tikhonov DB, Zhorov BS and Wang GK (2006) How batrachotoxin modifies the sodium channel permeation pathway: computer modeling and site-directed mutagenesis. *Molecular pharmacology* **69**(3):788-795.
- Wang SY, Tikhonov DB, Zhorov BS, Mitchell J and Wang GK (2007a) Irreversible block of cardiac mutant Na⁺ channels by batrachotoxin. *Channels* **1**:178-188.
- Wang SY, Tikhonov DB, Zhorov BS, Mitchell J and Wang GK (2007b) Serine-401 as a batrachotoxin- and local anesthetic-sensing residue in the human cardiac Na⁺ channel. *Pflugers Arch* **454**(2):277-287.
- Webster SM, Del Camino D, Dekker JP and Yellen G (2004) Intracellular gate opening in Shaker K⁺ channels defined by high-affinity metal bridges. *Nature* **428**(6985):864-868.
- Weiner SJ, Kollman PA, Case DA, Singh UC, Ghio C, Alagona G, Profeta S and Weiner P (1984) A New Force-Field for Molecular Mechanical Simulation of Nucleic-Acids and Proteins. *Journal of the American Chemical Society* **106**(3):765-784.
- Weiner SJ, Kollman PA, Nguyen DT and Case DA (1986) An All Atom Force-Field for Simulations of Proteins and Nucleic-Acids. *Journal of Computational Chemistry* **7**(2):230-252.
- Wright SN, Wang SY, Kallen RG and Wang GK (1997) Differences in steady-state inactivation between Na channel isoforms affect local anesthetic binding affinity. *Biophys J* **73**(2):779-788.
- Wright SN, Wang SY and Wang GK (1998) Lysine point mutations in Na⁺ channel D4-S6 reduce inactivated channel block by local anesthetics. *Mol Pharmacol* **54**(4):733-739.
- Wunderler D, Leonard RJ, Sanchez M and McManus OB (1999) Block of lymphocyte potassium channels by correolide, a triterpene natural product. *Biophysical Journal* **76**(1):A186-A186.
- Xie C, Zhen XG and Yang J (2005) Localization of the activation gate of a voltage-gated Ca²⁺ channel. *Journal of General Physiology* **126**(3):205-212.
- Xiu X, Puskar NL, Shanata JA, Lester HA and Dougherty DA (2009) Nicotine binding to brain receptors requires a strong cation- π interaction. *Nature* **458**(7237):534-537.
- Xu YQ, Crumb WJ, Jr. and Clarkson CW (1994) Cocaethylene, a metabolite of cocaine and ethanol, is a potent blocker of cardiac sodium channels. *J Pharmacol Exp Ther* **271**(1):319-325.

- Yamagishi T, Janecki M, Marban E and Tomaselli GF (1997) Topology of the P segments in the sodium channel pore revealed by cysteine mutagenesis. *Biophys J* **73**(1):195-204.
- Yamaguchi S, Zhorov BS, Yoshioka K, Nagao T, Ichijo H and Adachi-Akahane S (2003) Key roles of Phe1112 and Ser1115 in the pore-forming IIS5-S6 linker of L-type Ca²⁺ channel α 1C subunit (CaV 1.2) in binding of dihydropyridines and action of Ca²⁺ channel agonists. *Molecular pharmacology* **64**(2):235-248.
- Yang J, Ellinor PT, Sather WA, Zhang JF and Tsien RW (1993) Molecular determinants of Ca²⁺ selectivity and ion permeation in L-type Ca²⁺ channels. *Nature* **366**(6451):158-161.
- Yarov-Yarovoy V, Brown J, Sharp EM, Clare JJ, Scheuer T and Catterall WA (2001) Molecular determinants of voltage-dependent gating and binding of pore-blocking drugs in transmembrane segment IIS6 of the Na(+) channel α subunit. *J Biol Chem* **276**(1):20-27.
- Yarov-Yarovoy V, McPhee JC, Idsvoog D, Pate C, Scheuer T and Catterall WA (2002) Role of amino acid residues in transmembrane segments IS6 and IIS6 of the Na⁺ channel α subunit in voltage-dependent gating and drug block. *J Biol Chem* **277**(38):35393-35401.
- Zhen XG, Xie C, Fitzmaurice A, Schoonover CE, Orenstein ET and Yang J (2005) Functional architecture of the inner pore of a voltage-gated Ca²⁺ channel. *J Gen Physiol* **126**(3):193-204.
- Zhorov BS and Ananthanarayanan VS (1996) Structural model of a synthetic Ca²⁺ channel with bound Ca²⁺ ions and dihydropyridine ligand. *Biophys J* **70**(1):22-37.
- Zhorov BS and Bregestovski PD (2000) Modeling chloride channels of glycine and GABA receptors with blockers. *Biophys J* **78**:A2092.
- Zhorov BS, Brovtysna NB, Gmiro VE, Lukomskaya N, Serdyuk SE, Potapyeva NN, Magazanik LG, Kurenniy DE and Skok VI (1991) Dimensions of the ion channel in neuronal nicotinic acetylcholine receptor as estimated from analysis of conformation-activity relationships of open-channel blocking drugs. *The Journal of membrane biology* **121**(2):119-132.
- Zhorov BS, Folkman EV and Ananthanarayanan VS (2001) Homology model of dihydropyridine receptor: implications for L-type Ca(2+) channel modulation by agonists and antagonists. *Arch Biochem Biophys* **393**(1):22-41.
- Zhorov BS and Tikhonov DB (2004) Potassium, sodium, calcium and glutamate-gated channels: pore architecture and ligand action. *Journal of neurochemistry* **88**(4):782-799.
- Zhou M and MacKinnon R (2004a) A mutant KcsA K(+) channel with altered conduction properties and selectivity filter ion distribution. *Journal of molecular biology* **338**(4):839-846.
- Zhou M, Morais-Cabral JH, Mann S and MacKinnon R (2001a) Potassium channel receptor site for the inactivation gate and quaternary amine inhibitors. *Nature* **411**(6838):657-661.

- Zhou Y and MacKinnon R (2003) The occupancy of ions in the K⁺ selectivity filter: charge balance and coupling of ion binding to a protein conformational change underlie high conduction rates. *Journal of molecular biology* **333**(5):965-975.
- Zhou Y and MacKinnon R (2004b) Ion binding affinity in the cavity of the KcsA potassium channel. *Biochemistry* **43**(17):4978-4982.
- Zhou Y, Morais-Cabral JH, Kaufman A and MacKinnon R (2001b) Chemistry of ion coordination and hydration revealed by a K⁺ channel-Fab complex at 2.0 Å resolution. *Nature* **414**(6859):43-48.